STATISTICAL TREATMENT AND MODELING OF GEOCHEMICAL DATA OF VOLCANIC ARCS

by

Warren K. Lieu

APPROVED BY SUPERVISORY COMMITTEE:

____
Robert J. Stern, Chair

____
John W. Geissman

____
John F. Ferguson

____
Rita Economos

STATISTICAL TREATMENT AND MODELING OF GEOCHEMICAL DATA OF VOLCANIC ARCS

by

WARREN K. LIEU, MS

DISSERTATION

Presented to the Faculty of

The University of Texas at Dallas

in Partial Fulfillment

of the Requirements

for the Degree of

DOCTOR OF PHILOSOPHY IN

GEOSCIENCES

THE UNIVERSITY OF TEXAS AT DALLAS

May 2019

ACKNOWLEDGMENTS

I would like to thank my advisor, Bob Stern, for the guidance one needs to pursue an endeavor as noble as this. John Ferguson for his classes on analysis. John Geissman in the four summer field courses. Rita Economos in keeping me thinking about modeling. The Geosciences Department of The University of Texas at Dallas and its students: from them I learned many things beyond the scope of this dissertation.

December 2018

STATISTICAL TREATMENT AND MODELING OF GEOCHEMICAL DATA OF VOLCANIC ARCS

Warren K. Lieu, PhD
The University of Texas at Dallas, 2019

Supervising Professor: Robert J. Stern

This contribution concerns two projects based on statistical analysis of geochemical data of lava samples from global arc systems combined with standard geochemical treatments in order to extract trends, regularities and structures not readily apparent when done by studying individual volcanoes. Part I is an article "The robustness of Sr/Y and La/Yb as proxies for crust thickness in modern arcs." This paper considers three volcanic arcs – the Aleutians, Central America, and the Andes – and applies our understanding of trace element partitioning for four key elements and their dependence on pressure (i.e., depth) to derive crustal thicknesses along arcs and arc segments. We used geochemical data from the EarthChem.org repository and combined these with recent published igneous rock compositions vs. depth studies to derive crustal thickness profiles along modern arcs. We compare our methods with geophysical surveys to assess the viability of the correlation and our techniques. That the study at least partly agrees with geophysics is a boon for the conceptual methods we devised. That disagreements exist are, one, challenges for future geophysical surveys and geochemical studies to resolve and, two, a chance to interpret our results to reimagine and to incorporate existing theory of crustal processes into a

framework that is consistent with our results. Some arc's Moho may not have the sharp boundary that it is beneath continents but becomes an exchange interface with magma rising from the mantle injecting into the crust at the same time that magma cumulates (from fractionation) and crustal residues (from partial melting of the crust) founder into the mantle. The upper mantle beneath some active arc segment is then suffused with cumulates and restites separated from the lower crust such that seismic imaging of the Moho is difficult and ambiguous. Part II, "Fractionation and delamination in arc crust genesis," constrains models of fractional crystallization to generate lavas of the Alaska-Aleutian arc. The modeled dataset contains ~2,500 lava samples from ~30 volcanoes. We simulate first-order Earth processes that are heterogeneous, widely variable, and may not be in thermodynamic equilibrium, but that follow some principals that are statistically resolvable. This scheme reveals crustal processes that are plausible and produces cumulates that are similar to exposed mid and lower arc crust in Alaska and the Pakistani Himalayas. These modeled cumulates have variable compositions and densities to create a stratified crustal column as in exposed crust. Estimates of the physical characteristics and quantities of mineral assemblages can be inferred from the simulated crust to give insights into the mid and lower crust of the Alaska-Aleutian arc. For example, that the model solutions provide the quantity of the hydrous mineral amphibole in a crustal column allows me to estimate the amount of water stored in the crust, and explore the consequences of that. Furthermore, the results of fractionation modeling can be combined with approximate crustal geotherms and mineral densities to estimate the amount and rate that these dense cumulate masses are likely to sink into the upper mantle.

TABLE OF CONTENTS

LIST OF FIGURES

CHAPTER 1

THE ROBUSTNESS OF Sr/Y AND La/Yb AS PROXIES FOR CRUST THICKNESS IN MODERN ARCS

Authors - Warren Lieu and Robert Stern

Department of Geosciences, ROC 2.1

The University of Texas at Dallas

800 West Campbell Road

Richardson, Texas 75080-3021

A version of this chapter is "in press" and is used here under fair use permission granted by the Geological Society of America.

Abstract

Trace element (TE) ratios of convergent margin magmas have been found to vary with arc crustal thicknesses systematically. Here we use statistical smoothing techniques along with Sr/Y and La/Yb trace element Moho depth proxies to determine crustal thickness along the volcanic front for three arc segments: the central volcanic zone (CVZ) of the Andes arc, the Central America arc at Nicaragua and Costa Rica, and segments of the Alaska-Aleutian arc. The results are comparable to those from seismic surveys. TE depth proxies give ~70 km crust thickness beneath the CVZ's Altiplano region and show lower thickness (60 km for La/Yb, 43 km for Sr/Y) as the volcanic line crosses into the Puna region. In Central America, the proxy analyses show crustal thickness changes between the Chorotega block and the Nicaragua depression, with both proxies agreeing for Nicaragua (~27 km) but with La/Yb giving considerable thicker (~45 km) crust than Sr/Y (~30 km) for Chorotega. For these two arc segments, the La/Yb proxy approximated the seismically inferred Moho depth to within 10 km for the entire profile, but the Sr/Y proxy estimated crustal thicknesses diverge from those of the La/Yb proxy and seismic methods in the thin crust regions. For the Alaska-Aleutian arc, both TE proxies indicate that crust varies from thick (~35 km) for the western Aleutian segment (-175º E to 175º W), to thin (~22 km) for the transitional segment (175º W to 158º W), to thick (35+ km) for the eastern Alaska Peninsula (158º W to 150º W). Geophysical estimates favor a more modest change of 30 - 40 km for the same region. We propose that statistically treated geochemistry-based proxies can estimate useful crustal thickness when estimates from Sr/Y and La/Yb agree. We investigated the disagreement in the Alaska-Aleutian case in more detail. Alaska-Aleutian crustal thickness was found to correlate with calc-alkaline (CA) vs. tholeiitic (TH) segments of

the arc, as represented by along-arc smoothing of the volcanoes' CA-TH indices. The thin crust of the transitional segment trends tholeiitic while the thicker crust of the flanking segments trend calc-alkaline. We find that crustal thickness also plays a role in inferred magma flux (here approximated by volcano volume), with greater flux associated with thinner crust. Thin crust beneath the Alaska-Aleutian transitional segment may reflect continuing loss of cumulates from the lower crust/lithospheric mantle into the asthenosphere, leading to enhanced melting beneath this region.

1.1 Introduction

Convergent margin magmatism contributes significantly to the growth of Earth's continental crust (Rudnick, 1995; Kelemen et al., 2003, Davidson and Arculus, 2005). An essential process involves the partial melting of upper mantle and the subsequent modification of these melts to produce material with compositions that are broadly similar to bulk continental crust (the andesite model, Taylor and White, (1965), and its modifications, Gill, 1981). Details of these processes (e.g., mass-balancing of fractionated products and their cumulates) are continually being refined, but the fundamental tenets of this process are supported by the broad similarity of major and trace element compositions between modern arc igneous rocks and continental material, suggesting that similar processes generated both. Given that continental crust can form in arcs, a parameter to characterize crustal formation is the rate of crust addition. This requires that the volume of arc crust need to be estimated. Volume is a function of thickness, and the present-day crust thickness is most reliably obtained by crustal reflection and refraction techniques. But these are expensive and only a fraction of Earth's convergent plate margins have been studied in this way. These approaches are further complicated because the sub-arc Moho is often not marked by a sharp P-wave velocity (Vp) increase to 8 km/sec. This is because this region is composed of hot and partially melted mantle and delaminated cumulates acting to diffuse the seismically-defined crust/mantle boundary and making the Moho more difficult to discern (Arndt and Goldstein, 1989; Shillington et al., 2004; Kodaira et al., 2007; Shillington et al., 2013). Other geophysical approaches for estimating crustal thickness such as gravity modeling and receiver function analysis complement the active source techniques but are subject to uncertainties. Variations in some arc lava major elements were found to correlate with crustal thickness (Coulon and Thorpe, 1981), providing a non-geophysical method for crustal thickness determination. Refinements of these empirical studies have expanded into correlation of Moho depth with certain trace elements (Dhuime et al., 2015; Chapman et al., 2015; Profeta et al., 2015; Hu et al., 2017). This type of crustal thickness estimation comes with the possibility of inferring paleo-crust thicknesses. In this study, we examine trace element (TE) correlations with crustal thickness and compare these TE proxies' crustal thickness estimates against geophysics-derived Moho depths. We test the TE depth proxies' limitation and accuracy and extend their use by subjecting them to statistical assessments designed to quantify crust thickness variations on the scale of arc segments. As we will show, these correlation methods are not foolproof but in the best cases they match and complement estimates based on geophysical techniques. We also use our results to examine the implications of the Alaska-Aleutian arc system's crust thickness variation within the context of crustal evolution models.

1.2 Sr/y and La/Yb as Proxies For Crustal Thickness

The utility of arc TE crustal thickness proxies depend on the partitioning of certain TE (Sr, Y, La, and Yb) as melts interact with minerals through the lithospheric and crustal column through which they traverse, from the region of melt generation in the mantle wedge to the near-surface (we exclude TE from slab melt, for reasons discussed below). Here we briefly outline the origin of these correlations.

1.2.1 Arc Crust Formation And TE Ratios

New oceanic and continental arc crusts are derivatives of mafic magma generated from partial melting of the mantle wedge (Kimura, 2017). These mafic primary melts are generated by decompression melting accompanying flow in the mantle wedge and by flux melting when the subarc geotherm exceeds the wet solidus, which is in turn controlled by fluid released by the subducting oceanic slab. Primitive mafic magmas often underplate at the base of the crust (Annen and Sparks, 2002) where the magma's geochemistry are further modified by processes summarized as coupled assimilation-fractional crystallization (AFC; DePaolo, 1981, Spera and Bohrson, 2001) and magma assimilation, storage, and homogenization (MASH, Hildreth and Moorbath, 1988), which drive the mafic melts toward intermediate compositions. Additionally, there may be processes such as sinking of mafic-ultramafic cumulates from the lower crust (Kay et al., 1994; Lee et al., 2005; Behn and Kelemen, 2006; Jagoutz and Behn, 2013, see Discussion section), as well as accretion and underplating of buoyant subducted material (Kelemen and Behn, 2016). Magmas evolve further as they ascend and inject into the lower and mid-crust, where they change the local geotherm, fractionate, cause partial melting and mixing (Annen et al., 2006a, 2006b). They may then reside in one or more magma chambers and may further evolve before they are ultimately extruded from volcanoes or emplaced as plutons. Clearly, these processes make interpreting the geochemical components of a given igneous rock or lava sequence, from its inception as a mantle melt through its interactions with the crust en route to the surface, challenging and uncertain. However, the variability of these processes can be constrained and smoothed by statistics such that the complexity in their behaviors is averaged out and allow for broad patterns of chemical changes with pressure to emerge.

Here we concentrate specifically on the TE ratios Sr/Y and La/Yb of arc lavas and their relationship to different pressures in the upper mantle and crust beneath arcs where these melts form and evolve. These relationships arise because TE concentrations are by definition rarefied in magmas, and Henry's Law describes their activities, so linear equations govern mineral/melt partitioning during partial melting and crystal fractionation. Since the stability fields of equilibrium mineral assemblages are known, and their TE partition coefficients can be approximated, analysis of key TE ratios can reveal the conditions under which magma generation and differentiation occur. A bonus is that ratios of highly incompatible TEs (e.g., K/Rb, La/Nb) are conserved during magma fractionation, and therefore the initial ratios in the source region and primary melt (if not complicated by contamination and mixing) are preserved in the sampled lavas (White, 2013). Sr/Y and La/Yb ratios of arc igneous rocks are related to pressure due to the different affinity of these TEs to garnet ± amphibole and plagioclase (Moyen, 2009; Davidson et al., 2007). Garnet and plagioclase are stable at high (>1.4 GPa) and low (<0.4 GPa) pressure, respectively (amphibole is stable between 0.5 and 1.5 GPa for a typical arc geotherm), so La/Yb and Sr/Y in arc lavas reflect the pressure at which melting and fractionation occurred (middle diagrams of Figure 1.1 A, B). Partial melting or fractionation at high pressure (>~1.4 GPa), where garnet peridotite is stable, will result in a high Sr/Y melt due to the combined actions of stable garnet ± amphibole acting as a sink for the heavy Rare Earth elements (HREE) and Y, and the absence of plagioclase causing Sr to behave as an incompatible element (Moyen, 2009). At lower pressure (< ~1GPa) the absence of garnet ± amphibole causes Y to behave incompatibly at the same time that stable plagioclase absorbs Sr, leading to a melt with low Sr/Y. Similar processes control the La/Yb ratio with garnet ± amphibole absorbing Yb relative to La and plagioclase having no such effect. If we assume that partial melting of the mantle occurs just below the base of the arc crust and that MASH and AFC processes happen in the deep hot zones in the lower and mid-crust (Annen et al., 2006a, 2006b), we can use the systematics of these two sets of TE ratios to infer fractionating assemblages and thus indirectly crustal thickness and depth of the Moho.

High Sr/Y and La/Yb lavas of the far western Aleutians (west of ~175º E) (Kay, 1978; Kelemen et al., 2003; Yogodzinski et al., 2015) reveal processes likely related to highly oblique subduction and melting of the subducted slab (and subsequent interaction with the metasomatized upper mantle) producing variable silica with high Mg# andesites (Moyen, 2009). The Sr/Y- La/Yb ratios of these lavas likely do not reflect the processes we are interested in, and they do not form a statistically relevant population in the TE depth correlation studies used here; for these reasons they are excluded from this study (see Section 4 for region of study of the Alaska-Aleutian arc).

We note that there are additional processes that control subduction-related Sr/Y and La/Yb ratios, although these are probably second-order effects. We look at possible factors that could cause deviations from the TE ratios - depth correlation in Section 5.4 after the Results and Discussion sections.

1.2.2 Previous Geochemical Proxies For Arc Crustal Thickness

Global correlations of arc Moho depth with the variation of arc lava major elements (ME) have been established by a number of studies (Coulon and Thorpe, 1981; Leeman, 1983; Arculus, 2003; Mantle and Collins, 2008; Plank and Langmuir, 1998; Turner et al., 2015a, 2015b). Coulon and Thorpe (1981) concluded that crust thickness largely controls arc lava composition. They identified a crustal thickness threshold that separates dominantly tholeiitic volcanism on thin (< 20 km) crust and dominantly calc-alkaline volcanism on thick (> 20 km) crust. Leeman (1983) reported a relation between the silicic content of arc magmas and arc crustal thickness. He regressed global arc lavas' percent of andesite-dacite-rhyolite with arc crustal thicknesses and found a logarithmic fit with high r (correlation coefficient ~0.8) and concluded that arc magma evolution must scale with the amount of magma-to-crust interactions. These conclusions are corroborated by recent studies (e.g., Farner and Lee, 2017, discussed below).

While the early studies involved major elements, more recent works noted that some arc lava TE ratios also correlate to the thickness of the underlying crust (Chapman et al. 2015, Chiardia, 2015; Dhuime et al., 2015; Profeta et al., 2015; Farner and Lee, 2017). In particular, Chapman et al. (2015) showed that the trace element ratio Sr/Y in intermediate and felsic whole rock samples correlates linearly with crustal thicknesses to ~70 km. Profeta et al. (2015) showed similar correlations with low MgO calc-alkaline rock and added a power-law correlation between La/Yb and crustal thickness (Figure 1.2 A, B). Profeta et al.'s results are empirical curves fitted to large datasets of arc lavas from global geochemical repositories (e.g., GEOROC) with crustal thicknesses derived from the CRUST1.0 global model (Laske et al., 2013) and individual published studies (see their references). While the correlation is derived from global arcs and their median TE ratios, the authors proposed that the relationship could be extended to the scale of individual arcs. They demonstrated this possibility by superimposing Sr/Y and La/Yb vs Moho depth for individual volcanoes from the Southern Volcanic Zone (SVZ) of the Andes onto their Sr/Y and La/Yb vs. Moho depth regressions (red dots in Figure 2) and noted that these fall subparallel to the regressed curve. The interpretation is that the depth proxies of individual volcanoes (from at least this arc segment) conform to the correlation for global arcs, thus extending the correlations to a finer scale. The present study expands on Profeta et al.'s results and tests these correlations to infer crustal thickness along strike for three circum-Pacific arc segments: the Central Volcanic Zone (CVZ) of the Andes, the Central America arc at Nicaragua and Costa Rica, and part of the Alaska-Aleutian arc. We present the results as depth-to-Moho estimates, or equivalently to within a few km, crustal thicknesses, for these arcs, compare them with geophysical constraints, and examine implications of our results.

1.2.3 Robustness Of The TE-Moho Depth Correlations

While Profeta et al. (2015) interpolated their correlations from the arc scale to the scale of individual arc volcanoes, Farner and Lee (2017) investigated similar correlations at a more granular level. They argued that if arc crusts are in isostatic equilibrium, then an arc's elevation will reflect the total crust column thickness beneath it via an empirical relation derived in Lee et al. (2015), and elevations of lava samples are proxies for the crustal thickness. Then it is straightforward to construct correlation of the samples' inferred crustal thicknesses with their TE ratios. Farner and Lee's correlation is between mean TE values of samples binned into 10 km^3 volume (see below) and their derived crustal thickness via the isostasy relation. In Figure 1.3 we superimposed the La/Yb vs. crustal thickness curves of Farner and Lee onto the one from Profeta et al. The two regressed curves are sub-parallel and coincide for a large portion of the range of crustal thickness. The Profeta et al. curve is data-heavy for thin crust because it is skewed to more oceanic arcs (where marine seismic experiments can be conducted) whereas the Farner and Lee curve is derived from a more evenly distributed dataset (it is closer to being homoscedastic) since they can infer arc crust thicknesses merely by knowing the samples' mean elevations a.s.l. There is an offset of ~3 km in Moho depth (or a difference of ~6 in La/Yb value) between the two curves for thick crust, but in general, the curves are within each other's 95% confidence value. Notably, the two studies differ in the length scale treatment of the data: Farner and Lee's analysis involves taking the mean TE ratios from a collection of samples of a unit volume of crust (length x width = 10 km x 10 km and binned to their elevation $\Delta(h) = 0.1$ km) and using isostasy to obtain thicknesses, whereas Profeta et al.'s analysis relates median TE values of whole rocks and median Moho depths (from geophysics) of entire volcanic arcs. The quantitative agreement of the two studies, each uses a different method and performs at different data scale, bolsters confidence that correlations of TE ratios and crustal depth are robust. We propose that, given that the two approaches for estimating crustal thickness give comparable results, the correlations are plausible. In the present study, we further test the TE-crustal thickness relationship by applying the correlation to individual samples of volcanic and plutonic rock and use the rock sample population of the entire arc to derive crustal thickness variations along arcs.

1.2.4 Confidence Range Of The Profeta et al. (2015) Correlation And Conversion Of Geochemical Ratios To Arc Moho Depth

To reproduce and assess Profeta et al. (2015)'s results and to obtain a confidence level for the statistics of their approach, we re-analyzed their data (Figure 1.4). We produced least-squares best-fit lines and Pearson's coefficients (represented by r) for Sr/Y vs. crust depth using Monte Carlo simulation of their data assuming Gaussian distributions for their quoted one sigma errors. We calculate 10,000 bootstrapped regressed lines (~60 are shown) and the corresponding correlation coefficients (r). These form population distributions that we use to estimate confidence intervals. Our median simulated derived slope and intercept are 0.96, and 11.8, respectively, compared to Profeta et al.'s 1.11 and 8.05. The difference between the analyses is 10 to 30%, which corresponds to a depth difference that is generally less than 3 km (5 km maximum) for most Sr/Y. More importantly, our Monte Carlo derivation of r's gives their median as 0.84, with confidence interval (C.I.) between 0.61 and 0.92 (lower right of Figure 1.4). This implies that the correlation level of significance over the null hypothesis for these 22 arcs is over 99% and a median goodness-of-fit (R2) to be 0.71. We therefore accept the correlation between Sr/Y and depth, as conceptualized by Profeta et al. (2015) and Chapman et al. (2015).

A similar result was obtained for the La/Yb vs. depth correlation. For what follows below, we will use the correlation equations (Sr/Y and La/Yb vs. crustal thickness) of Profeta et al. (2015).

1.3 Methods

Our analysis depends on the assumption that globally-derived TE behavior holds at arc-segment and volcanic samples scales. We also rely on the assumption that the observed local-scale geochemistry of rocks is part of a rational representative of the underlying whole population. We accept that lavas from a given volcano are variable and may or may not follow Profeta et al. (2015)'s correlation. We show below that when we consider all the Sr/Y and La/Yb ratios from all available lava samples of an arc and treat these statistically we can map meaningful thickness variations for the arc using the correlation. We do this by employing a regression and smoothing algorithm to the sample suite and bootstrap for accuracy estimates. We show that such a procedure is equivalent to regressing the median value of each volcano for that arc; they both give nearly the same regression curve. We repeat the procedure using lava samples from three circum-Pacific arcs and compare each with geophysics-derived Moho depths to assess the robustness of our technique as well as the validity of the TE depth proxies.

1.3.1 Data Acquisition And Filtering Procedure

Data for volcanic samples were downloaded from Earthchem.org, which includes datasets from GEOROC, PetDB, and the USGS. A typical download includes all major elements, all available trace elements, isotope ratios, volatiles, location, etc. Harker-type diagrams were used to inspect the general geochemistry of the samples, and altered samples and other anomalous samples were deleted by inspection. We use robust statistics (e.g., median rather than mean) for our analysis to minimize influences of outliers. Extreme outliers were evaluated individually for inclusion or deletion. Finally, sample TE data used for crustal thickness estimation were subjected to filters following Chapman et al. (2015) and Profeta et al. (2015) in order to utilize their crustal thickness proxy correlation equations. One exception is that we did not apply the Thompson tau test for outliers per Chapman et al. (2015). A brief description of the filter used on the samples for inclusion is the following: major element totals between 97-103 wt% and SiO_2, MgO, and trace element ratio Rb/Sr ranges of 55-68 wt%, 1 to 6 wt%, and 0.05-0.2, respectively.

1.3.2 Sample Location Bias

In devising methods to characterize arc geochemistry from a population of samples accurately, we strive to minimize biases and sampling effects that may skew the dataset. The large number of samples gives some protection against bias from outliers. In addition, the estimators we used (median, boxplot, non-parametric regression, etc.) are less influenced by outliers than standard estimators (e.g., mean, standard deviation). The non-parametric lowess regression estimator described below uses polynomial regression in one of the steps that is model-based, but bootstrapping (see below) the regression adds robustness to the procedure.

When locations of lava samples are plotted as a function of distance along the arc, the distribution is usually uneven because volcanoes are unevenly sampled due to accessibility, regional politics, and other factors. In this situation, geochemical characterization of a given arc will be skewed by the more densely sampled volcanoes, which are overrepresented relative to the population. We seek a method to de-bias the over-represented volcanoes. One standard method is to "normalize" the geochemical value to the location parameter, e.g., 54 wt% SiO_2 per 10 km^3 of an arc (e.g., see Section 2.3 on Farner and Lee, 2017). The method we employ here to mitigate sampling bias is tied to the method of estimating accuracy when characterizing lava composition: the weighted bootstrap.

1.3.3 Weighted Bootstrapped Lowess Estimator

The lowess (locally weighted scatterplot smoothing) estimator (Cleveland, 1993) is a nonparametric regression devised to extract patterns in bivariate plots. It is nonparametric in that it does not rely on, for example, the sample population to be Gaussian, or any other a priori distribution. This estimator is well suited for characterizing Earth chemistry as we do not expect a parametric control in sample chemistry distribution (but if it is present the lowess regression is likely to detect it). It is not in the scope of this study to detail lowess operation, but a brief description is apt. A lowess regression fits a smoothed curve to characterize a set of bivariate data. Each particular point of this curve is calculated from data in the neighborhood of that point. The width of this neighborhood controls the smoothness of the final curve and this width constitutes one of two input parameters for the procedure. The lowess regressed value at this point is the fit of a weighted polynomial regression of the data within its neighborhood. For this study, we used a degree-1 linear regression (least squares) with a tri-cubic weight function throughout. The sharpness of the weighting function is the other parameter of the lowess. The lowess regressor can be thought of as a generalized "moving average" type regression. Its salient feature is that it is a nonparametric, adaptive, and outlier-resistance. We will further discuss the merits of using lowess regression in the next section.

To estimate the accuracy of the curves, we use the weighted bootstrap technique. Bootstrapping (Efron and Tibshirani, 1993) is an accuracy-estimating procedure that synthesizes many (typically from 100 to 10,000) populations of datasets by repeatedly resampling (with replacement) from the existing dataset. This synthesized population represents the underlying (unobservable) data of which the actual data is a subset. The relevant statistics that were performed on the original dataset is performed on these synthesized populations to obtain a distribution from which the variance and accuracy of the original dataset are extracted. It is bootstrapping in the sense that accuracy of the underlying large number of (inaccessible) samples can be estimated solely from the (typically small) number of accessible samples. Bootstrapping also allows for correcting bias in the resampling process (see data bias section above). To do this, we assign a weight to each sample during the bootstrap resampling. A sample's weight is based on the sample's proximity with all other samples of the arc system: a sample with many neighbors is weighted lower than a more isolated sample (see caption of Figure 1.5 for equation). This sample weight influences the probability of the sample being selected in the bootstrap resampling with the overall effect of a more even selection of samples among all the volcanoes. The sample biasing mitigation can be seen in data handling for the Alaska-Aleutian arc (Figure 1.5); specifically mitigating the larger number of samples in the Katmai region with the much smaller number of samples in the more remote western Aleutians (Figure 1.5 B). In Figure 1.5 C a weighted bootstrap resample dataset shows the Katmai data have been down-weighted and the western Aleutian data up-weighted. (If there is a small number of anomalous samples they will be up-weighted, but in practice, the smoothing process will tend to negate this type of leverage in producing the final, coherent curve.) This procedure results in a more balanced sampling of individual volcanoes for the whole arc from which statistical analysis is performed. We repeat this process thousands of times to derive a distribution of the statistics leading to a less biased dataset when operated on by the lowess estimator.

1.3.4 Equivalency Of Individual Samples And Volcano Medians

Here we demonstrate that we can subject lava samples to lowess regression to construct the geochemical variation trend along an arc and that doing so is equivalent to obtaining a trend by plotting median geochemical compositions for each volcano. The difference between using lowess regression of samples and taking volcano medians is nevertheless significant. This is because the lowess regressed curve takes values from a percentage of nearby samples to derive a value for any one point, so that that the generated curve does not allow for complete independence of samples from one location from those of its neighbors. Although it may seem restrictive that the constructed curve is so constrained and not completely independent, this is in fact what we assume when we calculate, for example, the mean silica wt% of a volcano: we assign a mean to that volcano and infer that all the lavas generated from it are related to (or constrained to be near) that mean. In lowess regression, we take this idea beyond a single volcano and say that at any single locale, lavas are related to, or are influenced by a certain percentage of lavas from other nearby locales. This means that, geochemically, the magmas originated from a process that was "simple" (i.e., partial melting of the mantle) but was acted upon by other processes that increase the variance of the magma compositions. For example, fractionation, anatexis, mixing, etc., contribute to the scattering of, say, a volcano sample's coordinates in a Harker diagram. However, in the limit of large number, perturbations that tend to increase an oxide's value are counteracted by others that tend to decrease it, so that lowess regression, which seeks the median of these scatters, can recover and better characterize the original signal. We propose that lowess regression can better represent the underlying geochemical signature of the relevant region by de-emphasizing the processes that scatter the sample data.

To demonstrate the near-equivalency of lowess regression and volcano medians we apply this regression to the SiO_2 content vs. location-along-arc for a suite of Alaskan-Aleutian arc lavas. The curve generated uses lowess regression on weighted bootstrapped resampling (Figure 1.6 A) with 5 and 95% confidence curves that bound the lowess estimate of the median value curve. All lava samples (n=3250) are plotted as black dots. Note the uneven density of samples of the Alaska Peninsula volcanoes versus the Aleutian island volcanoes are reflected in the spacing between the 5 and 95% bounding curves with a narrower spacing corresponding to denser data. This lowess regressed variation curve is interpreted here as the typical silica value at a locale along the arc. It clearly shows a slow decrease in silica from the western Aleutian island volcanoes to a sharp inflection at the continental shelf break (approximately the continent-ocean boundary), then a sharp increase from the peninsula to the continental interior. Figure 1.6 B shows boxplots for the median SiO_2 content of individual volcanoes. The lowess regression curve is shown for reference and to demonstrate the equivalency of the two plots. The inset shows a histogram of the residuals, the difference between the volcano median and the lowess curve at that longitude. The residuals histogram is close to Gaussian and symmetrical near 0, indicating that the difference between the prediction of the lowess regression curve is not biased from the volcano median. A feature of the lowess regressed curve that is distinct from the volcano medians is that the large number of samples guards against the curve being influenced by a few outliers, whereas in the volcano-median plot a small volcano with outlier median value may unduly influence the overall trend. That the generated curve gives a succinct and clear graphical representation (with accuracy estimate) of the underlying data is the main reason we propose that this type of curve characterizes the geochemical value against distance along an arc more accurately than other methods.

1.3.5 Null Hypotheses Check: Data Randomization

We have shown above that bootstrapped lowess regression is potentially useful for elucidating lava geochemical variations along an arc such as the Alaska-Aleutian system. We now address the question of what is the likelihood that such variation comes about from pure chance? To do this, we have devised a test to evaluate the possibility that the curve-generating procedure indicates a chemical variation vs. distance relationship when no relation exists in actuality. For this test we use data from the Alaska-Aleutian arc La/Yb proxy depths and, as before, perform lowess regression to examine their variation against along-arc distance (longitude). We pose the null hypothesis that the La/Yb variations have no dependency on longitude. If the null hypothesis is true, it means we can randomly permute the samples' longitude values, perform the lowess regression on this longitude-randomized sample set and expect a resultant curve that is equivalent to the original unpermuted dataset. We repeat this process one thousand times, then examine the distribution of these curves and compare them with the curve generated with the original data. Figure 1.7 shows a few dozens of the location-randomized La/Yb-depth variation curves along the arc (green curves). There are statistical variations and 'kinks' in the curve, where data density is low and a few samples control the curve. In the limit of taking the mean of the one thousand location-randomized curves, we obtain a near-horizontal curve (dark green) fluctuating near the mean value of the La/Yb of the population (here equal to 26 km crustal thickness), as is expected for a randomly located set of samples. Comparison of the randomized data with the actual variation of La/Yb vs. longitude (red curve, copied from Figure 1.13) shows how different the real variation is, compared to the ones made with the randomized data; the actual La/Yb variation with longitude is such that this curve barely intersect the field defined by the randomized curves. The lowess regression curve generated from the data is significantly distinct from those that come from chance alone. Thus the null hypothesis is false: the La/Yb variations along this arc do depend on longitude. The fact that there are two populations of La/Yb ratio (or Moho depth) amongst the samples is evident in the two distinct peaks in the histogram (left side of Figure 1.7). How these samples (as depth proxies) are actually distributed along the arc is the subject of the Results and Discussion section.

In general, given enough data, we can characterize lava geochemical variations along an arc using weighted bootstrap lowess regression as described in this Section. These characterizing curves can extract trends in noisy datasets, can correct for known bias, and come with estimation of accuracy.

1.4 Results Of Sr/Y And La/Yb Ratios As Depth Proxies For Three Arcs

Here we show results of crustal thickness estimates of the three arcs: the Central Volcanic Zone of the Andes, Central America, and Aleutian-Alaska. First, we show the studied regions (Figure 1.8, 1.9, 1.10 for CVZ of South America, Central America, and Alaska-Aleutian, respectively) with the regions superimposed with sample locations along with the tectonic boundaries. Seismic-derived Moho depths are also shown and referenced to the studies. Note that our curves are for the volcanic front (where the samples are located) but seismically determined Moho depths are for a much broader region. The relevant tectonic boundaries that define crustal thicknesses are shown. In the Alaska-Aleutian case (Figure 1.10), note the location of our boundaries ("west," "transition," and "east"): they differ from "western" and "eastern" denotations in past studies. Also, we emphasize that our Alaska-Aleutian studied area excludes the far western Aleutian (what is referred to by others as "Western Aleutian") because we only consider the arc associated with a subduction zone as being defined by the extent of the seismically detectable slab mapped by Syracuse and Abers (2006). In the Alaska-Aleutian arc, the slab is not defined west of ~180º, where the convergence velocity tends to very low value, and the tectonics are dominated by strike-slip faulting. The key TE correlations that we address do not apply there.

1.4.1 South America Convergent Margin Crustal Thickness

Crustal thicknesses are calculated from the individual samples' La/Yb and Sr/Y ratios based on the Profeta et al. (2015) correlations and regressed against arc strike (Figure 1.11).

Confidence interval curves (5% and 95%) are shown bounding the median (50%) curve in the figures. Both the individual samples' La/Yb and Sr/Y depth proxies and the derived curves plot close to each other and are in phase as they track changes along the northern (Altiplano) segment of the arc, estimating crustal thickness of 68-72 km. South of ~18ºS near the Puna and Altiplano boundary, there is a change in slope from flat to a decrease (at -3 to -6 km/° latitude for La/Yb and Sr/Y, respectively) in thicknesses to 21.5ºS, where the Sr/Y proxy predicts a shallower Moho depth than does the La/Yb proxy and the geophysics estimates by ~17 km (mid to high 40 km for Sr/Y vs. high 50 km for La/Yb, CRUST1.0 and McGlashan et al., 2008). In general the northern portion of the geochemically derived crustal thickness curves compare well with the McGlashan et al. (2008) teleseismic study and with the CRUST1.0 (Laske et al., 2013) estimates (we show both survey's data as lowess regressed curves made with the same method we used for the TE ratios). The density of samples increases the fidelity of the TE proxy curves along the arc with few gaps. The division between the Puna and Altiplano appears in the TE proxy curves as a difference in crustal thickness but is not as well resolved in the geophysically-derived Moho depths. The TE ratios depth proxies decouple in the Puna region, with Sr/Y depths ~20 km shallow than La/Yb depths and geophysics depths. This reflects the complex nature of the petrogenesis of the region as documented by Kay et al. (1994) and Kay and Coira (2009), where ignimbrite, calc-alkaline, intraplate, and shonshonitic centers are superimposed in a small region (23ºS - 27ºS). The Altiplano region is less complicated and the two TE proxies agree (to within 10 km) with the McGlashan et al. (2008) seismic depth, but are ~15 km thicker than the CRUST1.0 depth. The TE Sr/Y proxy depth departs from the La/Yb proxy depth and geophysics depths by ~15 km south of 19.5° S but is consistent with thinning of the crust south of the Altiplano (Kley and Monaldi, 1998; Kay and Coira, 2009). In general, the TE proxies give plausible Moho depths compared to those available from geophysics. The Sr/Y proxy may reflect the effect of plagioclase in cumulates or restites to lower Sr.

1.4.2 Central America Convergent Margin Crustal Thickness

We constructed lowess curves of crustal thickness derived from La/Yb and Sr/Y along the Central American volcanic arc, from latitude 9º to 15ºN (Figure 1.12). Here we compare our TE-based crustal thickness estimates with geophysically-based estimates from CRUST1.0 (Laske et al., 2013) and MacKenzie et al. (2008). Both Sr/Y and La/Yb Moho depth estimates decrease from the thick Chorotega block going north into the Nicaragua basin. The two geochemical proxies show different crustal thicknesses, with the La/Yb proxy predicting deeper Moho than the Sr/Y proxy by ~20 km. The La/Yb proxy predicts thick crust (50+ km) beneath the southern Chorotega block compared to the more moderate mid-30 to low 40 km estimate given by the Sr/Y proxy. The Sr/Y depth proxy predicts thinner crust beneath the center of the Chorotega block compared to the other estimates. The reason for this discrepancy may relate to excess plagioclase, or it may reflect the plume-influenced nature of magmatic processes beneath the southern Central American arc (Gazel et al., 2011). Both Sr/Y and La/Yb give slightly thinner crust beneath the Nicaragua basin as compared to the geophysically-based estimates but converge with the CRUST1.0 curve north of 12º. The two geophysical approaches show more moderate changes in crustal thickness beneath Central America. CRUST1.0 (Laske et al., 2013) indicates a gradual decrease in Moho depth of 10 km northward from 33 to 22 km in 5º of latitude while the MacKenzie et al. (2006) study shows a similar decrease of ~8 km (39 to 31 km) northward along 3º of latitude. The two geochemical proxies for Moho depth diverge in detail but consistently show modest crustal thinning from the Chorotega Block to the Nicaragua terrane.

1.4.3 Alaska-Aleutian Convergent Margin Crustal Thickness

We apply our method of estimating crustal thicknesses beneath volcanic arcs using TE ratios to the Alaska-Aleutian system (Figure 1.13). We note that the Alaska-Aleutian convergence system has an overriding plate that is oceanic in the west (Aleutians) and continental (Alaska Peninsula) in the east. We are especially interested to know whether the geochemical proxies show a significant crustal thickness difference for these two different crusts. Figure 1.13 shows the Moho depths inferred from La/Yb and Sr/Y along the arc. Crustal thicknesses agree between the two TE proxies and the curves are coherent and in phase. The proxies predict a crust thickness of ~20-25 km between 174° and 160°E, ~30 km crust west of 174°E, and notably, a ramp-like increase in thickness from ~23 to 35-40 km east of 155°E. This contrasts with estimates for Moho depth determined by the Alaska Seismic Experiment (ASE, 1994) line A1 and A3 (Figure 1.10), which show Moho depths of ~28 km at 172° E and 164°E, and along-strike Moho depth of 30±4 km (line A2, Figure 8 in Fliedner and Klemperer, 1999). Moreover, the CRUST1.0 (Laske et al., 2013) lowess regression curve shows Moho depth increasing eastward with a near-linear slope, from ~19 km at 180° to ~38 km at 153°E. A recent receiver function study by Janiszewski et al. (2013) placed the Moho at a (regressed) near-constant 39 km depth from 160º to 177º, almost 20 km deeper than the TE proxies' predictions.

Discrepancies between the geochemical proxies and the geophysics-derived crust thickness are further addressed in the Discussion section next.

1.5 Discussion

How reliable is the TE-based method of applying global correlation to a high-spatial resolution and geochemically-variable study of an individual arc? We note that in the case of Central America and the Andes CVZ, when the two TE ratios are coherent, they tend to agree with geophysical estimates, but when the two TE ratios disagree, they depart from geophysical estimates. We conclude that statistically-treated geochemistry-based proxies can estimate useful crustal thickness and are complementary to geophysical methods when estimates for the two ratios agree. Given this caveat, we look in more detail at the Alaska-Aleutian arc result and discuss the implications of the disagreement between our coherent TE-inferred Moho depths and seismically inferred Moho depths. We examine the geochemistry of this arc as it pertains to crustal thickness, then crustal thickness as it relates to volcanic output. Finally, we combine both analyses with a possible crustal model that may reconcile the thickness difference between the results of geochemistry and geophysics.

1.5.1 Alaska-Aleutian Lava Affinities

The Aleutian-Alaskan arc erupts both tholeiitic (TH) and calc-alkaline (CA) lavas (Kay et al., 1982; Kay and Kay, 1994; George et al., 2003; Mangan et al., 2009), but does the systematic relation noted by Coulon and Thorpe (1981) between CA-TH suites and crustal thickness exist in the Alaska-Aleutian arc? If so, what are the geodynamic implications? Recently, Farner and Lee (2017) observed in their global compilation that there was a correlation between elevation (their proxy for crustal thickness, see section 2.3) and calc-alkalinity. In this section, we apply lowess regression to construct curves to characterize calc-alkaline/ tholeiitic affinity of volcanoes and rock samples and correlate these with the crustal thickness proxies derived above. Figure 1.14 shows our resultant lowess regression curves of published calc-alkaline/tholeiitic indices (the tholeiitic index of Zimmer et al., 2010; and calc-alkaline/tholeiitic index of Hora et al., 2009) generated from volcanic samples of our compiled dataset. Zimmer et al. (2010)'s tholeiitic index (THI) is a measure of the Fe-enrichment of a volcano expressed in the ratio of FeO at 4% MgO over FeO at 8% MgO. THI is a per-volcano measurement whereas Hora et al.'s calc-alkaline/tholeiitic index (CATH) assigns an index to individual rock based on Miyashiro (1974)'s separation of arc tholeiitic and calc-alkalic rocks (see defining equations in Figure 1.14 caption).

Alaska-Aleutian igneous rocks define two distinct populations, with most plutonic samples having calc-alkaline affinities (Kelemen et al., 2003; Cai et al., 2015). For this reason, we performed the regression with only volcanic samples. For the per-volcano lowess curve generated by the THI index of Zimmer et al., tholeiitic volcanoes are preferentially located along the transitional segment of the arc with calc-alkaline volcanoes to the west (Aleutians) and east (Alaska Peninsula). CATH index shows a similar result with few exceptions (see Figure1.14). We conclude that Aleutian-Alaska tholeiitic arc lavas are associated with thinner crust (as inferred from our results) of the transitional segment between ~161° and 174°E, and that calc-alkaline lavas are associated with the thicker crust of the oceanic and continental arc on either side (Figure 1.13). The regression parameters we used are sensitive to long wavelength changes, so we did not reproduce results of Kay et al. (1982), in which CA and TH volcanoes are associated with the variable stress regime in and around rotated tectonic blocks. They proposed that TH volcanoes concentrate between rotated tectonic blocks, where magmas evolved at low pressure and ascended through extensional basins, whereas CA volcanoes are concentrated on the blocks, associated with a thicker crust and higher pressure magmatic evolution. This CA-TH relationship associated with tectonic blocks in the Aleutians is subsumed into the longer variation in the whole-arc treatment of the lowess regression of the geochemical data. In our analysis, the entire Aleutian-Alaskan arc from 176ºE (Buldir) to 152ºW (Spurr) manifests a single CA to TH to CA cycle.

1.5.2 Alaska-Aleutian Volcanic Activity And Crustal Thickness

Likely controls on the magma flux for a mature arc are convergence velocity, subducted fluids and sediment, magma plumbing system, and thermal structure of the mantle wedge. For example, Fournelle (1994), George et al. (2003) and others have pointed out a relation between Aleutian volcano volume (inferred to reflect magmatic flux) and convergence velocity. We checked their correlation with a polynomial fit (degree 1 or 2) and found that volume and velocity are related by an r-value = 0.4, with n = 34, a 95% significant correlation. Here we examined crustal thickness as a possible control of magma addition. We assumed that all arc volcanoes are about the same age (Jicha et al., 2006) and that each magmatic cell associated with an individual volcano reflects a similar proportion of intrusive to extrusive rocks. In this case, volcano volume scales with magmatic flux, and we will take the volcano volume as a proxy for flux. We plot the Alaska-Aleutian volcano volume along the arc (Figure 1.14, top), then we examine the relationship between volcano volume and crustal thickness. Figure 1.15 shows the correlation of the arc segment volcanoes' volume with the corresponding crust thickness beneath each. The negative correlation for the linear fit is significant (at 99% for $n = 34$, with similar significance for a polynomial fit). If the volcanoes are grouped by the three arc segments, the larger volcanoes tend to be located on the transitional segment (Figure 1.15, volume histogram). The distribution of volcano volume is similar for the eastern continental and western oceanic segments even though the two have a distributed crustal thickness values (Figure 1.15, thickness histogram). At the same time, the transition segment volcanoes are underlain by thin crust (21-25 km) and show a bimodal distribution of volumes. These observations reveal that the arc segments host distinct distribution of volcano volumes: the thin-crust transition segment volcanoes exist in two volume modes: ~75 km^3, and ~300 km^3, whereas the thicker-crust western oceanic (Aleutian) and eastern peninsula and continental (Alaskan) segments' volcano volumes are in a positively skewed distribution with median of 40 km^3. It is also noteworthy that the transitional segment contains most of the large edifices (7 out of 9 volcanoes with volume ≥ 200 km^3) but only 4 of 25 volcanoes with volume < 200 km^3.

We performed a randomization test (similar to the test described in Section 3.5) to see if the volcano volume vs. segment relation arose from chance alone. The test assumes a null hypothesis, in which case randomizing the relation between volume and crustal thickness would not affect the correlation. In fact, the real correlation is > 95%, significantly different than the randomized case. Thereby the null hypothesis is rejected and the correlation is significant. There is no similar correlation of volume vs. crustal thickness for the other studied arcs (CA and CVZ). The proposed correlation between magma addition and crustal thickness is simplistic in that it assumes all magma addition to be expressed in volcano volume, ignoring the cryptic addition of mass by mechanisms such as underplating and "relamination" of subducted material (Castro et al., 2013; Kelemen and Behn, 2016). However, the correlation exists and it is compelling. The thin-crust transitional segment of the arc hosts all the large volume volcanoes. This result suggests that thinner arc crust has a simpler plumbing system for magma migration to the surface, or that the Alaska-Aleutian transitional arc segment is a region that is more conducive to mantle melting. We explore the latter supposition in the next section.

1.5.3 Crustal Construction Model

We use derived crustal thickness along the Alaska-Aleutian margin to suggest reasons for the discrepancies with geophysical-derived Moho depths in the context of current ideas on arc crust construction. Assuming that the TE-inferred Moho depths are useful approximations of reality, we wonder what is responsible for thickening and thinning the crust between the transition segment and the continental segment of the arc. The lowess regressed curve predicts that the thin crust of the transition segment thickens to more continental-like thickness as the arc extends into the Alaskan peninsula, with the thin crust coincides with the high-volume, tholeiitic volcanoes' location on the transition segment, and the thick crust with the low-volume, calc-alkaline volcanoes of the western and continental segments (Figure 1.13, 1.14, 1.15). We relate these features to a model of oceanic arc crust evolving to continental crust, integrating observations from section 5.1, 5.2 and current crustal evolution theories.

It is known that the construction of continental crust from convergent margin magmatism is a multistage process that transforms basaltic mantle melts to the andesitic composition of bulk continental crust. The processes of fractionation, melting and mixing to evolve high Mg# andesite with TE that matches continental crust requires a complementary cumulate in the lower crust or upper mantle (Kay and Kay, 1993; Rudnick and Fountain, 1995; Holbrook et al., 1999; Kodaira et al., 2007). Seismic velocity profiles and fossil arc crust sections (e.g., Talkeetna; Greene et al., 2006) mostly do not show a mafic cumulate layer in the lower crust for the required mass-balance. Jagoutz et al. (2013) observed that the exposed Kohistan lower crustal section is denser than the upper mantle and suggested repeated delamination of the mafic lower crust as a mechanism to evolve andesitic arc crust and continental Moho. This also addresses the presence of a sharp seismic boundary at the continental Moho (Vp transitions from ~7 km/s to ~8 km/s in a step function) that is absent for the Moho beneath magmatic arcs. Most magmatic arcs show a thick (~10 to 15 km) transitional layer where Vp increases from ~7.4 km/s to ~7.8 km/s, which is generally assumed to represent upper mantle (Calvert and McGeary, 2013). However, these velocities are characteristic of lithologies such as pyroxenites and eclogites that are denser than the upper mantle peridotite, are weak and thus are likely to founder, as noted by Behn and Kelemen (2006). Similar lithologies compose the crustal section that Jagoutz et al. (2013) modeled as negatively buoyant and the absence of which creates a sharp P-wave velocity contrast between crust and mantle that characterizes continental Moho. Such a sharp Moho is exposed at the Talkeetna crustal section, whereas the analogous exposed Kohistan crustal section exhibits a more gradational crust-mantle boundary with a (calculated) gradual P-wave velocity ramp that may be more typical of arc crust.

Further insights into the nature of the lower crust and upper mantle beneath arcs are provided by measurements of shear wave splitting or SKS. Shear wave splitting reveals seismic anisotropy induced by preferred orientation of olivine in the upper mantle (Karato, 2009) or by melt-filled cracks oriented parallel to the maximum compressive stress direction (Yang et al., 1995). Both mechanisms are taken to indicate the direction of mantle flow. Measurement of seismic anisotropy beneath mid-ocean ridges shows that this is related to convection in the uppermost mantle, which is predicted to flow parallel to plate motion and perpendicular to the ridge strike. In arc settings, the fast-polarization directions are often oriented parallel to arc strike (see Yang et al. (1995) for seismic anisotropy beneath Shumagin Island within the Alaska-Aleutian transition segment), indicating paradoxically that mantle flow is perpendicular to the subduction vector. Behn et al. (2007) proposed that delamination (or Rayleigh-Taylor instability foundering) of dense lower arc crust as a mechanism that induced such trench-parallel flow. They modeled gravitationally unstable diapir-like sinking masses of ~15 km diameter (by a few kilometers thick) spaced ~40 km apart and observed induced flows that are similarly oriented to SKS fast directions documented in arcs. We propose that the transitional segment of the Aleutian arc is shedding dense lower crust granulite and pyroxenite (P-wave velocity of >7.4 km/s) formed as cumulates by basaltic fractionation at ~25 km depth, as indicated by the La/Yb and Sr/Y proxies (Figure 1.1 and 1.16). At 15 km diameter and a few km thick, these sinking masses will not be resolved in tomographic images, and their Vp contributions will be averaged into the surrounding mantle.

Furthermore, delamination of these cumulate masses induces upwelling of the sub-arc asthenosphere, leading to enhanced decompressional melting near the base of the crust (Kay et al., 1994; Behn et al., 2007) and the observed high-volume tholeiitic volcanism of the transition segment. Behn et al. (2007) estimated that each down-going mass could induce mantle upwelling to generate 10 km^3 of melt. We propose such processes are responsible for the enhanced volcanic activity of the transition segment. If the masses are spaced 40 km apart with a descent velocity of ~1 cm/yr and delamination occurs every 10^6 to 10^7 years (Behn et al., (2007) from arc-magma production estimates of Jicha et al., (2006)) the upper mantle beneath the volcanoes of the transition segment will accumulate, in volume, ~30% of cumulate rock, mixed in with the upper mantle peridotite, becoming a layer of mixed lithologies between lower crust and mantle, giving the high Vp structure at 20 - 40 km depth seen in teleseismic studies (Figure 1.1). This interpretation is consistent with the results of Shillington et al. (2013), who analyzed Vp/Vs ratio in addition to Vp to determine likely lower crustal lithologies in the Aleutian transition segment and concluded that a mixture of material is needed to explain the observed high Vp and low Vp/Vs ratio. These masses are smaller than delaminated slabs such as those proposed, say, for the Andes (Puna plateau, Kay et al., 1994) or the Sierra Nevada (Ducea and Saleeby, 1996; Manley et al., 2000; Farmer et al., 2002; Lee et al., 2015) where detachment of region-scaled lower crust/lithosphere occurred with the induction of prolonged region-wide uplift and magmatism. Our proposed scheme is more on the order of a dynamic exchange of material across the crust/mantle boundary, cycling at about 106 years; in this situation, uplift is suppressed by the balanced flux of cumulate loss and magma in-flow recharge. In our interpretation, the TE-inferred Moho depths mark the transition from the lower crust (at ~25 km) into a transitional lithological layer of melting and fractionating with a mixture of cumulate/peridotite rock, the bottom of which (at ~40 km) is interpreted as the Moho in the seismic survey.

1.5.4 Other Explanations For Proxies Vs. Geophysics Differences In Crustal Thickness

Here we address the discrepancy between the TE depth proxy predictions and the geophysics estimates (Holbrook et al., 1999; Lizarralde et al., 2002; Van Avendonk et al., 2004; Janiszewski et al., 2013; CRUST1.0; Shillington et al., 2013) without using the model discussed in section 5.3. The correlations of TE-estimated Moho depth seem robust because they are based solely on the abundance of four elements. The application of lowess regression to the correlations acts to average out the variable complexities of these elements in arc processes to exhibit the TE correlation to crustal thickness. This dependency on only four elements is also the correlations' weakness, for the correlations are vulnerable to systematic variations in those elements, as seen for the decoupled TE ratios in northern Puna of the CVZ and the Chorotega region of Central America. In those regions the TE proxies for crustal thickness may not be applicable: the multitude of processes operating in the region decoupled the two TE ratio correlations from showing an unambiguous and valid result. Similarly, for the crust of the Aleutian arc transition segment, there may be local processes acting to disturb the global correlation enough to invalidate its usage. The TE ratios there may reflect, for example, the variable mantle wedge chemistry such as Sr differentially leached from the subducted slab. These types of effects may be large compared to the global trend responsible for the correlation to crustal thicknesses. It is also possible that the Profeta et al. correlation itself may not be applicable to discern crustal thickness within an arc at the resolution we consider here. The global variations exist but have a variance that cannot be scaled down to show thickness variation at the resolution of this study. However, one must still explain the systematically lower Sr/Y for 15º along the arc that anti-correlates to both sediment input (Kelemen et al., 2003) and convergence velocity. There is also the possibility that geophysical techniques infer a Moho that is too deep: a crustal thickness of ~40 km at longitude 160° to 175° as proposed by Janiszewski et al. (2013) implies that the Moho at longitude 170° is less than 20 km from contacting the subducted slab as defined by the depth of the Wadati-Benioff zone of Syracuse and Abers (2006), a geometry that is problematic because it implies a cooler geothermal gradient in the mantle wedge than is capable of producing melt. The corresponding TE proxy Moho depth of 20 km gives a more realistic 40 km separation between the subducted slab and the lower crust (Figure 1.1). Beneath the easternmost continental volcanoes, the Wadati-Benioff surface gives what is probably the minimum separation of ~35 km for the TE proxy crustal thickness of 40 km. In the Central American arc, the TE proxies diverge from each other at latitude 10º - 11ºN, which is at the limit of the volcano line beneath which the subducting slab ceases to have seismicity and where the influence of the Galapagos plume (Cocos Ridge) may affect arc magma compositions.

1.6 Conclusions

We have demonstrated a proof-of-concept method using statistical techniques applied to geochemical data to extend the usage of the Sr/Y and La/Yb TE depth proxies to resolve variations in crustal thickness within arc segments. These estimates are plausible when compared to their geophysical refraction and reflection studies and thus serve as a complementary technique to model crustal thickness, especially for where geophysical coverage density is low. We have shown that when the two TE proxies are in phase, they can complement geophysics in the CVZ and the Central America cases. Then we examined an intriguing case in the Alaska-Aleutian where the TE proxies-geophysics disagreement necessitated novel interpretation of arc crust construction where the Moho interface of arcs maybe more opened, with influxes of mantle-derived magmas and delamination of fractionated cumulates and restites. This interpretation implies the Moho beneath an active magmatic arc may be more challenging to identify than generally acknowledged, with geophysical estimates being deeper than those from TE proxies.

REFERENCES CITED

Annen, C., Blundy, J.D., and Sparks, R.S.J., 2006a, The genesis of intermediate and silicic magmas in deep crustal hot zones: Journal of Petrology, v. 47, p. 505-539, doi: 10.1093/petrology/egi084.

Annen, C., Blundy, J.D., and Sparks, R.S.J., 2006b, The sources of granitic melt in deep hot zones: Transactions of the Royal Society of Edinburgh: Earth Sciences, v. 97, p. 297-309, doi: 10.1017/S0263593300001462.

Annen, C., and Sparks, R.S.J., 2002, Effects of repetitive emplacement of basaltic intrusions on thermal evolution and melt generation in the crust: Earth & Planetary Science Letters, v. 203, p. 937-956.

Arculus, R.J., 2003, Use and abuse of the terms calcalkaline and calcalkalic: Journal of Petrology, v. 44, p. 929-935, doi: 10.1093/petrology/44.5.929.

Arndt, N.T., and Goldstein, S.L., 1989, An open boundary between lower continental crust and mantle: its role in crust formation and crustal recycling: Tectonophysics, v. 161, p. 201-212, doi: 10.1016/0040-1951(89)90154-6.

Atwater, T., 1989, Plate tectonic history of the Northeast Pacific and western North America: Denver, CO, Denver, CO, United States: Geological Society of America, p. 21-72.

Behn, M.D., and Kelemen, P.B., 2006, Stability of arc lower crust: Insights from the Talkeetna arc section, south central Alaska, and the seismic structure of modern arcs: Journal of Geophysical Research B: Solid Earth, v. 111, doi: 10.1029/2006JB004327.

Behn, M.D., Hirth, G., and Kelemen, P.B., 2007, Trench-parallel anisotropy produced by foundering of arc lower crust: Science (New York, N.Y.), v. 317, p. 108, doi: 10.1126/science.1141269.

Cai, Y., Rioux, M., Kelemen, P.B., Goldstein, S.L., Bolge, L., and Kylander-Clark, A., 2015, Distinctly different parental magmas for calc-alkaline plutons and tholeiitic lavas in the central and eastern Aleutian arc: Earth and Planetary Science Letters, v. 431, p. 119-126, doi: 10.1016/j.epsl.2015.07.058.

Calvert, A.J., 2011, The Seismic Structure of Island Arc Crust, *in* Brown, D., Ryan, P.D., ed., Arc-continent collision: Berlin Heidelberg, Springer-Verlag, p. 87-119.

Calvert, A.J., and McGeary, S.E., 2012, Seismic reflection imaging of ultradeep roots beneath the eastern Aleutian island arc: Geology (Boulder), v. 41, p. 203-206, doi: 10.1130/G33683.1.

Castro, A., Vogt, K., and Gerya, T., 2013, Generation of new continental crust by sublithospheric silicic-magma relamination in arcs: A test of Taylor's andesite model: Gondwana Research, v. 23, p. 1554-1566, doi: 10.1016/j.gr.2012.07.004.

Chapman, J.B., Ducea, M.N., DeCelles, P.G., and Profeta, L., 2015, Tracking changes in crustal thickness during orogenic evolution with Sr/Y: An example from the North American Cordillera: Geology, v. 43, p. 919-923, doi: 10.1130/G36996.1.

Chiaradia, M., 2015, Crustal thickness control on Sr/Y signatures of recent arc magmas: an Earth scale perspective: Scientific Reports, v. 5, Article number 8115.

Cleveland, W.S., 1993, Visualizing Data: Summit, NJ, Hobart Press, 360 p.

Coulon, C., and Thorpe, R.S., 1981, Role of continental crust in petrogenesis of orogenic volcanic associations: Tectonophysics, v. 77, p. 79-93, doi: 10.1016/0040-1951(81)90162-1.

Davidson, J.P., and Arculus, R.J., 2005, The significance of Phanerozoic magmatism in generating continental crust, *in* Michael Brown and Tracy Rushmer, ed., Evolution and Differentiation of the Continental Crust: New York, Cambridge University Press, p. 135-172.

Davidson, J., Handley, H., Macpherson, C., Turner, S., and Dosseto, A., 2007, Amphibole "sponge" in arc crust? Geology, v. 35, p. 787-790, doi: 10.1130/G23637A.1.

DeMets, C., Gordon, R.G., Argus, D.F., and Stein, S., 1994, Effect of recent revisions to the geomagnetic reversal time scale on estimates of current plate motions: Geophysical Research Letters, v. 21, p. 2191-2194, doi: 10.1029/94GL02118.

Depaolo, D.J., 1981, Trace element and isotopic effects of combined wallrock assimilation and fractional crystallization: Earth and Planetary Science Letters, v. 53, p. 189-202, doi: 10.1016/0012-821X(81)90153-9.

Dhuime, B., Wuestefeld, A., and Hawkesworth, C.J., 2015, Emergence of modern continental crust about 3 billion years ago: Nature Geoscience, v. 8, p. 552-556, doi: 10.1038/ngeo2466.

Ducea, M.N., and Saleeby, J.B., 1996, Buoyancy sources for a large, unrooted mountain range, the Sierra Nevada, California: Evidence from xenolith thermobarometry: Journal of Geophysical Research B: Solid Earth, v. 101, p. 8229-8244, doi: 10.1029/95JB03452.

Efron, B., and Tibshirani, R., 1993, An Introduction to the Bootstrap: New York, New York: Chapman & Hall, 430 p.

Farmer, G.L., Glazner, Allen, and Manley, C., 2002, Did lithospheric delamination trigger late Cenozoic potassic volcanism in the southern Sierra Nevada, California? Geological Society of

America. Geological Society of America Bulletin, v. 114, p. 754-768, doi: 10.1130/0016-7606(2002)1142.0.CO; 2.

Farner, M.J., and Lee, C.A., 2017, Effects of crustal thickness on magmatic differentiation in subduction zone volcanism: A global study: Earth & Planetary Science Letters, v. 470, p. 96-108, doi: 10.1016/j.epsl.2017.04.025.

Fliedner, M.M., and Klemperer, S., 1999, Structure of an island-arc: Wide-angle seismic studies in the eastern Aleutian Islands, Alaska: Journal of Geophysical Research-Solid Earth, v. 104, p. 10667-10694.

Fliedner, M.M., and Klemperer, S.L., 2000, Crustal structure transition from oceanic arc to continental arc, eastern Aleutian Islands and Alaska Peninsula: Earth and Planetary Science Letters, v. 179, p. 567-579, doi: 10.1016/S0012-821X(00)00142-4.

Fournelle, J. H., Marsh, B.D., Myers, J.D., 1994, Age, character, and significance of Aleutian arc volcanism, *in* Plafker, G., and Berg, H.C., ed., The Geology of Alaska: Boulder, Colorado, Geological Society of America, p. 723-759.

Gazel, E., Hayes, J.L., Hoernle, K., Kelemen, P., Everson, E., Holbrook, W.S., Hauff, F., van den Bogaard, P., Vance, E.A., Chu, S., Calvert, A.J., Carr, M.J., and Yogodzinski, G.M., 2015, Continental crust generated in oceanic arcs: Nature Geoscience, v. 8, p. 321-328, doi: 10.1038/ngeo2392.

Gazel, E., Hoernle, K., Carr, M.J., Herzberg, C., Saginor, I., den Bogaard, P.v., Hauff, F., Feigenson, M., and Swisher, C., 2011, Plume–subduction interaction in southern Central America: Mantle upwelling and slab melting: Lithos, v. 121, p. 117-135, doi: 10.1016/j.lithos.2010.10.008.

George, R., Turner, S., Bacon, C.R., Nye, C., Stelling, P., and Dreher, S., 2004, Chemical versus temporal controls on the evolution of tholeiitic and calc-alkaline magmas at two volcanoes in the Alaska-Aleutian arc: Journal of Petrology, v. 45, p. 203-220.

George, R., Turner, S., Hawkesworth, C., Morris, J., Nye, C., Ryan, J., and Zheng, S., 2003, Melting processes and fluid and sediment transport rates along the Alaska-Aleutian arc from an integrated U-Th-Ra-Be isotope study: Journal of Geophysical Research-Solid Earth, v. 108.

Gill, J.B., 1981, Orogenic Andesites and Plate Tectonics: Berlin; New York: Springer-Verlag, 390 p.

Greene, A.R., DeBari, S.M., Kelemen, P.B., Blusztajn, J., and Clift, P.D., 2006, A detailed geochemical study of island arc crust: the Talkeetna arc section, south–central Alaska: Journal of Petrology, v. 47, p. 1051-1094, doi: 10.1093/petrology/egl002.

Hildreth, W., and Moorbath, S., 1988, Crustal contributions to arc magmatism in the Andes of Central Chile: Contributions to Mineralogy and Petrology, v. 98, p. 455-489, doi: 10.1007/BF00372365.

Holbrook, W.S., Lizarralde, W.S., McGeary, W.S., Bangs, W.S., and Diebold, W.S., 1999, Structure and composition of the Aleutian island arc and implications for continental crustal growth: Geology, v. 27, p. 31-34, doi: SACOTA>2.3.CO;2.

Hora, J.M., Singer, B.S., Wörner, G., Beard, B.L., Jicha, B.R., and Johnson, C.M., 2009, Shallow and deep crustal control on differentiation of calc-alkaline and tholeiitic magma: Earth and Planetary Science Letters, v. 285, p. 75-86, doi: 10.1016/j.epsl.2009.05.042.

Hu, F., Ducea, M., Liu, S., and Chapman, J., 2017, Quantifying crustal thickness in continental collisional belts: global perspective and a geologic application: Nature Scientific Reports, v. 7, p. 7058, doi: 10.1038/s41598-017-07849-7.

Jagoutz, O., 2014, Arc crustal differentiation mechanisms: Earth & Planetary Science Letters, v. 396, p. 267-278, doi: 10.1016/j.epsl.2014.03.060.

Jagoutz, O., and Behn, M.D., 2013, Foundering of lower island-arc crust as an explanation for the origin of the continental Moho: Nature, v. 504, p. 131-135, doi: 10.1038/nature12758.

Janiszewski, H.A., Abers, G.A., Shillington, D.J., and Calkins, J.A., 2013, Crustal structure along the Aleutian island arc: New insights from receiver functions constrained by active-source data: Geochemistry, Geophysics, Geosystems, v. 14, p. 2977-2992, doi: 10.1002/ggge.20211.

Jicha, B.R., Scholl, D.W., Singer, B.S., Yogodzinski, G.M., and Kay, S.M., 2006, Revised age of Aleutian Island Arc formation implies high rate of magma production: Geology, v. 34, p. 661-665, doi: 10.1130/022433.1.

Karato, S., 2009, Deformation of Earth Materials: An introduction to the rheology of solid Earth: Cambridge, UK, Cambridge University Press, 463 p.

Kay, R.W., 1978, Aleutian magnesian andesites: Melts from subducted Pacific ocean crust: Journal of Volcanology and Geothermal Research, v. 4, p. 117-132, doi: 10.1016/0377-0273(78)90032-X.

Kay, S.M., Coira, B., and Viramonte, J., 1994, Young mafic back arc volcanic rocks as indicators of continental lithospheric delamination beneath the Argentine Puna Plateau, Central Andes: Journal of Geophysical Research-Solid Earth, v. 99, p. 24323-24339, doi: 10.1029/94JB00896.

Kay, R.W., and Kay, M. S., 1993, Delamination and delamination magmatism: Tectonophysics, v. 219, p. 177-189, doi: 10.1016/0040-1951(93)90295-U.

Kay, S.M., and Kay, R.W., 1994, Aleutian magmas in space and time, *in* G. Plafker and Berg, H.C., eds., Geology of North America, The Geology of Alaska: Boulder, Colorado, Geological Society of America, p. 687-722.

Kay, S.M., and Kay, R.W., 1985, Role of crystal cumulates and the oceanic crust in the formation of the lower crust of the Aleutian arc: Geology, v. 13, p. 461-464, doi: ROCCAT>2.0.CO;2.

Kay, S.M., Kay, R.W., and Citron, G.P., 1982, Tectonic controls on tholeiitic and calc-alkaline magmatism in the Aleutian arc: Journal of Geophysical Research, v. 87, p. 4051-4072, doi: 10.1029/JB087iB05p04051.

Kay, S.M., and Coira, B.L., 2009, Shallowing and steepening subduction zones, continental lithospheric loss, magmatism, and crustal flow under the Central Andean Altiplano-Puna Plateau: Memoir - Geological Society of America, v. 204, p. 229-259.

Kelemen, P. B., G. M. Yogodzinski, D. W. Scholl, 2003, Along strike variation in the Aleutian Island Arc: Genesis of high Mg# andesite and implications for continental crust, *in* Inside the Subduction Factory: The American Geophysical Union, p. 223.

Kelemen, P.B., and Behn, M.D., 2016, Formation of lower continental crust by relamination of buoyant arc lavas and plutons: Nature Geoscience, v. 9, doi: 10.1038/ngeo2662.

Kimura, J., 2017, Modeling chemical geodynamics of subduction zones using the Arc Basalt Simulator version 5: Geosphere, v. 13, p. 992-1026.

Kley, J., and Monaldi, C.R., 1998, Tectonic shortening and crustal thickness in the Central Andes; how good is the correlation? Geology (Boulder), v. 26, p. 723-726, doi: TSACTI>2.3.CO; 2.

Kodaira, S., Sato, T., Takahashi, N., Ito, A., Tamura, Y., Tatsumi, Y., and Kaneda, Y., 2007, Seismological evidence for variable growth of crust along the Izu intraoceanic arc: Journal of Geophysical Research B: Solid Earth, v. 112, doi: 10.1029/2006JB004593.

Laske, G., Masters, G., Ma, Z. and Pasyanos, M., 2013, Update on CRUST1.0 - A 1-degree global model of Earth's crust: Geophysical Research, no. 15, Abstract EGU2013-2658, 2013.

Lee, C.A., Thurner, S., Paterson, S., and Cao, W., 2015, The rise and fall of continental arcs: Interplays between magmatism, uplift, weathering, and climate: Earth and Planetary Science Letters, v. 425, p. 105-119, doi: 10.1016/j.epsl.2015.05.045.

Lee, C., Anderson, D., and Cheng, X., 2005, Continental crust formation at arcs, the "garnet pyroxenite" delamination cycle, and the origin of fertile melting anomalies in the mantle: EOS, Transactions, American Geophysical Union, v. 86.

Leeman, W.P., 1983, The influence of crustal structure on compositions of subduction-related magmas: Journal of Volcanology and Geothermal Research, v. 18, p. 561-588, doi: 10.1016/0377-0273(83)90026-4.

Lehnert, K., Su, Y., Langmuir, C.H., Sarbas, B., and Nohl, U., 2000, A global geochemical database structure for rocks: Geochemistry, Geophysics, Geosystems, v.1, doi: 10.1029/1999GC000026.

Lizarralde, D., Holbrook, W., Mcgeary, S., Bangs, N., and Diebold, J., 2002, Crustal construction of a volcanic arc, wide-angle seismic results from the western Alaska Peninsula: Journal of Geophysical Research-Solid Earth, v. 107, doi: 10.1029/2001JB000230.

Mackenzie, L., Abers, G.A., Fischer, K.M., Syracuse, E.M., Protti, J.M., Gonzalez, V., and Strauch, W., 2008, Crustal structure along the southern Central American volcanic front: Geochemistry, Geophysics, Geosystems, v. 9, doi: 10.1029/2008GC001991.

Mangan, M., Miller, T., Waythomas, C., Trusdell, F., Calvert, A., and Layer, P., 2009, Diverse lavas from closely spaced volcanoes drawing from a common parent: Emmons Lake Volcanic Center, Eastern Aleutian Arc: Earth & Planetary Science Letters, v. 287, p. 363-373, doi: 10.1016/j.epsl.2009.08.018.

Manley, C., Glazner, A., and Farmer, G.L., 2000, Timing of volcanism in the Sierra Nevada of California: Evidence for Pliocene delamination of the batholithic root? Geology, v. 28, p. 811-814, doi: 10.1130/0091-7613(2000)282.0.CO; 2.

Mantle, G.W., and Collins, W.J., 2008, Quantifying crustal thickness variations in evolving orogens; correlation between arc basalt composition and Moho depth: Geology (Boulder), v. 36, p. 87-90, doi: 10.1130/G24095A.1.

McGlashan, N., Brown, L., and Kay, S., 2008, Crustal thickness in the central Andes from teleseismically recorded depth phase precursors: Geophysical Journal International, v. 175, p. 1013-1023, doi: 10.1111/j.1365-246X.2008.03897.x.

Miyashiro, A., 1974, Volcanic rock series in island arcs and active continental margins: American Journal of Science, v. 274, p. 321-355, doi: 10.2475/ajs.274.4.321.

Moyen, J., 2009, High Sr/Y and La/Yb ratios: The meaning of the "adakitic signature": Lithos, v. 112, p. 556-574, doi: 10.1016/j.lithos.2009.04.001.

Nowacki, A., Kendall, J., and Wookey, J., 2012, Mantle anisotropy beneath the Earth's mid-ocean ridges: Earth & Planetary Science Letters, v. 317-318, p. 56-68, doi: 10.1016/j.epsl.2011.11.044.

Plank, T., and Langmuir, C.H., 1998, The chemical composition of subducting sediment and its consequences for the crust and mantle: Chemical Geology, v. 145, p. 325-394, doi: 10.1016/S0009-2541(97)00150-2.

Profeta, L., Ducea, M.N., Chapman, J.B., Paterson, S.R., Gonzales, S.M.H., Kirsch, M., Petrescu, L., and Decelles, P.G., 2015, Quantifying crustal thickness over time in magmatic arcs: Scientific Reports, v. 5, p. 17786, doi: 10.1038/srep17786.

Reubi, O., and Blundy, J., 2009, A dearth of intermediate melts at subduction zone volcanoes and the petrogenesis of arc andesites: Nature, v. 461, p. 1269-1274, doi: 10.1038/nature08510.

Romick, J., Kay, S., and Kay, R., 1992, The influence of amphibole fractionation on the evolution of calc-alkaline andesite and dacite tephra from the central Aleutians, Alaska: Contributions to Mineralogy and Petrology, v. 112, p. 101-118, doi: 10.1007/BF00310958.

Rudnick, R.L., 1995, Making continental crust: Nature, v. 378, p. 571-579.

Rudnick, R.L., and Fountain, D.M., 1995, Nature and composition of the continental crust: A lower crustal perspective: Reviews of Geophysics, v. 33, p. 267-309.

Rudnick, R.L., and Gao, S., 2014, The composition of the continental crust, *in* Rudnick, R.L., ed., The Crust: Oxford, Elsevier-Pergamon, p. 1-51.

Ryan, W.B.F., Carbotte, S.M., Coplan, J.O., O' Hara, S., Melkonian, A., Arko, R., Weissel, R.A., Ferrini, V., Goodwillie, A., Nitsche, F., Bonczkowski, J., and Zemsky, R., 2009, Global multi-resolution topography synthesis: Geochemistry, Geophysics, Geosystems, v. 10, p. n/a, doi: 10.1029/2008GC002332.

Shillington, D.J., Van Avendonk, H.J.A., Behn, M.D., Kelemen, P.B., and Jagoutz, O., 2013, Constraints on the composition of the Aleutian arc lower crust from VP/VS: Geophysical Research Letters, v. 40, p. 2579-2584, doi: 10.1002/grl.50375.

Shillington, D.J., Van Avendonk, H.J.A., Holbrook, W.S., Kelemen, P.B., and Hornbach, M.J., 2004, Composition and structure of the central Aleutian island arc from arc-parallel wide-angle seismic data: Geochemistry, Geophysics, Geosystems, v.5, p. n/a, doi: 10.1029/2004GC000715.

Singer, B.S., Jicha, B.R., Leeman, W.P., Rogers, N.W., Thirlwall, M.F., Ryan, J., and Nicolaysen, K.E., 2007, Along-strike trace element and isotopic variation in Aleutian Island arc basalt: Subduction melts sediments and dehydrates serpentine: Journal of Geophysical Research B: Solid Earth, v. 112, p. , doi: 10.1029/2006JB004897.

Spera, F. J., Bohrson, W. A., 2001, Energy-constrained open-system magmatic processes I: General model and energy-constrained assimilation and fractional crystallization (EC-AFC) formulation: Journal of Petrology, v. 42, p. 999-1019.

Syracuse, E.M., and Abers, G.A., 2006, Global compilation of variations in slab depth beneath arc volcanoes and implications: Geochemistry, Geophysics, Geosystems, v. 7, doi: 10.1029/2005GC001045.

Taylor, S.R., 1989, Growth of planetary crusts: Tectonophysics, v. 161, p. 147-156, doi: 10.1016/0040-1951(89)90151-0.

Taylor, S.R., and White, A.J.R., 1965, Geochemistry of Andesites and the Growth of Continents: Nature, v. 208, p. 271, doi: 10.1038/208271a0.

Tukey, J.W., 1977, Exploratory Data Analysis: Reading, Mass., Reading, Mass.: Addison-Wesley Pub. Co, 499 p.

Turner, S.J., and Langmuir, C.H., 2015a, The global chemical systematics of arc front stratovolcanoes: Evaluating the role of crustal processes: Earth and Planetary Science Letters, v. 422, p. 182-193, doi: 10.1016/j.epsl.2015.03.056.

Turner, S.J., and Langmuir, C.H., 2015b, What processes control the chemical compositions of arc front stratovolcanoes? Geochemistry, Geophysics, Geosystems, v. 16, p. 1865-1893, doi: 10.1002/2014GC005633.

Turner, S.J., Langmuir, C.H., Katz, R.F., Dungan, M.A., and Escrig, S., 2016, Parental arc magma compositions dominantly controlled by mantle-wedge thermal structure: Nature Geoscience, v. 9, p. 772-776, doi: 10.1038/NGEO2788.

Van Avendonk, H.J.A., Shillington, D.J., Holbrook, W.S., and Hornbach, M.J., 2004, Inferring crustal structure in the Aleutian island arc from a sparse wide-angle seismic data set: Geochemistry, Geophysics, Geosystems, v. 5, doi: 10.1029/2003GC000664.

White, W.M., 2013, Geochemistry: Hoboken, N.J., Hoboken, N.J.: John Wiley & Sons Inc, 478 p.

Yang, X., Fischer, K., and Abers, G., 1995, Seismic anisotropy beneath the Shumagin Islands segment of the Aleutian-Alaska subduction zone: Journal of Geophysical Research-Solid Earth, v. 100, p. 18165-18177, doi: 10.1029/95JB01425.

Yuan, X., Sobolev, S.V., and Kind, R., 2002, Moho topography in the central Andes and its geodynamic implications: Earth & Planetary Science Letters, v. 199, p. 389-403.

Yogodzinski, G.M., Brown, S.T., Kelemen, P.B., Vervoort, J.D., Portnyagin, M., Sims, K.W.W., Hoernle, K., Jicha, B.R., Werner, R., 2015, The Role of Subducted Basalt in the Source of Island Arc Magmas: Evidence from Seafloor Lavas of the Western Aleutians: Journal of Petrology, v. 56, p. 441-493, doi: 10.1093/petrology/egv006.

Yogodzinski, G.M., Lees, J.M., Churikova, T.G., Dorendorf, F., Woerner, G., and Volynets, O.N., 2001, Geochemical evidence for the melting of subducting oceanic lithosphere at plate edges: Nature, v. 409, p. 500-505.

Zimmer, M.M., Plank, T., Hauri, E.H., Yogodzinski, G.M., Stelling, P., Larsen, J., Singer, B., Jicha, B., Mandeville, C., and Nye, C.J., 2010, The role of water in generating the calc-alkaline trend: new volatile data for Aleutian magmas and a new tholeiitic index: Journal of Petrology, v. 51, p. 2411-2444, doi: 10.1093/petrology/egq062.

APPENDIX - FIGURES AND CAPTIONS

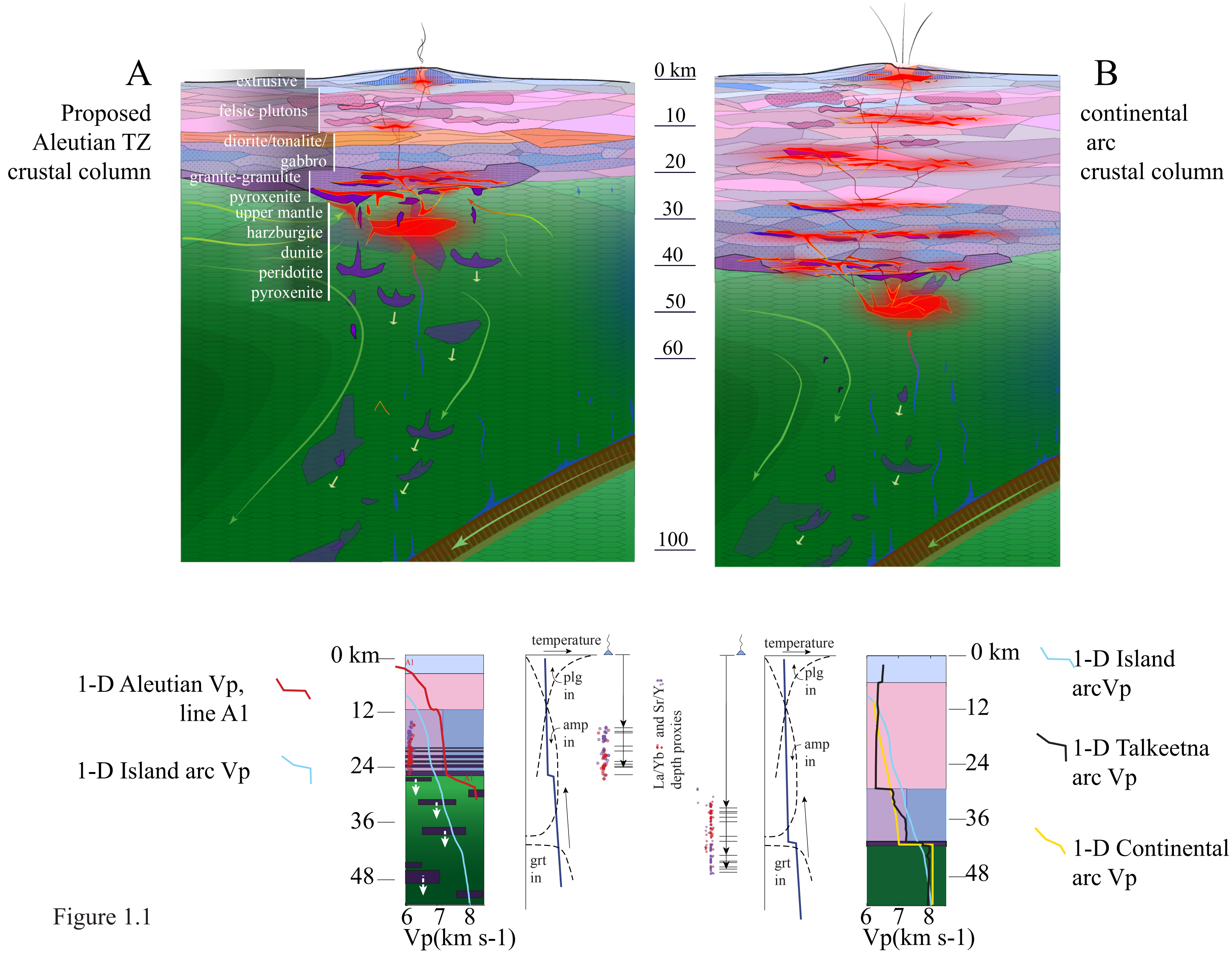
A
Proposed
Aleutian TZ
crustal column
extrusive
felsic plutons
diorite/tonalite/
gabbro
granite-granulite
pyroxenite
upper mantle
harzburgite
dunite
peridotite
pyroxenite
0 km
10
20
30
40
50
60
100
B
continental
arc
crustal column
1-D Aleutian Vp,
line A1
1-D Island arc Vp
0 km
12
24
36
48
6 7 8
Vp(km s-1)
temperature
plg
in
amp
in
grt
in
La/Yb and Sr/Y
depth proxies
temperature
plg
in
amp
in
grt
in
0 km
12
24
36
48
6 7 8
Vp(km s-1)
1-D Island
arcVp
1-D Talkeetna
arc Vp
1-D Continental
arc Vp

Figure 1.1

Figure 1.1. Drawings contrasting arc magmatism and trace element-derived crustal thickness for thin (oceanic) and thick (continental) end members. Figures show convergent margin with schematic (A) thin (~20 km) and (B) thick (~40 km) crustal columns (left and right sides of figures). Lower middle of the figures shows Sr/Y and La/Yb proxy depths (the subject of this study) from representative volcano lava samples from the Aleutian transition arc segment (defined in the text and Figure 10) for thin crust (A) and Alaska continental arc segment for thick crust (B). Crustal columns with Vp curves (see Discussion) are generated from schematic crustal columns of Jagoutz and Behn (2013) and Behn and Kelemen (2006) for the thick-crust member (B) while a proposed crustal column for the thin-crust member is shown in (A) with Vp profile of line A1 of the ASE (taken from Calvert, 2011). For both members, a schematic phase diagram for plagioclase, amphibole and garnet stability field is shown with the respective thin and thick crust geotherm (blue curve). Tectonic sketches show arc crust over the serpentinized subarc mantle with the subducting and dehydrating oceanic crust and lithosphere at lower right. Fluxed melting of the mantle is shown with ascending melts ponding at the Moho and injected into various levels of the lower and mid crust (Annen et al., 2006). Various crustal-melt interactions (crustal hot zone, MASH, AFC, etc.), crystallization of plutons, magma chamber, and eruptions are shown, these processes presumably imbue the magmas with the trace element ratios Sr/Y and La/Yb marking depths base on the mineral stability field in the phase diagram. Mantle flow lines are shown as curves with arrowheads. Negatively buoyant cumulate masses are shown separating from the lower crust and sinking into the convecting mantle. The amount of detached mass (purple) shown for (A) the thin crust arc is approximately equal to the estimate by Behn et al., (2007), the thick crust arc (B) is shown at a more quiescence delamination state. Refer to the Discussion section (and Figure 15) for crustal construction/evolution model based on the results of this study.

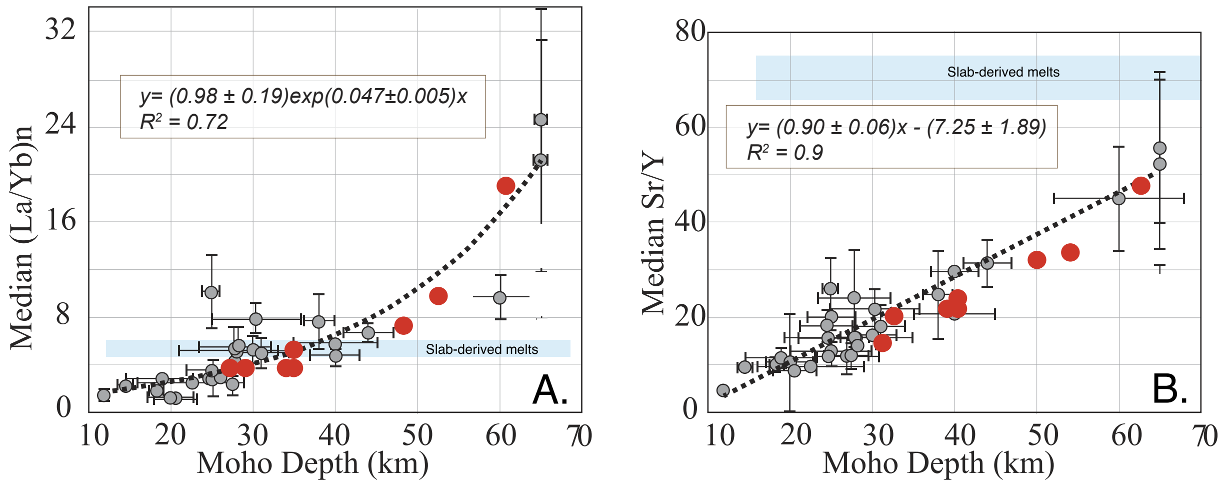

Figure 1.2

Modified from Figure 1 of Profeta et al. (2015)

Figure 1.2. Modified Figure 1 of Profeta et al. (2015): Correlation between the trace element proxies and crustal thickness (Moho depth) used in this study. Goodness-of-fit is given as 0.72 and 0.9 for La/Yb and Sr/Y, respectively. Red dots are Sr/Y and La/Yb vs. crustal thickness values of individual volcanoes of the Andes SVZ superimposed on the correlation graphs, implying that the correlations are valid for within an arc. See Figure 4 for identities of arcs used in the Sr/Y correlation.

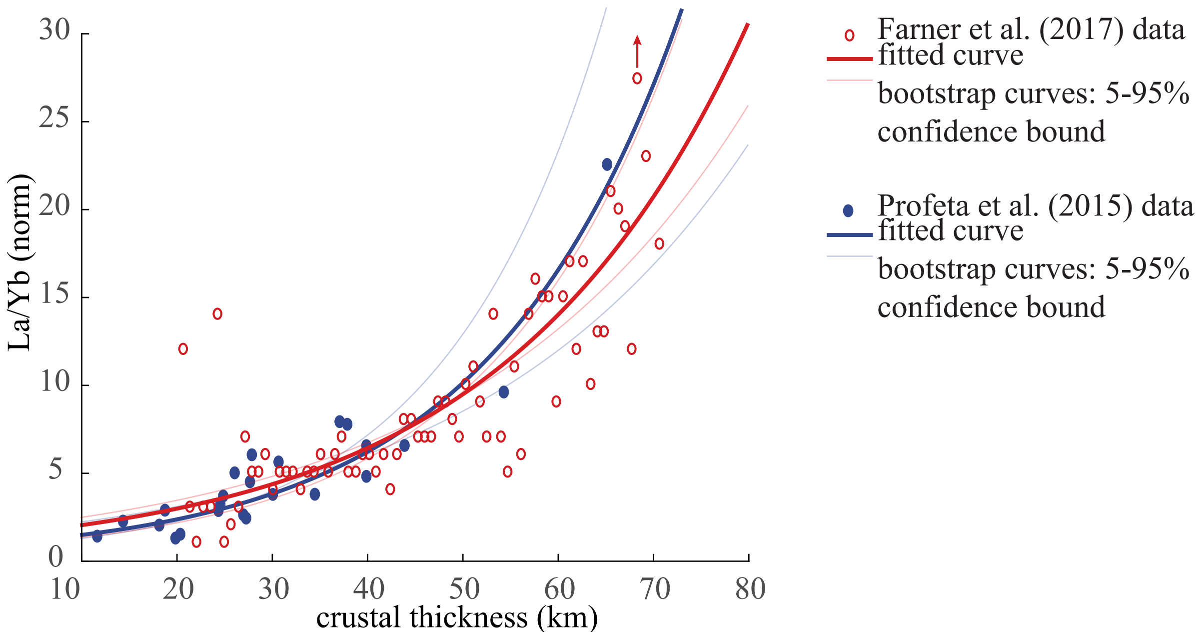

Figure 1.3

Figure 1.3. Comparison of Profeta et al. (2015) vs. Farner and Lee (2017) correlation curves for La/Yb in arc lavas vs. crustal thickness. Exponential regression lines for the two studies are within each other's 95% confidence level. Data are from the respective papers' supplemental materials.

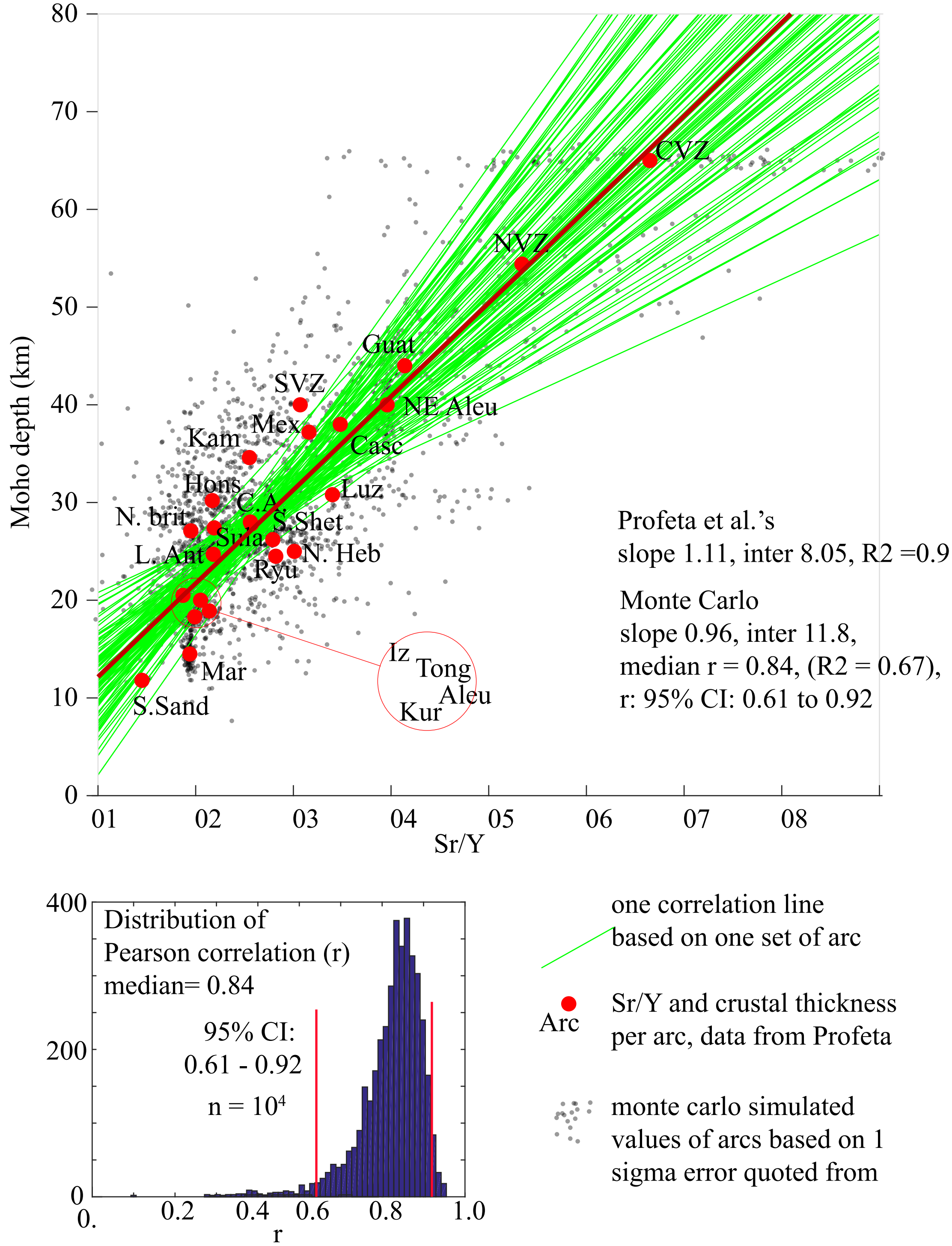

Moho depth (km)
Sr/Y
S.Sand
Mar
L. Ant
N. brit
Hons
Kam
Mex
SVZ
C.A
Suia
S.Shet
Ryu
N. Heb
Luz
Casc
NE Aleu
Guat
NVZ
CVZ
Iz
Tong
Aleu
Kur
Profeta et al.'s
slope 1.11, inter 8.05, R2 =0.9
Monte Carlo
slope 0.96, inter 11.8,
median r = 0.84, (R2 = 0.67),
r: 95% CI: 0.61 to 0.92
Distribution of
Pearson correlation (r)
median= 0.84
95% CI:
0.61 - 0.92
n = 10⁴
r
one correlation line
based on one set of arc
Arc
Sr/Y and crustal thickness
per arc, data from Profeta
monte carlo simulated
values of arcs based on 1
sigma error quoted from

Figure 1.4

Figure 1.4. Profeta et al. (2015) Monte Carlo simulation. 10,000 simulated arc Sr/Y and crustal thickness values regression lines (green) based on Profeta et al. (2015) data and Gaussian distribution of error. For clutter reduction, we show only a few dozens simulations. The median regression line has the equation:

Crust thickness (km) = 0.964(Sr/Y) + 11.8, (1)

as compared to Profeta et al. (2015):

Crust thickness (km) = 1.11(Sr/Y) + 8.05. (2)

The median of 10,000 simulated correlations has $r = 0.84$ with 5% to 95% of r's between 0.61 and 0.92, the distribution of which is shown at lower right. See text for details. Arc abbreviations: Aleu: Aleutian, CA: Central America, Cas: Cascades, CVZ: Central volcanic zone, South America, Guat: Guatemala, Hons: Honshu, Iz: Izu-Bonin, Kam: Kamchatka, Kur: Kurile, L. Ant: L.Antilles, Luz: Luzon, Mar: Mariana, Mex: Mexican, NE Aleu: NE Aleutian, N. Brit: New Britain, N. Heb: New Hebrides, NVZ: Northern volcanic zone, South America, Ryu: Ryukyu, S.Sand: South Sandwich, S. Shet: S. Shetland, Sula: Sulawesi, Sun: Sunda, SVZ: Southern volcanic zone, South America, Tong: Tonga.

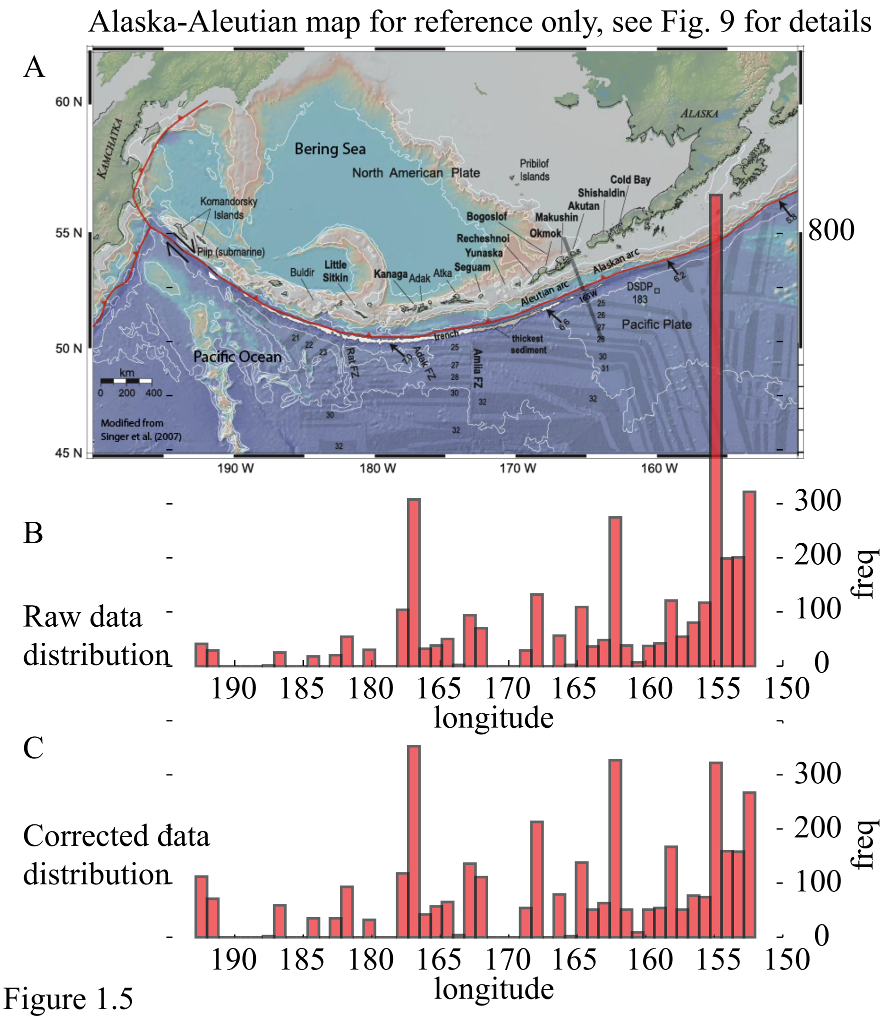

Figure 1.5

Figure 1.5. Sampling bias mitigation for the Alaska-Aleutian arc system (A). (B) Histogram of the number of samples downloaded from EarthChem.org showing the uneven sampling of lava as a function of location along the Alaska-Aleutian arc. Volcanoes of the Alaska Peninsula are overrepresented while the Aleutian island volcanoes are underrepresented. (C) Weight function based on the density of a sample's neighbor is applied to each sample during the bootstrap resampling procedure. The resampled selection histogram is shown to be more representative along the arc.

Weight function: $Wti = \mathrm{sumj}\,(|Xi - Xj|)^{0.4}$, (3)

where Wti = weight of i-th sample, Xi = location of i-th sample, Wti is obtained from the sum of the 0.4 power of the difference between the i-th sample location and all other (j) sample locations.

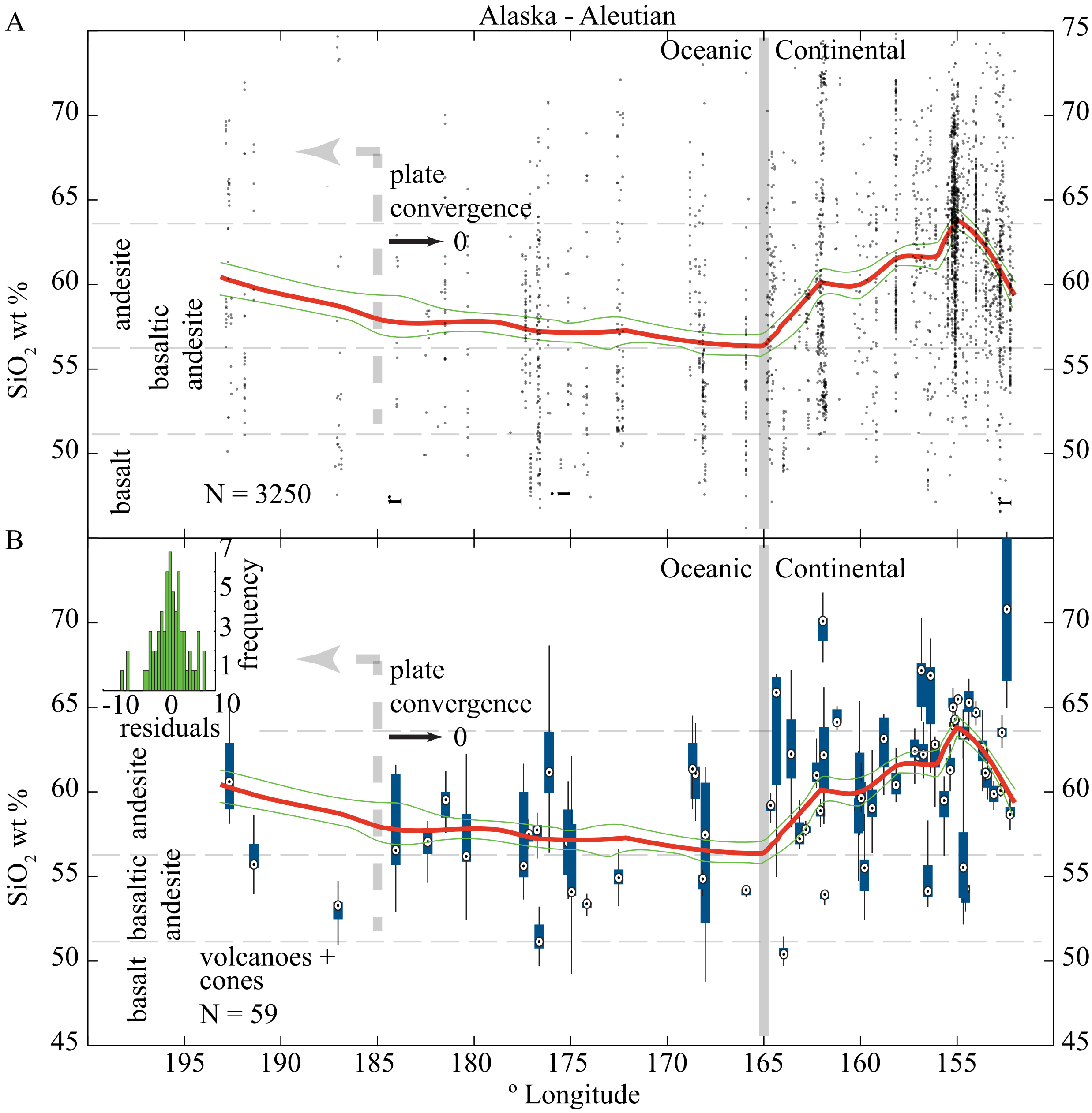

Figure 1.6

Figure 1.6. Weighted lowess smoothed regression for SiO_2 along the Alaska-Aleutian arc. (A) The weighted lowess smoothed regressed estimate curve of median SiO2 (red) for the arc with 5-95% confident curves (green). (B) The median curve is shown with boxplots of samples per volcano. Box-and-whisker symbols represent sample values of a volcano: Each box encompasses silica value for 50% of the samples for a volcano. The whiskers extend to the 5 and 95 percentile of samples and the circle-with-dot marking the median value. Inset: histogram of the difference between the medians of the volcanoes and the lowess median curves at that longitude.

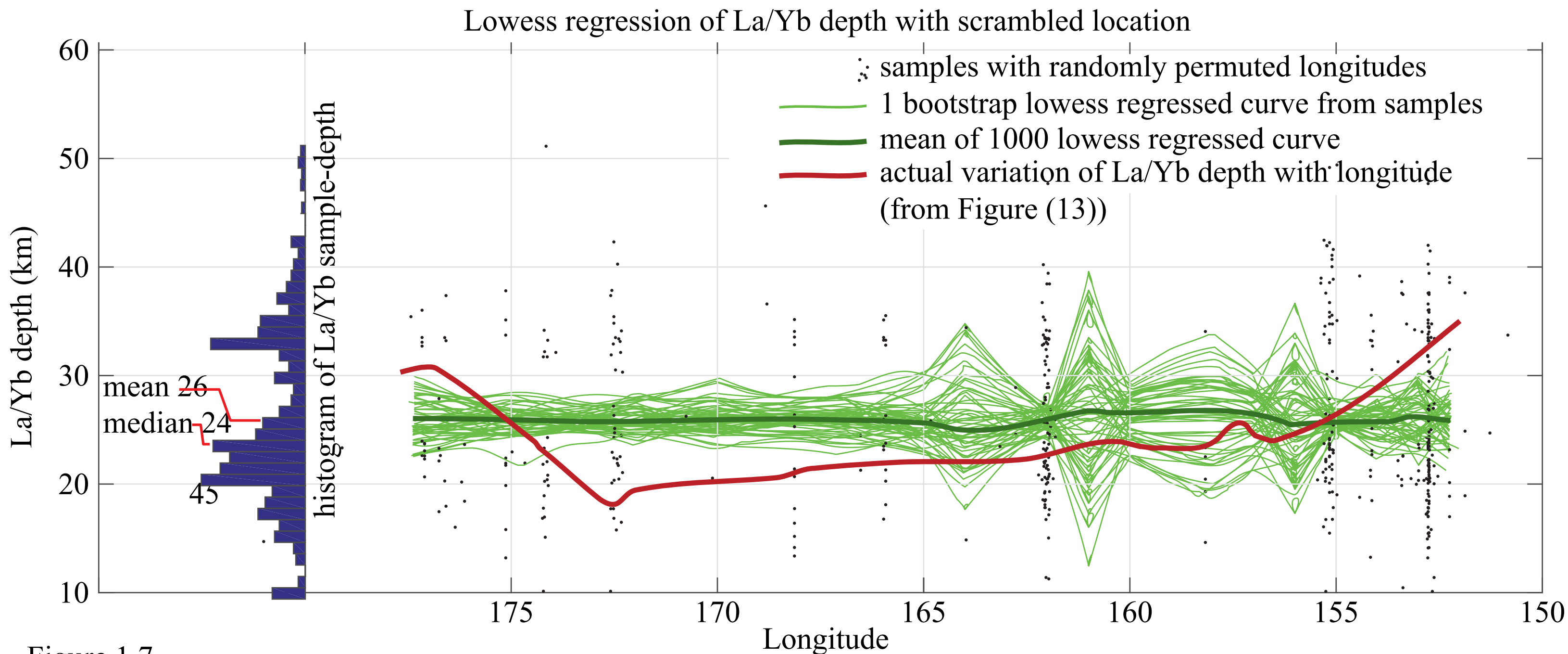

Figure 1.7

Figure 1.7. Null hypothesis test for lowess regression. One set of randomly permuted location value for La/Yb samples is plotted as black dots. Green lines are 100 bootstrapped lowess regressed curves of 100 sets, the mean value of which is the thick dark green curve wavering at the La/Yb proxy depth of ~26 km, which is the mean value of the population, as shown at left. Actual data-produced curve of La/Yb depth along arc variation is shown as the thick red curve. Histogram shows the overall La/Yb proxy depth distribution of the samples. Refer to text for discussion.

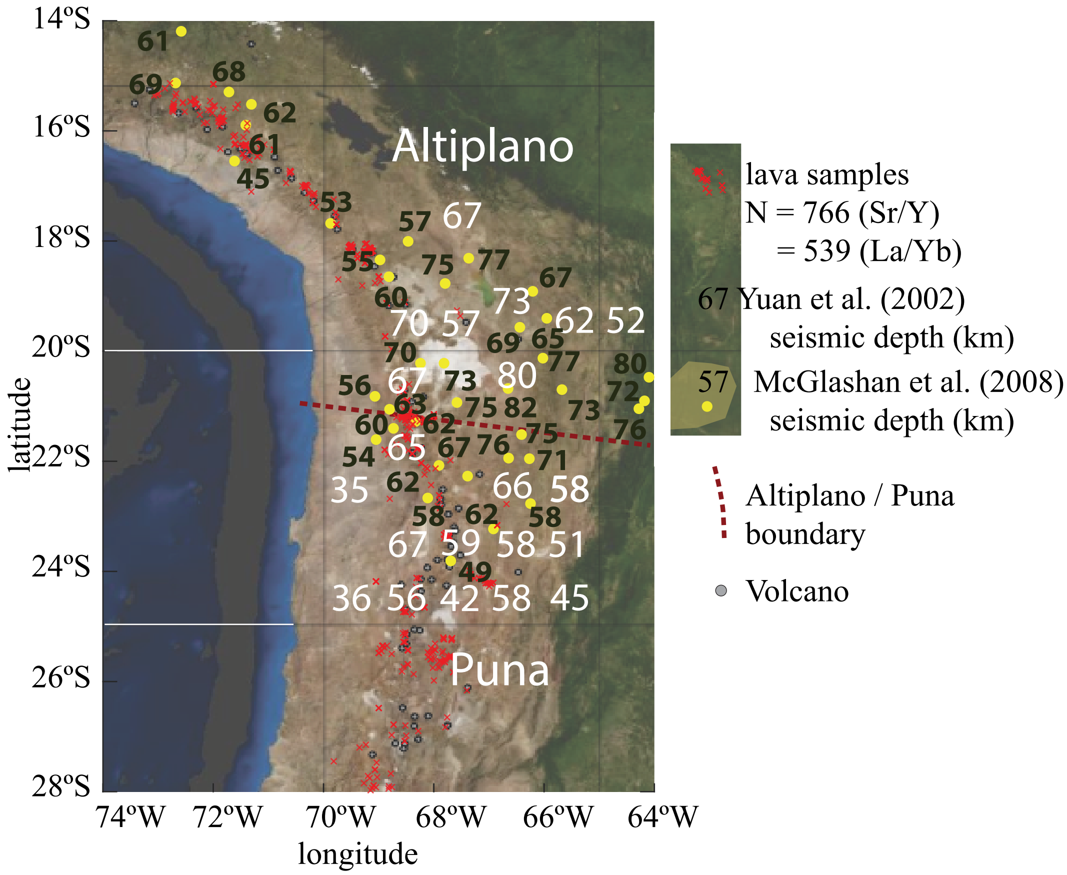

Figure modified from McGlashan et al. (2008)

Figure 1.8

Figure 1.8. Andes Central Volcanic Zone arc lava samples (red 'x's) are shown overlain on McGlashan et al. (2008)'s Moho depth model (black numbers indicate Moho depth in km at yellow dots) with Yuan et al. (2002)'s square-degree depth model (white numbers indicate Moho depth in km, averaged over 1º square at number locations). Approximate Puna-Altiplano boundary is shown by dashed line.

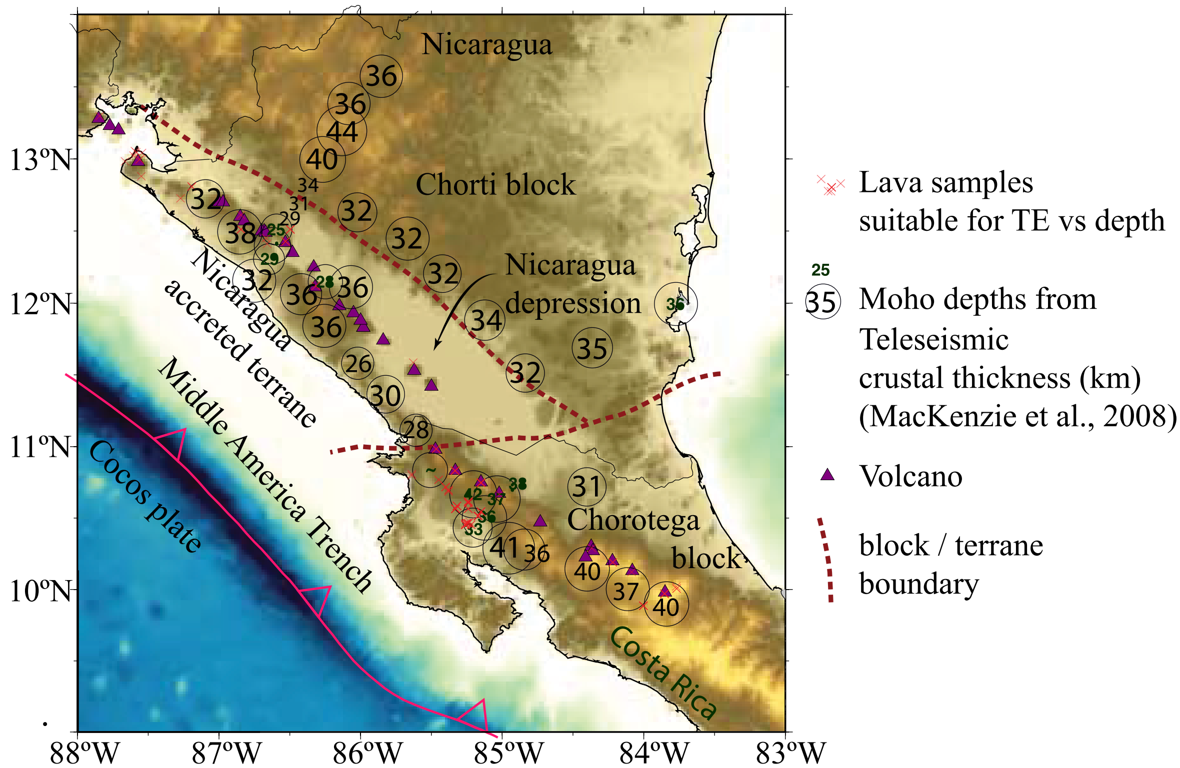

Modified from MacKenzie et al., 2008)

Figure 1.9

Figure 1.9. Central American Volcanic Arc sample locations are shown overlain on MacKenzie et al. (2008)'s seismic Moho depth model. Note that some volcanoes are not represented because of exclusion due to the filtering process (see Methods). Dashed lines show tectonic boundaries.

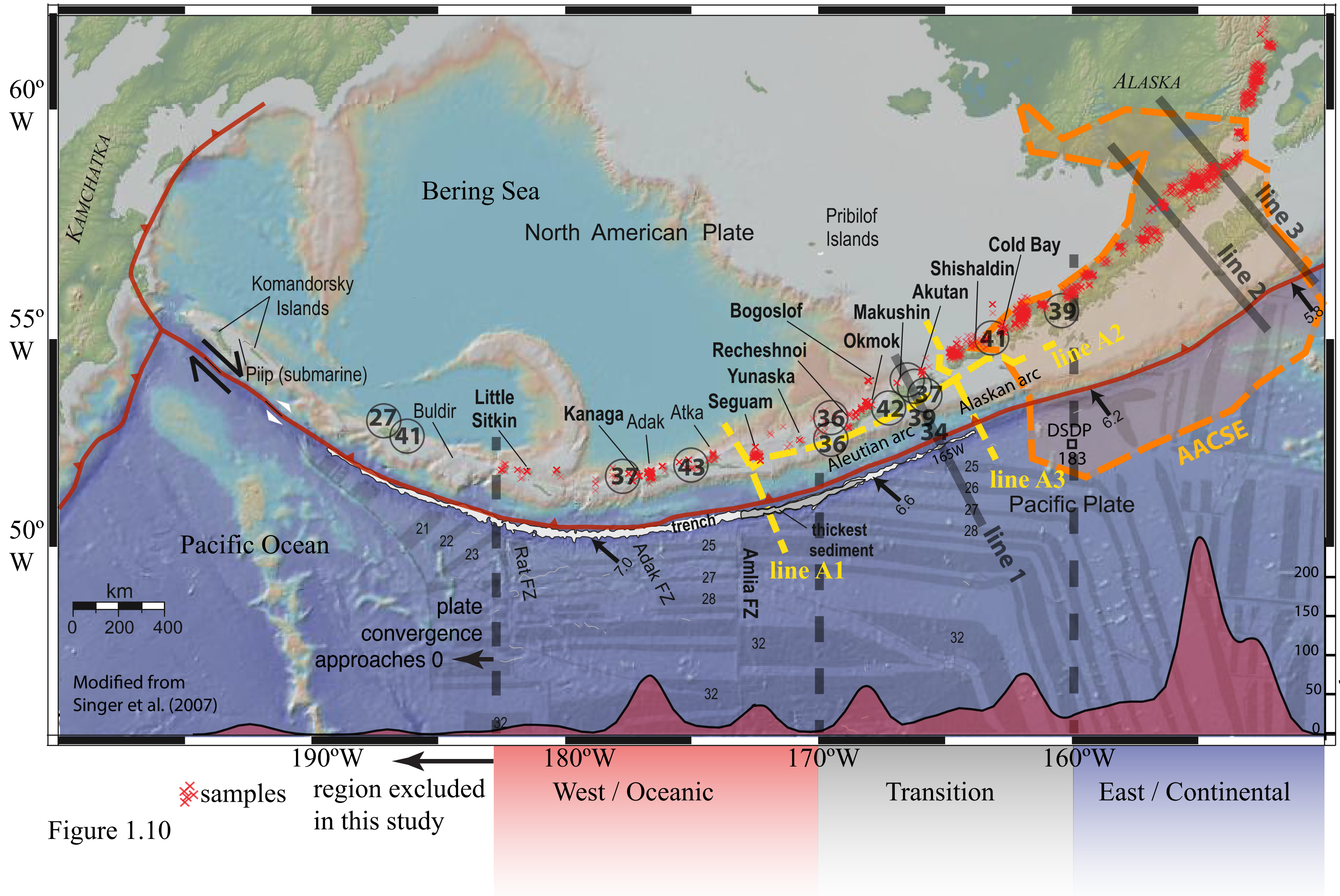
60º W
55º W
50º W
KAMCHATKA
ALASKA
Bering Sea
North American Plate
Pribilof Islands
Komandorsky Islands
Piip (submarine)
Buldir
Little Sitkin
Kanaga
Adak
Atka
Seguam
Yunaska
Recheshnoi
Bogoslof
Okmok
Makushin
Akutan
Shishaldin
Cold Bay
Aleutian arc
Alaskan arc
line A1
line A2
line A3
line 1
line 2
line 3
AACSE
DSDP 183
Pacific Plate
Pacific Ocean
trench
thickest sediment
Rat FZ
Adak FZ
Amlia FZ
165W
km
0 200 400
plate convergence approaches 0
Modified from Singer et al. (2007)
~frequency
190ºW
180ºW
170ºW
160ºW
samples
region excluded in this study
West / Oceanic
Transition
East / Continental

Figure 1.10

Figure 1.10. Alaska-Aleutian arc volcanic sample locations plotted as "x"s. The gray line near 165ºE marks the approximate boundary between oceanic (Aleutian) and continental (Alaska Peninsula) portions of the arc system. Approximately ±5º of 165°E is designated as the "transition" segment (shown at bottom). Major volcano /island names are written on top. Circles with number refer to depth to Moho (km) from Janiszewski et al. (2013). Line A1, A2, A3 are tracks of the Alaska Seismic Experiment (ASE, 1994). Orange dashed line outlines the Alaska Amphibious Community Seismic Experiment planned for 2018-2019. Gray lines labeled "line 1, 2, and 3" reference locations of cross sections depicted elsewhere (Figure 1, Figure 13, Figure 16). Sample distribution curve is shown along the bottom of the map in kernel density function form. The map is modified from Singer et al. (2007), it includes relative plate velocity from DeMets et al. (1994) and marine magnetic anomalies from Atwater (1989). Colored base map was generated with GeoMapApp (www.geomapapp.com, Ryan et al., 2009).

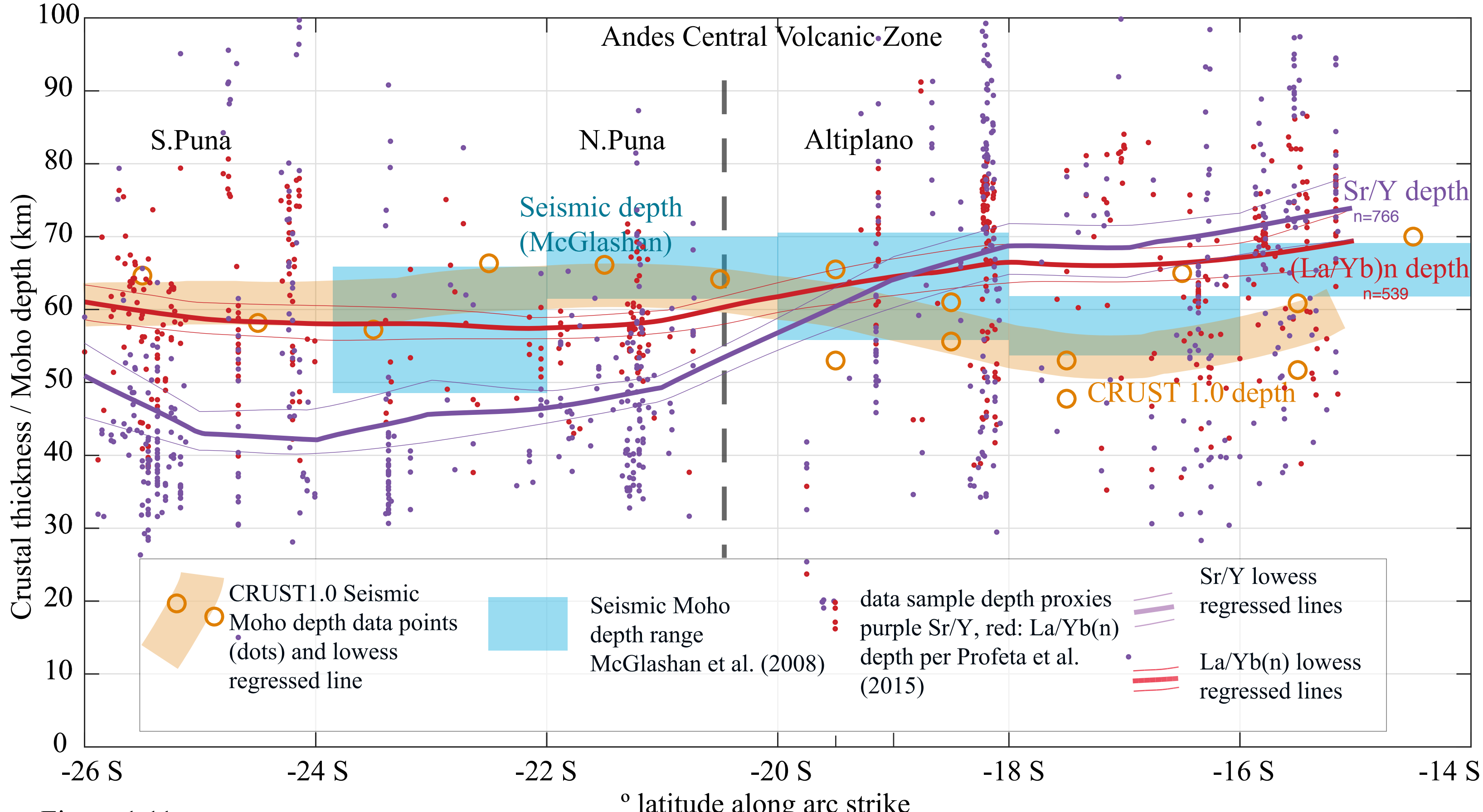

Andes Central Volcanic Zone
S.Puna
N.Puna
Altiplano
Seismic depth
(McGlashan)
Sr/Y depth
n=766
(La/Yb)n depth
n=539
CRUST 1.0 depth
CRUST1.0 Seismic
Moho depth data points
(dots) and lowess
regressed line
Seismic Moho
depth range
McGlashan et al. (2008)
data sample depth proxies
purple Sr/Y, red: La/Yb(n)
depth per Profeta et al.
(2015)
Sr/Y lowess
regressed lines
La/Yb(n) lowess
regressed lines
Crustal thickness / Moho depth (km)
100
90
80
70
60
50
40
30
20
10
0
-26 S
-24 S
-22 S
-20 S
-18 S
-16 S
-14 S
º latitude along arc strike

Figure 1.11

Figure 1.11. Application of the bootstrap weighted lowess regression to the central volcanic zone (CVZ) of the Andes. The Sr/Y and (La/Yb)n depth proxy curves are derived from the samples' predicted crustal thickness depth per Profeta et al. (2015). TE samples' converted depths shown as dots, colored to correspond to Sr/Y or La/Yb curves. Blue field denotes the range of Moho depths from the central Andes teleseismic survey of McGlashan et al. (2008), adapted for depth near the volcanic arc front. The teleseismic curve is consistent with the CRUST1.0 (Laske et al., 2013) curve, shown in orange dots with lowess regressed curve in orange; both show thinning at latitude 16° to 18°S. The depth proxies Sr/Y and (La/Yb)n generally agree with the geophysics-derived Moho depths and plausibly depict the increase in crustal thickness (of ~10 km thickness) from the southern volcanic zone (Puna region, thinner crust) to the central volcanic zone (Altiplano, thicker crust). Note the bifurcation of the two proxy curves in the Puna region, with La/Yb closer aligned with the geophysics curves while Sr/Y depicts a 10-15 km thinner crust.

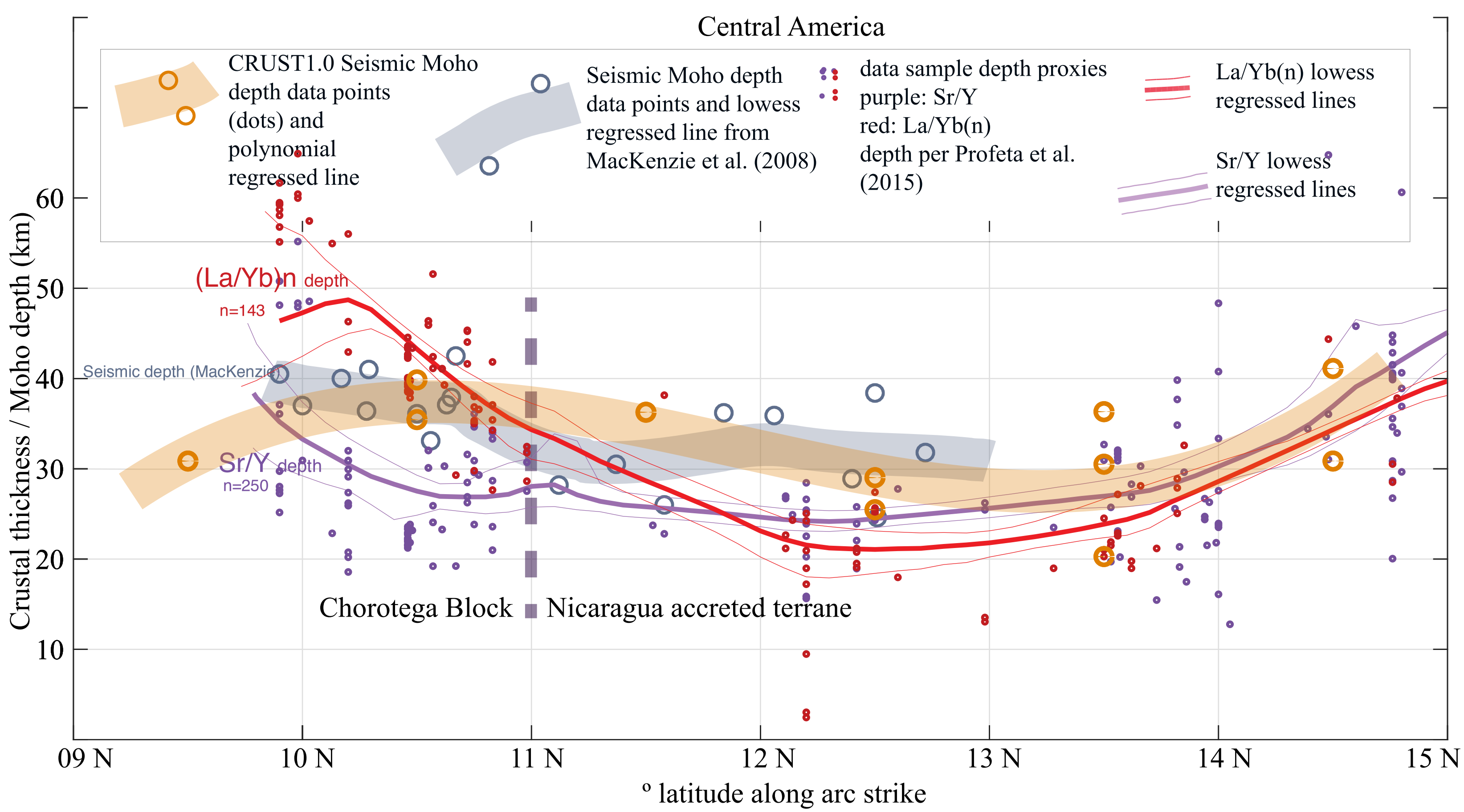
Central America
CRUST1.0 Seismic Moho depth data points (dots) and polynomial regressed line
Seismic Moho depth data points and lowess regressed line from MacKenzie et al. (2008)
data sample depth proxies
purple: Sr/Y
red: La/Yb(n)
depth per Profeta et al. (2015)
La/Yb(n) lowess regressed lines
Sr/Y lowess regressed lines
(La/Yb)n depth
n=143
Seismic depth (MacKenzie)
Sr/Y depth
n=250
Chorotega Block
Nicaragua accreted terrane
Crustal thickness / Moho depth (km)
60
50
40
30
20
10
09 N
10 N
11 N
12 N
13 N
14 N
15 N
º latitude along arc strike

Figure 1.12

Figure 1.12. Central American arc Moho depth along strike as approximated by trace element ratio proxies Sr/Y and (La/Yb)n. TE depth proxy curves and samples shown here are as described in Figure 11. The thick grey line is the lowess regression curve for crustal thicknesses beneath seismic stations (heavy gray dots) of the TUCAN array of MacKenzie et al. (2008). CRUST1.0 (Laske et al., 2013) estimates are green dots with lowess regressed curve superimposed. The dashed line corresponds to the boundary between the Nicaragua depression/accreted terrane and the Costa Rica Chorotega Block, which also corresponds with ~50 km right-lateral step of the volcanic front. A dashed vertical line separates the Chorotega Block and Nicaragua terrane.

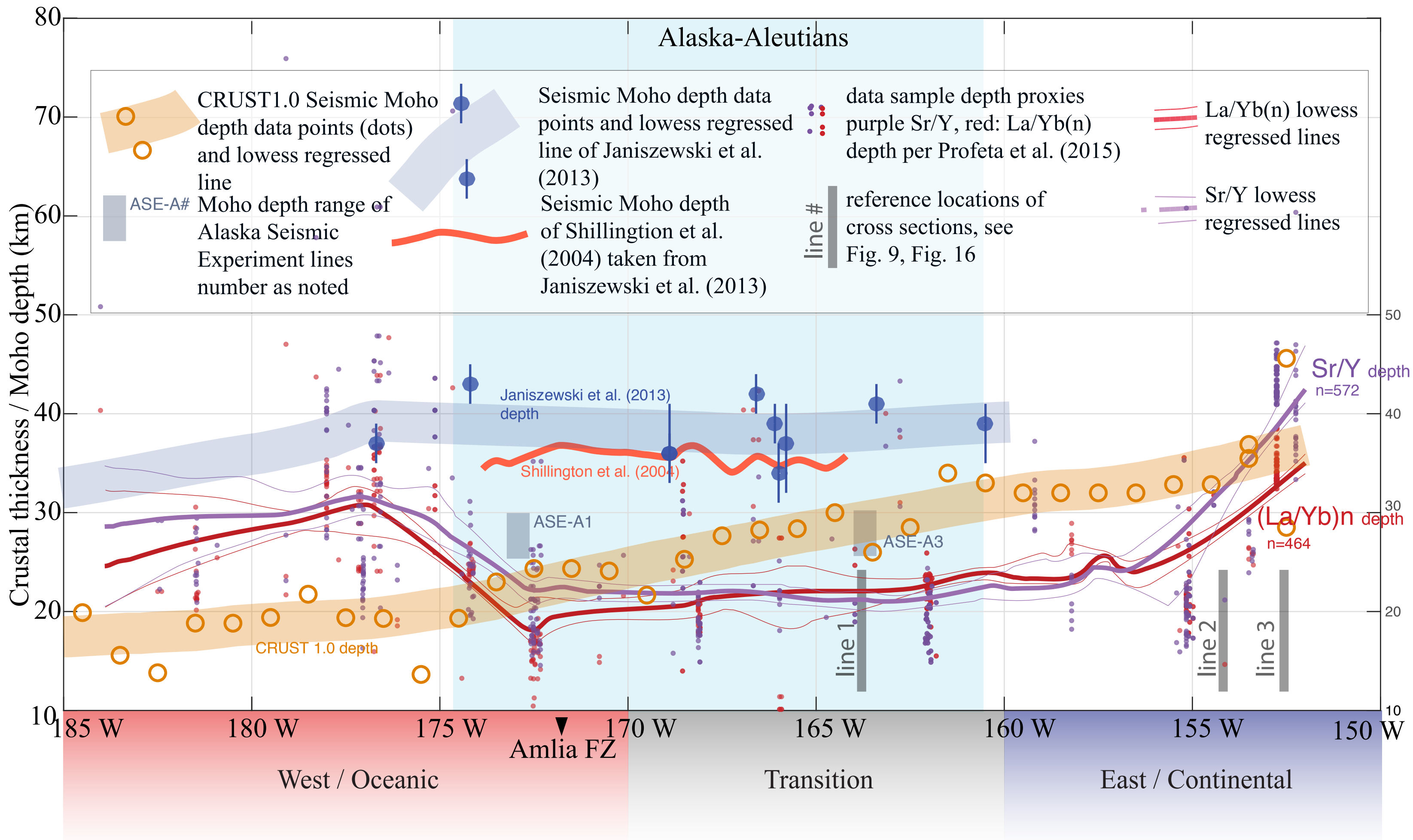

Alaska-Aleutians
CRUST1.0 Seismic Moho depth data points (dots) and lowess regressed line
ASE-A# Moho depth range of Alaska Seismic Experiment lines number as noted
Seismic Moho depth data points and lowess regressed line of Janiszewski et al. (2013)
Seismic Moho depth of Shillingtion et al. (2004) taken from Janiszewski et al. (2013)
data sample depth proxies purple Sr/Y, red: La/Yb(n) depth per Profeta et al. (2015)
line #
reference locations of cross sections, see Fig. 9, Fig. 16
La/Yb(n) lowess regressed lines
Sr/Y lowess regressed lines
Crustal thickness / Moho depth (km)
Janiszewski et al. (2013) depth
Shillington et al. (2004)
ASE-A1
ASE-A3
CRUST 1.0 depth
Sr/Y depth
n=572
(La/Yb)n depth
n=464
line 1
line 2
line 3
185 W
180 W
175 W
170 W
165 W
160 W
155 W
150 W
Amlia FZ
West / Oceanic
Transition
East / Continental

Figure 1.13

Figure 1.13. Alaska Aleutian arc Moho depth along strike as approximated by trace element ratio proxies Sr/Y and (La/Yb)n. TE depth proxy curves and samples shown are as described in Figure 11. The two blue-gray lines (ASE-A1 and ASE-A2) encompass modeled seismic reflection Moho depths of Fliedner and Klemperer (2000), Holbrook et al. (1999), from the 1994 Alaska Seismic Experiment (ASE). CRUST1.0 (Laske et al., 2013)) data points are lowess regressed into the curve shown. Shillington et al. (2004)'s along strike Moho depth curve is shown in dark orange. The Janiszewski et al. (2013) receiver function Moho depth data are shown regressed with Monte Carlo simulated error based on the given depth range (shown as vertical bars at the data point). The blue-shaded region is Aleutian transitional arc segment (see text) with tholeiitic affinity, as defined by the CATH and THI indices (see Figure 14). The vertical dashed line corresponds to the boundary between continental (Alaska Peninsula) and oceanic (Aleutian) arc segments. This approximates the transition between oceanic and continental arc, where geochemistry predicts thinner crust than the western and eastern region of the arc. This is in contrast to the Sr/Y variation of basalt (see Singer et al., 2007) that shows no variation along strike. The discrepancy between geochemical proxy depths and geophysics depths is discussed in the text.

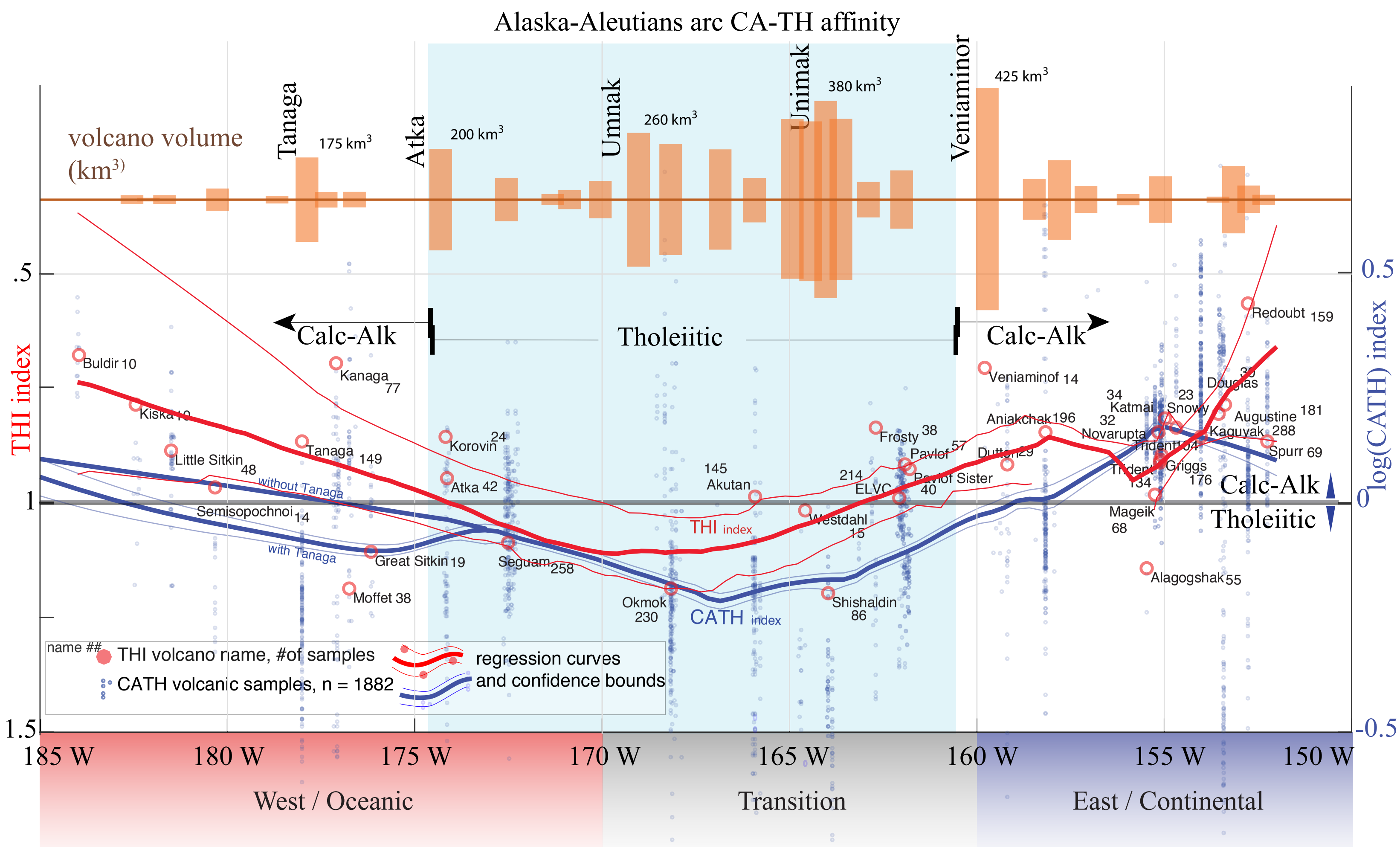
Alaska-Aleutians arc CA-TH affinity
volcano volume
(km3)
Tanaga
Atka
Umnak
Unimak
Veniaminor
175 km3
200 km3
260 km3
380 km3
425 km3
Calc-Alk
Tholeiitic
Calc-Alk
THI index
log(CATH) index
.5
1
1.5
0.5
0
-0.5
Buldir 10
Kiska 10
Little Sitkin 48
Semisopochnoi 14
Kanaga 77
Tanaga 149
without Tanaga
with Tanaga
Great Sitkin 19
Moffet 38
Korovin 24
Atka 42
Seguam 258
Okmok 230
Akutan 145
THI index
CATH index
Westdahl 15
Shishaldin 86
ELVC 214
Frosty 38
Pavlof 57
Pavlof Sister 40
Dutton 29
Veniaminof 14
Aniakchak 196
Novarupta 32
Katmai 34
Snowy 23
Douglas 30
Trident 134
Griggs 176
Mageik 68
Alagogshak 55
Augustine 181
Kaguyak 288
Redoubt 159
Spurr 69
Calc-Alk
Tholeiitic
name ## THI volcano name, #of samples
CATH volcanic samples, n = 1882
regression curves
and confidence bounds
185 W
180 W
175 W
170 W
165 W
160 W
155 W
150 W
West / Oceanic
Transition
East / Continental

Figure 1.14

Figure 1.14. Alaska-Aleutian arc in calc-alkaline or tholeiitic affinity of the lava, as characterized by the CATH and THI indices of Hora et al. (2009) and Zimmer et al. (2010), respectively. Weighted lowess regression of THI (per volcano, red dots, weighted by the number of samples per volcano) and CATH (rock sample, blue points) are shown. The horizontal line at THI = 1 (left ordinate) and CATH = 0 (right ordinate) separates the tholeiitic/calc-alkaline affinity of the volcanoes and samples. Note the discrepancy between the two curves, especially at Tanaga, Akutan, and Aniakchak where the indices give opposite indications. This is caused by the complexity of including silica in the CATH index (see discussion in Zimmer et al., 2010). We take THI to be the more robust index and use it to define the tholeiitic region of the arc (THI < 1, shaded blue) that coincides with the region of thinner crust of Figure 13. Top portion shows a bar graph of volcano volumes, adapted from Fournelle et al. (1994).

CATH index = (wt%SiO_2 - 42.8) / (6.4 × FeO^*/MgO), (4)

THI = $FeO_{4.0}/FeO_{8.0}$, subscripts indicate MgO wt %. (5)

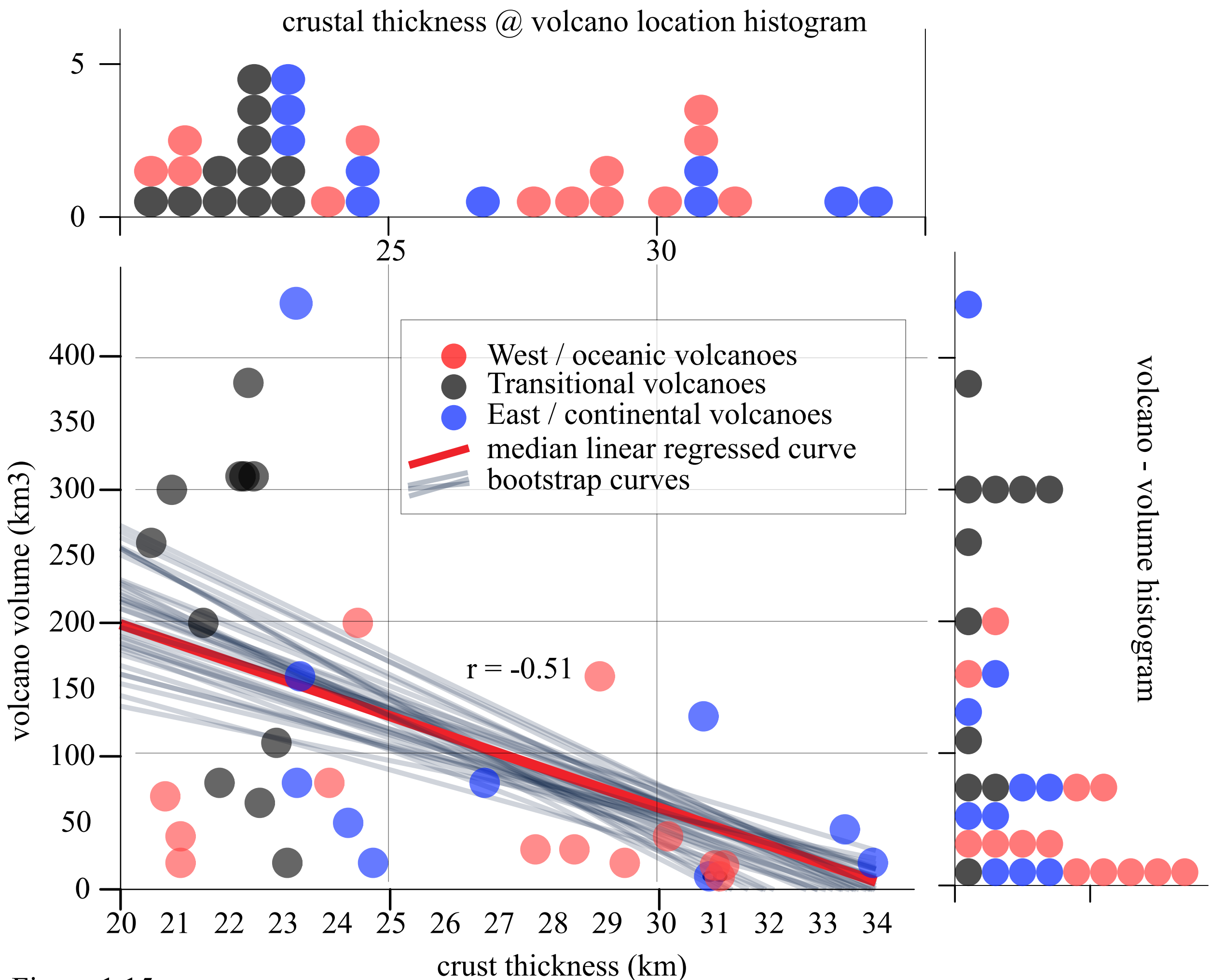

Figure 1.15

Figure 1.15. Crustal thickness vs. volcano volume. TE proxy crustal thicknesses of this study are regressed with volcano volumes from Fournelle et al. (1994). The r-value of bootstrapped linear fit is shown (gray lines) with median r = -0.51 (red line), similar r is found for exponential fit. Histograms of volcano volumes (right) and crustal thicknesses (top) are shown with volcanoes grouped by color into transitional, oceanic and continental segments. Distinct populations of volcano volume appear when volcanoes are grouped by arc segment, with the thin-crust transitional volcanoes showing two volume modes of volcanoes, with one mode dominating the high-volume volcanoes, see text for discussion.

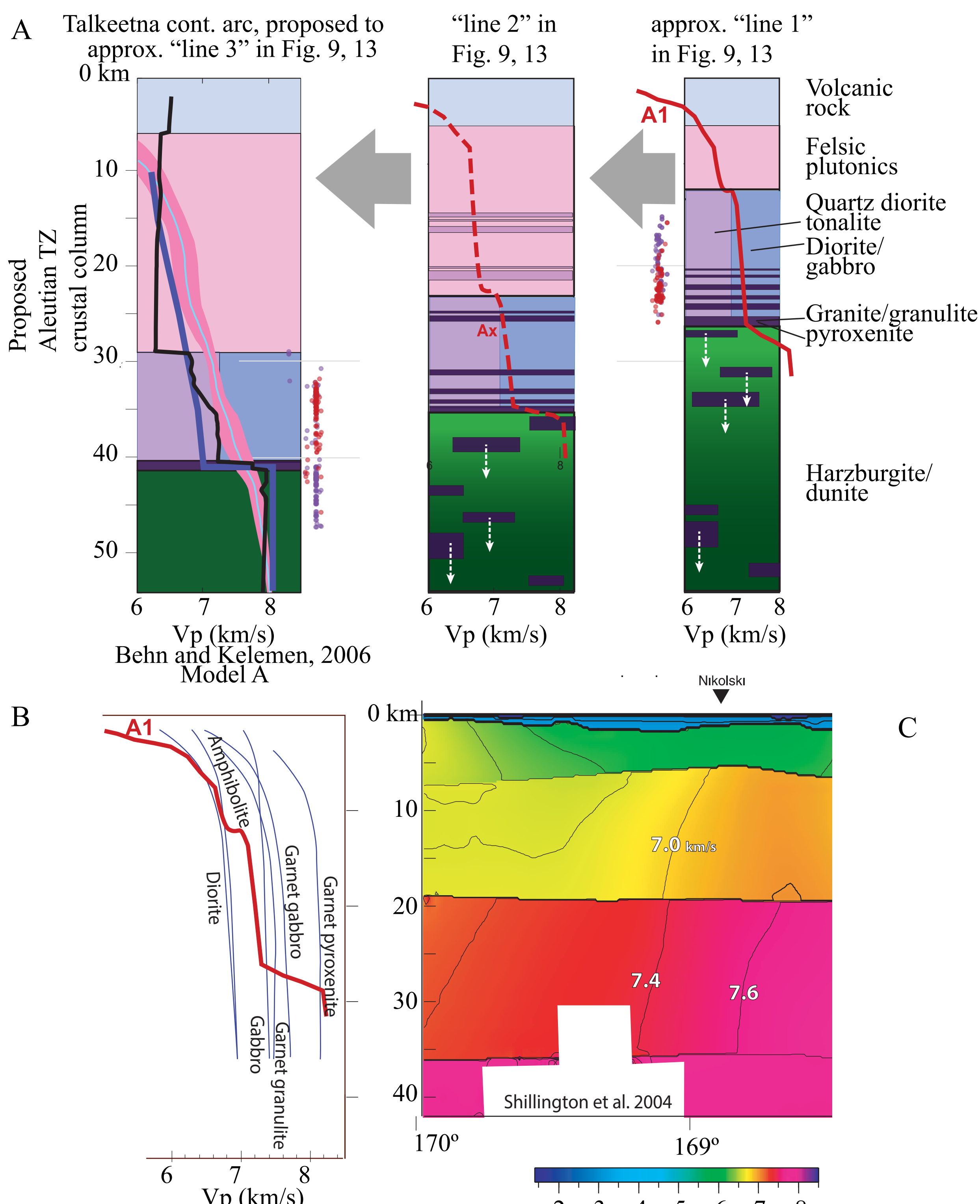

Figure 1.16 Aleutian A1, 1-D profile with lithologies depth vs Vp

Figure 1.16. Crustal structure, Vp and lithologies. (A) Simplified crustal columns with lithologies, adapted from Jagoutz et al. (2013) and Behn and Kelemen (2006), showing the proposed transition segment of the Aleutian arc with cumulate masses created from injections of magma at random levels 20 - 35 km deep in the lower crust (Annen et al., 2006). Gravitationally unstable cumulate masses just above the mantle detach from the crust and descend into the upper mantle. The sites of the sinking cumulates are also sites of enhanced de-compression melting induced by in-flowing mantle moving into the vacated space behind the sinking masses. If the descent speed of the cumulate is on the order of cm/yr and these delamination events recur at period of 106 yr, then 30% of the upper mantle volume will be suffused with mafic cumulates, and the overall Vp of the upper mantle would come from this mixed lithology as discuss in Shillington et al. (2013). Large gray arrows lead to crustal column evolution toward thick "continental" crust approximated here by the Talkeetna exhumed arc section (far left). An intermediate column is proposed and shown between the TZ (transition segment) column and the Talkeetna column, at approximate location of "line 2" in Figure 10 and Figure 13. (B) Vp vs depth of ASE line A1 (see Figure 10), shown with Vp vs depth of crustal lithologies, modified from Calvert (2011). Note the continental-crust-like profile of ASE line A1's sharp increase in Vp at 27 km depth from ~7 km/s to ~8 km/s. (C) Along-strike P-wave velocity model of Shillington et al. (2004) (modified partial enlargement of their Figure 11) shows that from 20 to 35 km depth the Vp (~7.2 to ~7.8 km/s) is in the range of lithologies (garnet gabbro, pyroxenite, etc.) that is denser than the upper mantle and thus gravitationally unstable. The velocity model does not preclude a transitional crust between 20 to 30+ km depth that is fractionating and shedding cumulate masses, as shown in (A).

CHAPTER 2

FRACTIONATION AND DELAMINATION IN ARC CRUST GENESIS

Authors - Warren Lieu and Robert Stern

The Department of Geosciences, ROC 2.1

The University of Texas at Dallas

800 West Campbell Road

Richardson, Texas 75080-3021

Abstract

For the lavas of the Alaska-Aleutian arc system, we performed least-square mass-balanced modeling of crystal fractionation using known compositions and proportions of minerals in cumulate arc rocks, and the available arc lava geochemical data from each volcano to simulate the liquid-line-of-descent for 8 major elements. We test for magma fractionation as the lone mechanism that accounts for the diversity of lavas from these arc volcanoes. We examine the fractionated cumulates and estimate the crust's compositions, its density stratification, and explore the implications for delamination. Our novel method uses a bootstrapped lowess regression procedure to approximate a geochemical liquid line-of-descent for the assumed co-genetic lava. From these approximations, we generated large populations of major element data which are used as inputs to least-square modeling to find the fractionated culminates. We did this for eight fractionation steps, each separated by 1 wt% MgO increments (from MgO 8 to 1 wt%). We interpret these result as a first-order characterization of the geochemical processes operating in the magmatic arc. The least-squares model results in solutions (in proportion of crystallized minerals and their fractionation %) that are plausible with the chosen inputs, giving a composition- and density-stratified crust column under each arc volcano. The cumulate phase amphibole is examined in detail for its role in crustal water storage. We found a nearly constant 1 wt% of mantle-derived water can be stored in hornblende-rich mid- and lower crustal cumulates. Density re-organization (Glazner, 1994) of this hydrous mafic materials may sequester them into a lower crust reservoir, where the water could be released from the thermal breakdown of amphibole ~900ºC due to heating from repeated influx of mantle-derived magma

(Annen et al., 2002). These episodic hydrous pulses could also be the origin of bimodal calc-alkaline/tholeiitic suites of continental arc igneous activity.

We modeled primary magma fractionation with published primary magmas as parents and the 8 wt% MgO lava from Part I above as daughter melts, using published ultra-mafic cumulate for mineral assemblages. Percent fractionation estimates inform estimates of the total volumetric flux across the Moho of the Alaska-Aleutian arc and the percentage of ultramafic cumulate removed from the lower crust. For the Alaska-Aleutian system, we derived a whole-arc mean primary melt % fractionation of ~38%, and if applied to a current crust volume of 8,000 km3/km and an age of 46 My (Jicha et al., 2006), then mass flux was up to 120 km3/km /My (depending on location along the arc) of ultramafic cumulate delaminates into the upper mantle. This result agrees with the calculated volume of foundered masses of Behn et al. (2007) and implies that the active magmatic arc dynamically sheds dense cumulates and residues into the upper mantle.

2.1 Introduction

This study uses a simple least squares technique to model fractionation in a magmatic arc. Fractionation of mantle-derived magma is believed to be the main mechanism from which basaltic liquid is converted to andesite, which is the mean composition of the earth's arc crust. Since continental crust may originate as arc crust, the study of arc crust genesis serves as a link to the formation of earth's continents. The bases of the study of continental crust origin began with noting that the relatedness of lava major elements, trace elements and isotopes between arc-general lava and continental crust is such that it is probable that arc processes contribute some fraction of global continental crust production (Taylor and White, 1965). Thus the 'andesitic model' of Taylor (1967, 1977) posits that andesitic arc crusts accreted over time to become continental crust. However, the flux of mantle melt into the crust in arcs is basaltic (Gill, 1981), rather than andesitic as first thought. The andesitic continental crust cannot be generated from the mantle in a single step, and additional processes are required to further evolve the melt into the compositions seen in exposed continental crust column (Rudnick, 1995; Rudnick and Fountain, 1995) and in inferred seismic inferred arc crust compositions (Shillington et al., 2013). Differentiation (or fractionation) processes are required to evolve basaltic melt into a more silicic material. Melting of and mixing with existing crust are processes proposed to drive the basaltic magma to the observed Mg# of bulk continental crust (Jull and Kelemen, 2001). In some tectonic settings, melting of the subducted oceanic crust (Kay, 1978) and its subsequent equilibration with the mantle wedge can produce high Mg# andesitic melts that may be juvenile continental crust (Kelemen et al., 2003). Here we test whether the principal mechanism, magma fractionation, can be responsible for magma evolution from a primitive first melt to intermediate magma. We reserve the other mechanisms as separate (and ~equal) and narrow our focus on fractionation alone. Fractionation likely begins in the primary melt ponded at the Moho and continues to occur in sills as the magma ascends through the crust, or as fresh magma is injected into sills. Crystal fractionation takes a parental melt to produce daughter liquid and fractionated cumulates. The daughter liquid is the evolved melt that further differentiates whereas mafic and ultramafic cumulates remain behind. This process repeats as the daughter liquid ascend the crust and further fractionation. This provides a simple mechanism to compositionally stratify the crust as magma ascends and evolves, leaving its fractionated products to modify the crust. To first order, the continental crust expresses a stratified record of cogenetic differentiation, i.e., related by fractionation, partial melting, and magma mixing. While differentiation can drive the melt toward silicic compositions, the complementary cumulates and restites constitute some fraction of the Earth crust, posing a mass-balance problem: there does not seem to be enough mafic cumulate in mid to lower continental crust. Calculations suggest at least a 1:2 (and up to 1:10+) ratio of felsic crust to mafic cumulate in order to produce the observed intermediate and felsic crustal composition and thickness. These cumulates do not seem to exist within the seismically imaged crust section.

This problem is resolved if cumulates are shown to be dense, become negatively buoyant, and form drips and delaminate into the upper mantle (Figure 2.1). The evidence and implication and indeed direct imaging of this process are an intense and ongoing research subject for geoscientists. Much geochemical research has focused on entrained xenoliths or obducted crust exposed for analysis (Greene et al., 2006; Kay and Kay, 1985; DeBari et al., 1987; DeBari and Coleman, 1989). Here we take a different approach: we seek to construct a crustal section based on modeled cumulates derived from least-square modeling of Alaska-Aleutian arc lavas. The derived "crustal sections," made of cumulates from solutions of mass-balanced fractionation of geochemical parent/daughter pairs, acts as a statistical window to view into fractionation in the crust. This is the main process this exercise attempts to simulate. Additional processes, such as partial melting of, mixing with and assimilating of pre-existing crust material, MASH (Hildreth and Moorbath, 1988), AFC, (DePaolo, 1981) play important roles but are ignored here.

2.2 Geologic Setting

Figure 2.2 depicts the Alaska-Aleutian arc as it spans ~2,500 Km from southwestern continental Alaska westward through the peninsula, into the oceanic island arc province, terminating in eastern Kamchatka. This system consists of some 50 main edifices and a similar number of cones that together form an arcuate shaped convergent plate boundary that extends across oceanic, transitional, and continental lithosphere, with the Pacific plate subducting slab from the southeast. The convergence vector of the system is orthogonal to the trench at the eastern continental segment and because of the arcuate shape, the vector tends to small value west of 175° E and gradually the plate boundary switches to strike-slip along strike. Longitude 175° E also corresponds to the cessation of the seismically detectable subducted slab (Syracuse and Abers, 2006). The present project concerns the arc above the subducted Pacific slab: between longitude ~150ºW to ~175ºE. We will adopt Lieu and Stern (2018)'s terminology for the tripartite division of this arc: the western oceanic arc segment (175° E to ~ 175° W), the transition segment (~175° W to ~160° W), and the eastern continental segment (160° W to 150° W).

2.3 Methods

Presently geochemical modeling is performed with the energy-minimized thermodynamic transport algorithm (pMELTS, Ghiorso et al., 2002) and energy-conserved fractionation with open system anatectic melting, magma recharge and mixing (EC-AFC, Bohrson and Spera, 2001). These give accurate predictive reactions for defined inputs (rock chemistry, extensive and intensive parameters) and precise adherence to the algorithms' assumptions. Thermodynamic equilibrium (pMELTS) and energy balance (EC AFC) are assumed to have been achieved between the phases, and rigorous solutions are produced. However for many instances in arc magma genesis, disequilibrium between phases is common (e.g., Conrad and Kay, 1984) and thermodynamic models have difficulty converging to solutions (Greene et al., 2006). Here we use a modeler that strive to achieve results outside the realm of thermodynamics: the least squares approximation.

2.3.1 Least Squares Fitting

We use least squares estimation as a method to simulate fractionation. The least squares method as applied to magma fractionation, partial melting, and mixing follows the formulation of Wright and Doherty (1970). They laid out the equations, provided the algorithm and solved simple examples in the usage of linear least squares approximation to solutions to petrologic problems. Though it is simple in terms of petrologic concept--it is essentially a sophisticated application of the lever rule--it can simulate solutions of parent and daughter magma that follow a liquid line of descent. It must be emphasized that least squares fitting approximates a mass-balance solution and is not a thermodynamic minimal energy solution such as pMELTS. The advantage of least squares fitting is that it, by design, always fits the input lava parent, daughter, and cumulate fractionates with some linear combination of phases, with a residual that characterizes the goodness-of-fit. This procedure does not consider physical reality. One must decide on the meaning of the results as they relate to geology. A part of my procedure is to filter out unrealistic solutions and keep those that make geologic and petrologic sense. The least-squares result assemblages also depend on the quality of the input data. The results are reliable if reasonably accurate input phases are used. In spite of these limitations, numerous workers have successfully used the method to forward and reverse model magma fractionation, partial melting and mixing, as discussed in the next section.

2.3.2 Least Squares Method in Other Studies

Wright and Doherty (1970) developed the least squares method to find the best solution based on the level rule of weight % mass balance. As such, it is used in petrology for forward and reverse problems in fractionation, partial melting, and mixing. I describe my approach for least squares approximation for petrologic problems in greater detail below. Here I review selected projects that successfully employed the technique to model parent-daughter-cumulate relations. Arculus (1976) studied lavas of Granada of the Lesser Antilles arc and related alkaline basalt to melts of mantle garnet peridotite source by least squares forward modeling with crystallization of observed phenocrysts (olivine, clinopyroxene, and spinel). The relevance of this study to the present one is the assessment made by Arculus (1976) of the fractionated assemblage based on the square of the residuals of the solution (Sum r^2): by adding amphibole (not observed as phenocryst) the solution gives a better match (lower r^2) so that petrological consideration has to be given to amphibole as a viable fractionated phase. Greene et al. (2006) modeled cogenetic lava and gabbronorite and pyroxenite of the exposed Talkeetna crustal section in southern Alaska. They found that least squares fitting solutions matched observed trends, supporting the interpretation that Talkeetna igneous rocks were related by fractionation. They chose cumulate phase compositions by assuming equilibrium between crystals and liquid via

Fe/Mg K_d value. This is a step that my study omits; my selection of cumulates is discussed below. Greene et al. also derived (from cpx addition to the ultramafic cumulates to find primary melt composition) that melts of mantle peridotite crystalized >25% to form pyroxenites. Conrad and Kay (1984) also used least-squares fitting of Aleutian arc lavas to infer 21% fractionation of a primary melt. Their least squares model followed a more nuanced path that matched oscillatory-zoned clinopyroxene crystals. They used multiple cycles of open system fractionation and melt replenishment/mixing to arrive at the steady state composition of the observed crystal. We will compare these primary magma % fractionation results with our results in the Discussion Section.

While the cases mentioned above used least squares to model specific magma parent/daughter pairs of collected samples, we intend to use the least squares method to give insights into the large-scale, whole-population view of the system using all the available lava of the system. In the next section, I provide a brief formulation of the problem and the method to solve it.

2.3.3 A "0 + 7" Steps Least Squares Crustal Model

A distinguishing aspect of my study is access to a large geochemical dataset. Least-square modeling is used because it allows for calculating solutions that number in the 100,000, after perhaps some millions of individual calculations. This makes it possible to simulate, as described below, least squares fractionation with 8 major elements from 28 volcanoes in 8 fractionation steps (the "0 + 7" steps, see below) with some 10,000 simulated line-of-descent geochemical suites per volcanoes. The solutions I seek are the phase proportions of the cumulate minerals and the % fractionation of the "reaction." At the end we have an approximated geochemical crustal section, ordered by MgO wt %, under the 28 volcanoes along the Alaska-Aleutian arc that can be combined along arc strike so that a 2 dimensional spatial-chemical profile of the arc can be constructed. The most important result of the study may be the first-order estimates of quantities of crustal minerals and the total % fractionation needed to evolve the mafic melt delivered to the base of the crust to more felsic melt in the midcrust. This requires constructing populations of line-of-descent paths for existing lavas from each volcano for each of the 8 considered major elements (SiO_2, TiO_2, Al_2O_3, FeO*, MnO, MgO, CaO and Na_2O). These line-of-descent constructs are described in the next section: they are bootstrapped lowess regressed lines derived from existing lava plotted in MgO Harker diagrams. I bootstrapped 10,000 of these lines and from them I extracted 10,000 oxide values, each set separated by 1 wt% MgO from MgO 8 wt% to MgO 1 wt% so that least squares solutions could be applied for the 7 fractionation steps. This is the "7" of the "0 + 7" step approach. The "0" refers to the step that is the fractionation of mantle-derived primary magma to magma of MgO 8 wt%. This 0-th step is important for calculating the amount of ultramafic cumulates that fractionated from the primary melts (probably at the Moho). These cumulates are suspects for delaminating into mantle and never invade into the lower crust en masse. Therefore this step is described and shown separately in the subsequent plots even though procedurally, they are obtained exactly the same as the other 7 steps. The least squares solutions of a set of mineral mass fractions that compose the crystalized assemblages and the accompanying % fractionation from the parent melt means that the solutions identified the cumulate rock fractionated at that step. At the end we have a simulation of 7 "layers" of cumulate rocks, each is related to the fractionation proxy, MgO wt%. If MgO wt% is used as a proxy for depth into the crust, then we have modeled the structure of the crust under a volcano.   This is done for the 28 volcanoes along the arc and, using lowess regression as outlined in Lieu and Stern (2018), we can construct crustal composition variations along arc strike that characterize the entire arc. We now describe more details about this method.

2.3.4 Bootstrapping to Derive Liquid Lines of Descent

It would be ideal to have analyses all lava from each volcano; this is of course not possible. However, for the analyses that we do have, we can statistically determine from what population distribution they came. This is the essence of bootstrapping (Efron and Tibshirani, 1993). Here bootstrap resampling of the lava samples is used to create a population of lavas on which lowess regression is applied to derive lines of descent. Bootstrapping strives to obtain information on the underlying (and unobserved) population of samples from which the observed samples form a subset. By repeated resampling (with replacement) of the observed samples, populations are synthesized from which statistics can be performed to give information of accuracy, variance, etc., of the total sample suite. It should be said that these synthesized samples are used only to provide statistics related to the actual samples, they are not taken to have physicality. This point is emphasized as we bootstrap populations of lava from observed samples and use the bootstrapped population for subsequent geochemical modeling.

We use bootstrapping in combination with *lowess regression* (Lieu and Stern, 2018) to extract trends in geochemical Harker diagram. These trends are taken as liquid-lines-of-descent for the magma suite and are used to generate synthetic lava samples from which to perform the least squares approximation. These simulated lavas are the unobserved lava constructed from the observed samples. They are 'real' in the sense that the collected samples constrain them. An assumption in the validity of the bootstrapping technique is that the observed samples are representative of the total population of interest (all the un-sampled lavas that have similar genesis history but laid buried by younger flows), and if that is the case, then the bootstrapped population can give information on the variational behavior of the observed sample suite.

The bootstrapped-lowess regression estimates a volcano's geochemical line-of-descent based on Harker diagrams. The eight considered major elements of a volcanic suite are plotted against MgO as the fractionation index. Each scatterplot is then smoothed by lowess regression to generate variation curves for the oxides. Lowess regression predicts variation curves without a priori assumptions about the parametric model curve shape (i.e., a lowess regression curve's shape depends solely on the data that generates it, it is model-independent). As emphasized previously, the lowess regression curves in the Harker diagram are taken to approximate a lava suite's liquid line of descent. Conceptually, the lowess curve seeks out the median curve as defined by the existing lava compositions. The original lavas have been scattered by multiple processes such that they departed from their original position in the line-of-descent, but lowess curve may better approximate the original path. Deviational processes that tend to "pull" an oxide value one way is countered by other processes that "push" an oxide the other way so that in the limit of many such interactions the resultant path tends toward the line-of-descent path without the influences of these processes, and this is what the lowess regressed line recreates. Lowess regression is statistical in nature and therefore can be bootstrapped to reveal the underlying distribution from which the actual curves are derived. For each oxide-MgO pairing, 10,000 bootstrapped lowess curves were calculated. This process is illustrated in Figure 2.3 for the FeO-MgO relationships of lavas from one volcano.

The lowess regression algorithm generates samples that are likely to be close to the mean of the samples around it, but it does not duplicate the scatter of samples that are displayed in the Harker diagrams. This is evident in Figure 2.3, the volcano samples are scattered, but the lowess regressed curve is more tightly constrained because it approximates the mean of the samples around it. Using synthesized samples from the lowess regressed mean is more constraining than synthesizing more of the real samples. We treat the synthesized (mean) samples as the bases upon which the rest of our analysis is built.

The lack of 'relatedness' of the bootstrapped samples between the oxides, i.e., they are separately generated in each Harker diagram and are not from 10,000 individual (simulated) rocks, seems to make this exercise 'ungrounded.' This is not avoidable but the mitigating factor is that when each of these simulated samples from a set selected randomly from the 10 oxides, they sum to near 100 wt%. The bootstrapped samples are not representations of 'real' rocks, but their compositions are constrained by real samples, and bootstrapping constructs a distribution of synthesized samples that can inform on the statistics of the real samples. This is the key to the exercise as we are extracting overall trends (means, medians, SD) to see how they vary across the entire arc. I.e., these samples are grounded by the fact that they are constrained representations of real samples. Our modeling scheme is distinct from modeling on rocks from a single volcano, where the geochemistry of individual rock may be precisely modeled but the result does not have distributional data to give confidence level of the model (how representative is the one sample), is isolated to one locale along an arc, and is seldom comparable to another author's model on an adjacent volcano because the modeling assumptions may be different.

2.3.5 Least Squares Approximation

At the core of our scheme is reverse modeling in mass-balanced least squares model of fractionation. At its core, the least-square method solves a system of linear equations by solving for the solutions with the smallest residuals. Modern computers working in matrix formulation can easily calculate the solutions. I follow the formulation of White and Doherty (1970) with code implementation similar to that of Janousek (2016) running on codes written in MatLab scripts on Windows and Mac operating systems.

Our reverse problem is the following: given a parental liquid, what mass fractions and % fractionation of a particular assemblage of minerals (with fixed compositions) are needed to generate a given daughter liquid? The linear equations in matrix form are straightforward (Janousek, 2016) and their solutions (with residuals) are a classic application of linear algebra. The least-square modeling proceeds with using 10,000 random (Monte Carlo) pairings of parent and daughter samples and each pair is solved with 18 possible/likely cumulates (described below). The Monte Carlo sampling simulates the large and possibly variable line-of-descent paths taken by actual magmas in their evolution as they rise through the crust. This is done for the 7 steps (the 0-th step, primary magma to MgO 8 wt%, is described separately in Section 3.8 forward). At this point, we have data matrices of least squares solutions for 10,000 simulations of 7 fractionation steps for 18 cumulate sets for the 28 studied volcanoes totaling some 30 million solutions. We collect the solutions for examination and filtering. We described those next.

2.3.6 Filters

With the 10,000 parents and daughter liquid composition and 18 cumulate compositions fixed, a least squares solution of fractionation of cumulate minerals is done to fit parent to daughter liquid for each of the 7 steps. However, least squares fitting gives purely analytical solutions, and we must apply conditions to screen for physically sensible solutions. The criteria for an acceptable solution are the following: least squares residual is less than 0.1, the fraction of fractionated mineral has to be positive values, the summation of all mineral fractions plus residual liquid is between 95 and 105%, and fractionated crystallization for each step is between .01 and 0.9.

The screening reduced the total number of bootstrapped solutions considerably. The remaining solutions for a particular set of cumulate assemblages can indicate the 'appropriateness' of that assemblage as a real solution as applied to that volcano's bootstrapped lavas (and therefore, is a believable solution). That is, the viability of a solution from a particular cumulate composition (and its % fractionation) is proportional to the number of filtered solutions it generated. Later, a weight based on this is assigned to a particular mineral solution set when I take the mean or median of quantities from all the solutions. This step will be discussed in the Results Section. Next, I summarize the origins of the cumulate compositions used in the model.

2.3.7 Fractionated Cumulate Assemblages For Step 1 to 7

Compositions of xenoliths and gabbros from the Alaska-Aleutian oceanic and continental arc and the Lesser Antilles Arc are used to define the cumulate assemblage used in modeling.

These include oceanic arc xenoliths from Adak Island, Aleutian arc (Conrad and Kay, 1984), dunite, hornblendite, and amphibolite from Adagdak, Aleutian arc (DeBari et al., 1987); continental crustal column cumulate gabbros and gabbronorite from Talkeetna fossil arc exposed in the Chugach mountain, Alaska (Greene et al., 2006), and one suite from the Lesser Antilles arc (Arculus and Willis, 1980). In total, 18 cumulate mineral sets were used as potential fractionates from the parental liquid. These cumulates are used for all seven fractionation steps (8-7, 7-6,…, 2-1 wt% MgO). A description of cumulate mineral assemblages used is given below. They are graphically represented in Figure 2.4A.

3.7.1 Arculus and Wills (1980): (CsAr in Figure 2.4A)

This assemblage is taken from a study of mineralogy of plutonic blocks ejected from the eruption of Soufriere volcano in St. Vincent (Lewis, 1973). This assemblage contains olivine (Fo79-Fo67), plagioclase (An96-An89), aluminous pyroxene, hastingsitic amphibole and magnetite. The blocks are ejecta buried in ash flow deposits and the minerals are described as unzoned and quenched at high temperature. Arculus and Wills. (1980) obtained plausible results from least squares modeling to establish the genetic relation of their Lesser Antilles basalt-basaltic andesite pair using this assemblage for fractionated cumulate.

3.7.2 "CsAr_Ol"

This is the same as outlined in 3.7.1 but olivine was omitted from the fractionating assemblage.

3.7.3 Conrad and Kay (1984): ("ConKay_Ol, "ConKayFo76", etc. in Figure 2.4A)

These seven assemblages were copied from analyses of ultramafic cumulate xenoliths entrained in andesitic magma erupted at Adak documented in Conrad and Kay (1984). These assemblages were constructed from gabbroic xenolith minerals that they used in open-system crystallization modeling. Their study concluded that the cumulates were derived from magma in equilibrium with spinel lherzolite near the Moho. Here we constructed 8 mineral assemblages similar to those used by Conrad and Kay (1984) in their least squares modeling effort. Four of this series of mineral assemblages have identical compositions of clinopyroxene, magnetite, plagioclase, and amphibole, but with 3 different compositions of olivine (Fo 89, 85, 76). Three assemblages that excluded amphibole and olivine are also included.

3.7.4 DeBari et al. (1987): ("ADAG81", "ADG1", "Dun30", "DeBari")

These four assemblages reflect dunite, wehrlite, pyroxenite and amphibolite xenoliths from Adagdak on Adak, which are interpreted as cumulates from primary melt fractionation beneath the crust-mantle boundary. While this collection is related to the near-by suite of cumulates of Conrad and Kay (1984) as being fractionates from Aleutian arc magmas, differences exist. One each dunite, wehrlite, and hornblendite were selected as candidate cumulates from this study. We also constructed a mean cumulate composition ("DeBari") from the range of these xenoliths.

3.7.5 Greene et al. (2006): ("Gr1", "Gr2", "Gr3")

These four cumulate assemblages are from Talkeetna. The fossil roots of the Jurassic continental Alaskan arc is represented by the cumulate rocks exhumed in the Talkeetna range in southeast Alaska, a section of exposed arc crustal column with layered cumulate gabbros and pyroxenites that genetically link the fractionates and the lavas. Greene et al. performed least-square modeling with three steps, each step paired with a cumulate and its phases. We use these cumulate gabbro and pyroxenite phases as documented by Greene et al. without modification. Here cumulate Gr1, Gr2, and Gr3 in Figure 2.4 A refer to their step 1 (parent MgO 8.17 wt. % to daughter MgO 7.24 wt. %), step 2 (7.24 to 6.05 wt. % MgO) and step 3 (6.05 to 3.87 wt. %

MgO), respectively. Greene et al.'s step 1 and 2 roughly correspond to this study's step 1 and step 2, and their step 3 corresponds to this study's step 3, 4, and 5.

3.7.6 cumulate constructs ("GrPlgPrx", "Kay", "Ol89")

These three cumulate assemblages come from the work of Green et al. (2006) and Conrad and Kay (1984). Cumulate 16 is a norite, composed of plagioclase, orthopyroxene and clinopyroxene. Cumulate 17 is a cumulate of Conrad and Kay (1984). Cumulate 18 is a peridotite constructed from olivine from Conrad and Kay (1984), and orthopyroxene and clinopyroxene from Greene et al. (2006).

2.3.8 Fractionated Cumulate Assemblages For Step 0

For fractionation of the primary magmas to MgO 8 wt% data (step 0) and MgO 8 to 7 wt% (step 1*, which is a re-do of the lavas of step1 with the cumulate assemblage described here), I selected ultramafic-mafic assemblages from xenoliths in the Tonsina complex, Alaska, as documented by DeBari and Coleman (1989), a clinopyroxenite from Conrad and Kay (1984), and a hornblendite from DeBari et al. (1987). Ultramafic-mafic cumulate "AK-10", "AK-23b", "ALu-60" are xenolithic websterite, garnet gabbro, wehrlites, respectively from DeBari and Coleman (1989); "ADG-1" is a hornblendite from DeBari et al. (1987) already described above; "MM-102" is an olivine hornblende clinopyroxenite from Conrad and Kay (1984). These ultramafic assemblage compositions are shown in Figure 2.4 B.

2.3.9 Primary Magma For Step 0

Figure 2.5 shows the major elements (ME's) compositions of a population of primary magmas used as parents for step 0 (primary magma to MgO 8 wt%). The oxides are normalized to OK4, a tholeiitic basalt (see below). These are published primary magmas from the Alaska-Aleutian arc, the Lesser Antilles, and Japan. We are inclusive in our primary magma choices in order to represent the maximum diversity of the mantle from which we fractionate. We have few constraints on the homo- or heterogeneity of the mantle source under the arc, so we chose to err on the side of less restrictive mantle geochemistry. These eight primary magmas are assumed to represent the compositional range of first melt in the mantle beneath the Alaska Aleutian arc system. This assumption is simplistic, but I used it here to represent the heterogeneity of Earth's mantle which enables us to derive first-order information from the least-square fractionation model (which is itself an approximation of a thermodynamically accurate model). The primary basalts used are the following:

OK4: Byers (1961), tholeiitic basalt (Kay et al., 1982).

FAMOUS: tholeiitic MORB basalt Bender et al. (1978); Conrad and Kay (1984).

TH basalt: Tatsumi (1982), olivine tholeiite in equilibrium with peridotite, Setouchi volcanic belt, (Conrad and Kay, 1984).

Ash basalt: Byer (1961), Ashishik basalt, Conrad and Kay (1984).

ADAG81: DeBari et al. (1987), Adagdak volcano basalt

ID16 NR: Nye and Reid (1986) unfractionated basalt from Okmok volcano

Fuji 85: Fuji and Scarfe (1985), basalt from spinel lherzolite (DeBari et al., 1987).

Following the same least squares procedure for step 1 to 7, I did 10,000 Monte Carlo pairing of these 8 primary magmas with the one thousand synthesized MgO 8 wt% lava from each of the 28 volcanoes, using the cumulate assemblage compositions described in Section 3.8 (ultramafic cumulates) to derive cumulate mineral fractions and % fractionation. The solutions from these go through the filtering process as described above for the solutions of step 1 to 7.

2.3.10 Lowess Regression

The lowess (locally weighted regression) nonparametric smoothing regression (Cleveland, 1993) was applied to the data for volcanoes along the whole arc. Such a curve characterizes the geochemical variations of the arc more comprehensively because it contains geographic information and it implies the variation exists *between* volcanoes. Since lowess regression is a statistics, we bootstrap the data and generate hundreds to thousands of curves and extract estimates on confidence level (usually we include 5- and 95-% bounds). We conjecture that lowess regression curves show an underlying (smoothed) pattern from which the discrete data points emerge. For a fuller discussion of the usage of the lowess regression characterization of arcs, refer to Lieu and Stern (2018).

2.4 Results

When all the calculation of this scheme are performed, the outputs we are interested in are the mass fractions of the fractionated cumulates from the 18 mineral assemblages, and the % fractionation undergone by the magma from MgO 8 to MgO 1 wt% (plus the primary magma to

MgO 8 wt% pairs). There are some 4 million solutions of the synthesized parent-daughter pairs and ~4 million residuals to consider for interpretation. I have filtered for criteria as described in the Methods section and derived fractionation for each step for each volcano. Here I plot and examine the resulting compositional and fractionation variation along the arc. Then I analyze the fractionated cumulates with various statistical and graphical means and draw inferences from these about the implication a for Alaska-Aleutian arc magmagenesis.

2.4.1 Solutions Of Least Squares Modeling, (Step 1 To 7) Bar Graphs

Graphical representation of the solutions of the least squares cumulate compositions of the arc lavas from MgO 8 to 1 wt % (step 1 to 7) for the volcano Great Sitkin is shown in Figure 2.6. These represent the cumulate mineral fractions based on each of the 18 cumulate assemblage chemical make-ups for the parent/daughter pair for each of the 7 MgO steps (ultra-mafic cumulate of step 0, fractionation from primary magmas to MgO 8 wt% is described in the next section). The number of solutions (after filtering out the nonsensical solutions) obtained per step per cumulate assemblages is also shown: these give a sense of how the assemblages 'fit' a certain condition to fractionate. I assert that the number of cumulate solutions obtains per 10,000 Monte Carlo simulation scales to the likelihood of the validity of that particular set of mineral fractions and % fractionation beneath the volcano. That is, I take the number of solutions as a quantitative indication of the actual fractionation event that occurred there.

It is evident from examining all the solutions that specific patterns emerge: the cumulate assemblages of Conrad and Kay (1984) and Arculus and Wills (1980) produce the most solutions, regardless of the step number. These yield cumulates of hornblende gabbro, gabbro, and olivine gabbro. Cumulate mineral assemblages of DeBari et al. (1987) yielded the fewest solutions: in many cases, they yield no solutions. This is not surprising given that the cumulate assemblages of DeBari et al. (1987) are considered ultramafic and derivatives of primary melts. These cumulates should yield more solution in step 0, described below. The Greene et al. (2006) cumulate assemblages give a variable number of solutions for the whole arc but their assemblages for low MgO (Gr3) gives, in many cases, the most solutions, regardless of step number.

From a macroscopic view, these fractionated cumulates are predominately gabbros, olivine gabbros and hornblende gabbros. Amphibole is ubiquitous among the solutions, hinting at the importance of this hydrous phase in arc magmatism (Davidson et al., 2007). This point is explored further in the Discussion section.

Regardless of the appropriateness of each of the 18 assigned cumulate assemblages, I infer from all of the solutions as reflecting the heterogeneity of the fractionation processes--with the caveat that we use the number of solutions of each cumulate assemblages as a pseudo-weight factor when we perform statistics on the arc as a whole. The solutions to the least squares model shown represent cumulate rocks, and to discern possible trends and cumulate variations from these data, we plot these cumulate in mafic and ultramafic ternary rock classification diagrams.

2.4.2 Solution To Ultramafic Least Squares Modeling, (Step 0) Bar Graphs

Graphical representation of the ultramafic cumulates least squares solutions for the primary magmas to MgO 8 wt% (step 0) for the 28 volcanoes are shown in Figure 2.6. These solutions are obtained from least squares model similar to the mafic cumulates step 1 to step 7 of the in-crust model, and Figure 2.6 is similarly arranged as in the previous section's bar graphs of Figure 2.4. Here the least squares modeling is less successful regarding the number of solutions found for the ultra-mafic cumulate assemblages. Nevertheless, they are assessed as derived cumulates and information extracted from these solutions are shown in the Discussion section.

2.4.3 Ternary Diagrams

To assess the diversity of the derived cumulates of the last two sections, I plot them in four ternary diagrams (Figure 2.7, 2.8 , 2.9, 2.10) with labeled fields defined by Stanley (2017). The large scatter of the cumulate solutions is evident in the plots, and it seems to suggest these are bad solution matches for each of the least-square solution steps. But the reality is that cumulate rocks as collected in the field that is likely to be genetic fractionates of lavas, such as the exposed crustal section of the Talkeetna arc in southern Alaska, are compositionally diverse. For example Greene et al. (2006) have described lower crustal gabbros to have 30-80% plagioclase, 5-35% orthopyroxene, 0-30% clinopyroxene, 0-10% amphibole, and 0-15% spinel. Such a range of phase % would have similar scatter on a ternary diagram as our cumulate solutions. The ternary diagrams of the synthesized cumulates populations show our derived rocks are (1) are within the ranges of Talkeetna lower, and mid crust gabbro and gabbronorite populations of Greene et al. (2006), (2) are similar to, e.g., those of Hacker et al. (2008)'s gabbros, hornblende gabbronorites pyroxenites. To summarize the cumulates generated:

~15%: pyroxenite peridotites, websterites, anorthosites, and norites

~30%: olivine-bearing pyroxenites,

~55%: olivine hornblende-bearing pyroxenite, olivine pyroxenite-bearing hornblendites, hornblende pyroxenites, olivine gabbros, pyroxenite gabbros, pyroxenite hornblende-bearing gabbros, plagioclase hornblende-bearing pyroxenite, and orthopyroxene-bearing gabbros, gabbros.

2.4.4 Density Stratification In Cumulates Of The Arc Crust

Here I show results that simulate the distribution of cumulates in the crust. The fractionated assemblages vary in their mineral proportions according to MgO content of the parent-daughter pair such that they usually give systematically increasing density as a function of MgO, or depth. Here I used the density-estimating algorithm of Hacker and Abers (2004) to derive the cumulates' density. Figure 2.11 shows that the crust beneath 18 volcanoes exhibits an increased density of cumulates with depth, and 9 that do not; these are plotted separately in (A) and (B), respectively. All parent-daughter pairs with 1-2 wt% MgO fractionate cumulates with densities less than the upper mantle value of 3.25 g/cm^3 (pyrolite, Jull and Kelemen, 2001) but higher than continental crust. Rudnick and Fountain (1995) compiled mean mid- and lower-crustal density to be ~2.8 g/cm^3, with felsic gneisses at ~2.7 g/cm^3 and garnet-bearing mafic granulite at ~3.0 g/ cm^3. Cumulate densities increase systematically with increased MgO so that at MgO of > 6 wt% cumulates for 11 of the 27 volcanoes have densities that exceed that of the upper mantle.

2.4.5 % Fractionation Vs. Longitude: Step 0 - Ultramafic Cumulates

The density of cumulates generated for the fractionation step 0 (primary magmas to MgO 8 wt%) is nearly constant along the arc: most of these are denser than the uppermost mantle and would be gravitationally unstable and prone to sinking into the mantle. The extent (%) of fractionation to produce these cumulates along the Aleutian arc is shown in Figure 2.12. The lowess regression indicates variable, but > 40% fractionation in the western Aleutians, ~30% in the transitional segment, trending to a bimodal but higher (> 40%) median % F in the eastern continental segment. Percent fractionation is (1 - melt fraction) so that the lower %F in the transitional segment may signify enhanced (higher) degree of melting due to delamination of the lower crust (see Discussion Section). If the Alaska-Aleutian arc formational parameter from Jicha et al. (2006) is added (far right axis of Figure 2.12) then the % fractionation curve may reflect the rate of delamination. We show Vp vs longitude on the same plot to compare with the % fraction variation. We calculated the cumulates' median Vp per volcano, the purple dots on Fig. 12, from Hacker and Abers (2004)'s software. Behn and Kelemen (2006) considered a Vp that is > 7.4 km/s to indicate gravitationally unstable material above upper mantle. The lowess regressed curve shows that first stage cumulates beneath the transition segment (shaded region between 176 º and 160 ºW) have Vp > 7.4 km/s, and the flanking continental and western segments have Vp < 7.4 km/s.

2.4.6 % Fractionation Vs. Longitude: Step 1 To 7 - Mafic Cumulates

I now describe the % fractionation of the derived cumulate rocks of the crust (steps 1 to 7). The 7 fractionation steps (from MgO 8% to 1%) are best combined into 3 combined steps: "A" combines steps 1-2 (MgO 8% to 7%, MgO 7% to 6%); "B" combines steps 3-4 (MgO 6% to 5%, MgO 5% to 4%); "C" combines steps 5-6-7 (MgO 4% to 3%, MgO 3% to 2%, MgO 2% to 1%). Each volcano then gets three points on Fig. 13 corresponding to the fractionation % for the three combined steps, which are more easily color-coded. These three steps represent early (A), intermediate (B), and evolved (C) state of the volcano's magma column. I plot these % fractionation values of all the volcanoes and calculate bootstrapped lowess-regression curves for step A, step B, and step C. These three curves represent the state of the arc's % fractionation, or its complement: the state of % melt (which is 1 - % fractionation), as proxies by the volcanoes, and as modeled by our least square method from the synthesized population of lavas. Figure 2.13 shows that steps B and C reflect low extents of fractionation (15 - 25%) and vary little along the arc, i.e., most volcanoes stay within a small range of % F for the intermediate and evolved fractionation states. Step A, however, shows considerable variation as well as greater fractionation amongst some of the volcanoes, it is the main agent that dictates the state of magma evolution along the arc system. These variations are arc segment-dependent: Step A %F is high for the western island-segment and in the eastern continental segment volcanoes and low-to-intermediate for the transition segment. Fractionation at step A has a greater effect in the overall %F due to the way the subsequent % F is summed up so that it is this contribution of step A (lava modeled at MgO 8 - 6 WT%) which dictates the overall fractionation budget of the total, final lava.

2.5 Discussion

Figures 2.6 from the Result Section show all the solutions to the synthesized-magma least-square fractionation model for the Alaska-Aleutian arc volcanoes from primary magma (step 0) to very fractionated magmas (step7). Quantitative results such as density, % fractionation, compositions and others will be extracted from these data by standard robust statistics (median, weighted median, lowess regression, etc.). These will be used to generalize my finding for the state of the arc structure in what follows. My model simplifies details of the fractionation process, e.g., it ignores thermodynamic energy minimization of phase generations and neglects other mechanisms contributing to magma evolution in the crust (AFC, MASH), as discussed previously. Nevertheless, the simple model presented here has the advantage of focusing on the process of fractionation and allowing for the statistics of large number to smooth out the myriad of processes operating in the crust--that is, it enables ancillary processes to cancel each other out, so the results reflect the primary process of fractionation. That the model generated viable solutions, given the input of the erupted lavas, that reasonably approximate the cumulates that actually formed (see bar graphs and ternary diagrams in the Result section), is a first-order result.

Moreover, the result indicates that magmatic fractionation is the primary mechanism that can generate the diversity of cumulates likely to have formed deep in the crust beneath an active magmatic arc, and that melting, mixing and assimilating mechanism within the existing crust are probably second-order controls on magma evolution. As a rough comparison, the total fractionation from step 1 to step 7 is ~60% to 85% (Figure 2.13). This implies for a crustal column a mass ratio of cumulate vs. evolved magma of 3 to 7 to 1. Tatsumi et al. (2008)

modeled the construction of the Izu-Bonin Mariana arc by mixing (between felsic crustal magma and differentiated basalt) and anatexis (of basaltic lower crust) and showed that lower crust restite and cumulate are under-observed seismically by factors of 3 to 9. That the present study's result falls within their range is a modest validation of the procedure. However, this means the synthesized cumulates of this study have any bearing on reality, their existence and eventual fate have to be explained in a model that is reasonable and testable. For the rest of the Discussion section, I assume the modeled fractionation mechanism does occur beneath the Alaska-Aleutian arc and work out implications that can be drawn from that assertion.

2.5.1 The Role Of Amphibole In Arc Magma Fractionation

A main result from the modeling is that fractionation of amphibole is important in arc magma evolution. Hornblende gabbros compose the largest percentage of the modeled cumulate. They are notably greater than the more commonly exposed olivine gabbros and gabbronorites. Using Dy/Yb and La/Yb vs. SiO2 systematics Davidson et al. (2007) hypothesized that amphibole is pervasive as a fractionated mineral in arcs. That hornblende gabbro is not exposed in greater proportion is attributed to the sensitivity of the amphibole to temperature rendering it "cryptic" as it breaks down at low T and P (Medard et al., 2005). Davidson et al. (2007) used Dy/Yb-based fractionation systematics to argue that many arcs produce lava with trends that are controlled by amphibole rather than garnet or anhydrous gabbro (clinopyroxene + plagioclase ± olivine) fractionation. This assertion is due to the opposite slope in the partitioning of MREE and HREE of the two minerals (Figure 2.14 inset). I found a similar systematic variation in Dy/Yb vs. SiO_2 for almost all Alaska-Aleutian volcanoes (Figure 2.14). Inspection of Figure 2.14, especially the cpx and garnet fractionation vectors, indicates that we can rule out cpx (in gabbro) and garnet as the main controlling phases for magma compositions. Amphibole seems to have more leverage in controlling magma composition: its fractionation is more efficient in driving liquid to higher SiO_2 content than does clinopyroxene (because amphibole has less SiO_2 than gabbro/cpx). Garnet fractionation produces trends that differ from observed trends. I show next that the synthesized cumulate results support this conclusion and examine some of the predictions of these results using Alaska-Aleutian arc lavas.

2.5.2 The Amphibole Sponge: Crustal Water Storage

Davidson et al. (2007) hypothesized that amphibole fractionation in the mid/lower crust would sequester ~20% of H2O from hydrous mantle-derived magma on its passage through the crust: amphibole in the crust acts a "sponge" for water. They assumed that the H2O content of amphibole is ~2-4 wt% so a cumulate composed of 50% amphibole would contain ~1 wt% water. If arc water content of mantle-derived arc magma is 5 wt% (see, e.g., Plank et al., 2013), then as this magma traverses through the crust, 20% of it is sequestered in amphibole.

In my derived solutions of cumulates for Alaska-Aleutian volcanoes, it is straightforward to extract mineral phase quantities and analyze implications from them, since all mineral assemblages of the fractionated cumulates are known. From estimated amounts of amphibole, it is easy to estimate the amount of water stored in the crust under each volcano. I can then lowess-regress and smooth the data to derive curves to characterize the arc. Table 1 summarizes these calculations, which are obtained this way: the synthesized number-of-solutions of cumulates are taken to represent a proportion of rock in the crust. Each step is then summed across the 18 cumulates set of solutions weighted against the total number of solutions obtained for each cumulate. This is done for each volcano. The result is a characteristic cumulate for each of the steps (recall the steps are proxies for depth in the crust). The sum of the 7 steps gives a mineral assemblage taken as approximating the crustal mineralogy under that volcano, according to the modeling. From this, the proportion of amphibole that resides under each volcano is obtained. We now need water content from the incoming magma from the mantle. Zimmer et al. (2010) gave an estimate of the water content of arc magma based on global melt inclusion studies and correlated to volcano's THI ("tholeiitic index"). THI is a quantification of the tholeiitic vs. calc-alkalic affinity of a suite of cogenetic lava based on the iron-enrichment trend in the FeO vs. MgO systematic. Zimmer et al. coupled THI from magmatic systems from various settings with water content in the corresponding melt-inclusions to obtain a correlation between THI and magmatic water content. We use this to derive water input from the mantle for each arc volcano: the lowess regressed curve (and the individual volcano data points) is shown. Figure 2.15 shows amphibole as a fraction of the cumulate per volcano. Amphibole fraction for the crust under each volcano varies between 16 and 26% with a median of 21%. If we assume amphibole contains 4 wt% water (high end of Davidson et al.'s estimate), we obtained for the wt% of water contained in each crustal column, and by lowess regression, the estimated stored water content along the entire arc. This is shown in Figure 2.16 as a flat curve under 1 wt%. The amount of water stored along the Alaska-Aleutian arc is a nearly constant 1 wt%. The mantle magma-water content under most Alaska-Aleutian volcanoes is greater than 2 wt% (green curve, Figure 2.16), but notably, 6 of the transitional and western volcanoes have less. The overall curve reflects the THI curve obtained in Lieu and Stern (2018), i.e., calc-alkaline/thick crust/high water content beneath the western oceanic segment, tholeiitic/thin crust/low water content beneath the transitional segment, and calc-alkaline/thick crust/highest water content beneath the eastern continental segment. Note that the total amount of water is not considered here, only wt%, and the thickness (overall volume) of the crust is neglected. The fraction of water from the mantle intercepted and stored in amphibole of the lower- and mid-crust is shown (orange curve with right ordinate axis). The remaining water that is not bounded in amphibole is shown in the blue curve. This is water present in the magma and can take part in subsequent reactions and add to the volatile budget of erupting lava. It is evident that the tripartite division of the arc as proposed by Lieu and Stern (2018) is exhibited here with the amphibole crustal water storage curves: the transitional tholeiitic segment is dryer than the western and eastern calc-alkaline segment bounding it. This curve may just reflect the THI variation of Zimmer et al. but I propose an alternative interpretation: since the fraction of crustal amphibole is near constant across the arc (~20%) and the wt% of water locked in amphiboles is ~1 wt%, the absolute *volume* of water in amphibole then depends on the thickness of the crust. From Lieu and Stern (2018)'s analysis we accept that the transition segment of the arc is 2/3 the thickness of the east and west segment, and therefore the transition segment holds 2/3 the amount of water as the east and continental segment. I explore the significance of this assertion combined with ideas in the next section.

2.5.3 Density Stratification Of The Arc Crust And Implications For Foundering Of Mafic Cumulates

If we take the synthesized cumulates to resemble a natural geochemical system, they should resemble a physical system as well. Here I examine cumulate densities and their implications for understanding arc processes. The Earth's crust is density stratified, an interpretation derived from seismic velocity profiles that show increased Vp with depth (Meissner, 1986). Arc crusts show average mid crustal P-wave velocities of 5 - 6 km/s, increasing to 7 - 7.2 km/s in the lower crust, then jump from >7.4 to 8 km/s below the Moho (see, e.g., Rudnick and Fountain, 1995). These velocities correlate with lithologies (Jull and Kelemen, 2001; Shillington et al., 2013). For igneous rocks under crustal pressures, P-waves velocity varies approximately linearly with density (Fowler, 1990) so that lithologic density is expected to increase with depth. I calculate the synthesized cumulate densities with an algorithm from Hacker and Abers (2004) and plot the results. Figure 2.11 shows that these cumulates increase in density with increasing MgO. Denser cumulates are fractionated with higher MgO parent-daughter pairs, or higher pressure if MgO serves as a depth proxy. It is worth noting that all the cumulates are denser than normal crust so that they are gravitationally unstable and tend to sink to their buoyancy-neutral depths if the ambient crust is weak enough to allow this. I do not examine sub-arc crustal strength, but likely temperatures in the crust beneath arc volcanoes makes it likely that the weakest crust is found in the midcrust and below. These considerations explain a dearth of mafic rocks in the middle crust because these cumulates would undergo foundering, perhaps by forming inverted diapirs that sink when critical mass is reached (Glazner, 1994).

The density vs. MgO diagram (Figure 2.11) explains the observed Vp vs. depth profile: cumulate densities calculated here are all greater than the ambient crust's. These range from 3 to 3.4 gm/ccm, with a density contrast of > 0.2 gm/ccm. This implies that these cumulates would sink at 1 to 50 km/my when they accumulate and reach a diameter of a few km (Glazner, 1994). This continuous mass-redistribution means that at any instant the subarc middle and lower crust will have some percentage of fractionated mafic masses sinking toward the Moho. If we assume that the arc system is in a dynamically steady state of chemical fractionation and mafic cumulate foundering, the deeper toward the Moho, the more volume will be occupied by these mafic masses (and thereby increasing the Vp velocity profile with depth). Eventually, some of these masses would settle at the Moho (Griffin and O'Reilly, 1987) whereas those with density > 3.3 g/cm^3 would sink deeper into the upper mantle. This results in a sub-arc crustal seismic profile that increases with depth, but which may not have a sharp reflection to mark the Moho because of the mixture of delaminating mass with upper mantle lithology. Shillington et al. (2004) show a 7.4+ km/s layer from 20 to 35 km beneath line A2 of the 1994 Alaska Seismic Experiment (see Figure 2.2 for ASE line A1 location). This may be interpreted as a sub-Moho region of mixed mantle and delaminated lithologies (see below and Lieu and Stern, 2018).

Dense, sunken cumulates containing ~20 wt% amphibole will suffuse the lower arc crust and the upper mantle with structurally-bound water. The lower and midcrust of the continental Alaska-Aleutian arc would seem to be a particularly significant "amphibole sponge" of Davidson et al. (2007), sequestering mantle-derived water in cumulates. This growing layer is likely to be destabilized by the continuous (or periodic) introduction of new mantle melts injected into the lower and midcrust. Over time these repeated injections will heat and weaken the crust, maintaining a lower crustal “hot zone” (Annen et al., 2002, Annen et al., 2006).

The sub-arc geotherm may eventually increase above the stability of amphibole, the breakdown of which will suffuse the hot zone with additional H_2O (Davidson et al., 2007). pMELTS modeling on selected cumulates shows that a 5% melt fraction at 1025ºC will have 5 wt% water, and by ~1050ºC most hornblende is consumed, and the melt will contain 4% water.

This addition of water from amphibole breakdown in the lower crustal hot zone into mantle-derived magma is likely to lead to magmas with enhanced water contents which would also promote calc-alkaline differentiation trends by suppressing plagioclase crystallization. These processes may be important for continental crust construction and thickening. The overall process is a positive feedback mechanism where thicker crust, by having an already thick layer of dense cumulate above the Moho, increases both the chance of more cumulate settlement so that even the densest cumulates are trapped at the crust base, and the chance of magma injections into sills. Both mechanisms increase the crust thickening rate and the continued release of water from amphibole breakdown. This mechanism of trapping cumulates at the crust base which then are heated further and release water into the sub-arc melt environment may also be responsible for the large range in tholeiitic/calc-alkaline magma trends seen in the continental segment (see the CATH index in Figure 2.17). The repeated injection of mantle-derived magma into lower crustal sills and dikes that raises the local geotherm requires a few million years to accomplish (Annen et al., 2006). Magma injection from the mantle may be episodic and locale-specific so that the release of water that promotes calc-alkaline differentiation trends are episodic. It is possible that an active arc with a thick crust (> 30 km as in the Alaska-Aleutian continental segment) goes through alternating cycles of tholeiitic vs. calc-alkaline magma generation dictated by the maturation of the lower crustal hot zone. This effect is less pronounced beneath the Alaska-Aleutian transitional segment, where there is less volume of settled cumulate and structural water remains in amphibole, reinforcing the likelihood that the magma trend there is more tholeiitic. Figure 2.18 graphically illustrates and compares the above conjectures as applied to thin and thick crustal sections.

2.5.4 Fractionation Of Primary Magma And Implications For Foundering Rate

Arc magmagenesis is the most complex mechanism of mantle melting because it combines adiabatic asthenospheric upwelling and solidus depression induced by fluid from the subducted slab (see Pearce and Parkinson, 1993). These two types of melting are seen explicitly in Central America, where geochemistries of arc front lavas were found to be decoupled from backarc lava (Walker et al., 1995), i.e., calc-alkaline trend for arc front volcanism and tholeiitic trend for back-arc volcanism. They proposed that this distinction reflect the melt extractions' physical locales in the mantle wedge: the tholeiitic-like lavas are derived from shallow upwelling of circulating mantle before it dives into the deeper, fluid-rich portion adjacent to the subducting slab, which generates the calc-alkaline arc front lava. Here I use my modeling result to explore the supposition that sinking masses of lower crust cumulates from primary magma fractionation could induce additional mantle upwelling, increase melt fraction and thereby promote more tholeiitic signature that is discernable in our lava analysis.

I built on ideas from Behn et al. (2007) who proposed a model of detaching mass of cumulate/restite from the lower crust into the mantle due to gravitational instability to explain observed trench-parallel fast seismic shear wave velocities. These shear waves' fast polarization direction, interpreted as indicating mantle flow vector, are orientated trench-parallel (Shumagin island, the Aleutian, Yang et al., 1995), perpendicular to the expected direction of flow induced by the subducting slab, which should be trench normal. Behn et al. (2007) explain the trench-parallel anisotropy as reflecting mantle flow induced by sinking masses of the lower crust. They modeled 3D flows of mantle induced by the periodic sinking of slightly denser (> ~0.05 gm/ccm) small-scale (~30 km^2 by ~3 km thick) masses, spaced 40 km apart. These sinking masses drive upper mantle convection and could produce the observed trench parallel seismic anisotropy. I identify these masses as cumulates and restites from primary magma fractionation at the base of the crust and possibly mafic cumulates foundered from lower and midcrust (described in the previous section). This model for trench-parallel seismic anisotropy also have the additional benefit of providing the necessary mechanism of mass-delamination in continental crust generation (see Kodaira et al., 2007). The accompanying adiabatic decompression melting of the mantle induced by sinking cumulates and restites adds complexity to melting of mantle above subduction zones, as summarized by Pearce and Parkinson (1993) and Walker et al. (1995). Induced convection and associated water flux from sinking cumulates and restites beneath arc volcanoes is an additional aspect of convergent margin melt generation. The effects of this additional mechanism would be difficult to distinguish from the accepted mechanisms of adiabatic decompression and flux melting.

Kelemen et al. (2004) studied Talkeetna mafic plutonic rocks (see their Figure 24). They concluded that there is not enough pyroxenite at Mg# > 86 to explain the additional pyroxene needed to generate primary magma estimated by (a later published study) Greene et al. (2006)'s least-square modeling. This is evidence that cumulate masses may have been lost from the lower crust soon after these formed. Behn et al. (2007) used 50% fractionation of primary magma for their modeled cumulates: they modeled delaminated masses of ~60 km3 per few million years, assuming a magma production rate of 50 to 150 km^3/km. This model dynamically removes mantle magma-derived cumulates so that these do not underplate the crustal base, explaining the absence of ultramafic cumulates (note that these are distinct from the mafic cumulates that collect above the Moho discussed in the previous section). My analysis on the least-squares model using synthesized primitive magma at MgO 8 wt% (daughter liquid) with known primary magmas (parent) and known cumulate phases can give detail to these processes. The extent of fractionation needed to generate the cumulates indicates the degree of melting of the primary magma beneath the volcanic front, which informs on the rate at which the delamination mechanism proposed by Behn et al. (2007) operates. Figure 2.12 shows arc overall median %F is ~0.38. This is lower than Behn et al. (2007)'s estimate of 50% and higher than the estimates of 25%, 21%, and 18% by Greene et al. (2006), Conrad and Kay (1984), and DeBari and Sleep (1991), respectively. If I use Jicha et al. (2006)'s parameters for the Aleutian arc crust volume of 8,000 km3 and its age as 46 Ma, and if ultramafic cumulates from the primary magma fractionation delaminate and do not underplate the base of the crust, then the Aleutian arc crust addition rate is 185 km^3/km/Ma (Jicha et al, 2006). If this represents 0.62 (1 - 0.38) of the observed fractionate then it means that 115 km^3/km/Ma of ultramafic cumulates foundered into the mantle dynamically as they form, collect, become increasingly unstable and detach. Thus the total flux from the mantle to the for the arc is (185 + 115) 300 km^3/km/Ma with variation in losses by foundering along the arc expressed in the lowess curve shown in Figure 2.12. It is noteworthy that the along-strike delamination rate reflects a one-cycle of high-low-high for the west to transition to east arc segments, in-phase with a similar CA-TH-CA cycle and thick-thin-thick crust (Lieu and Stern, 2018). This cycle also correlates with the derived Vp curve of the fractionated ultramafic cumulates (Figure 2.12), with higher Vp in the thin transition segment.

2.6 Conclusions

The main result from this chapter is that magmatic fractionation alone can produce compositionally stratified crust at convergent plate margins. This stratification reflects variations in density of multistage cumulates the formed from primary melts to magma with MgO 1 wt%. This was shown using calculates liquid lines of descent constructed by lowess regression of lavas of the Aleutian-Alaskan magmatic arc. That the least squares model produced viable solutions implies that it is fractional crystallization and not crustal melting that is the primary control on the compositional trends seen in these lavas. By generating crustal columns for each of the 28 volcanoes of the Alaska-Aleutian arc, I constructed lowess regression curves to characterize the cumulate mineral assemblages beneath each volcano and used the extracted mean-arc mineral compositions to make general inferences on arc crust construction. Cumulates formed in the mid and lower crust are rich in amphibole and denser than the ambient crust such that they are likely to sink deeper into the lower crust or upper mantle. In this case, the arc lower crust is a repository for water, structurally bound in the mineral amphibole, where it could be released when amphibole is heated sufficiently from repeated injection of mantle magma and breaks down. Water released in the lower crust or upper mantle may have greater control on magmatic trends (tholeiitic vs. calc-alkalic) than heretofore considered. Sub-Moho fractionation of primary melts to MgO 8 wt% magma was also successfully modeled. This gives ultramafic cumulate information such as density and Vp that generally agree that continuous sinking of dense cumulates and residues is a likely mechanism complementing magmatic addition to the crust beneath arcs. From the % fractionation for these cumulate I estimated the mean rate of crustal loss by foundering for the arc to be ~115 km^3/km/my, from the arc crustal growth rate of ~186

km^3/km/my (of Jicha et al., 2006), or a 38:62 cumulate to crust ratio, which is intermediate between the estimates of other studies.

REFERENCES CITED

Annen, C., and Sparks, R.S.J., 2002, Effects of repetitive emplacement of basaltic intrusions on thermal evolution and melt generation in the crust: Earth & Planetary Science Letters, v. 203, p. 937-956.

Annen, C., Blundy, J.D., and Sparks, R.S., 2006, The sources of granitic melt in deep hot zones: Transactions of the Royal Society of Edinburgh: Earth Sciences, v. 97, p. 297-309, doi: 10.1017/S0263593300001462.

Arculus, R.J., and Wills, K.J.A., 1980, The petrology of plutonic blocks and inclusions from the lesser Antilles Island arc: Journal of Petrology, v. 21, p. 743-799, doi: 10.1093/petrology/21.4.743.

Arculus, R.J., 1976, Geology and geochemistry of the alkali basalt-andesite association of Grenada, Lesser Antilles island arc: Bulletin of the Geological Society of America, v. 87, p. 612-624, doi: GAGOTA>2.0.CO;2.

Atwater, T., 1989, Plate tectonic history of the Northeast Pacific and western North America: Denver, CO, Denver, CO, United States: Geol. Soc. Am, p. 21-72.

Bédard, J.H., 2006, A catalytic delamination-driven model for coupled genesis of Archaean crust and sub-continental lithospheric mantle: Geochimica Et Cosmochimica Acta, v. 70, p. 1188-1214, doi: 10.1016/j.gca.2005.11.008.

Behn, M.D., and Kelemen, P.B., 2006, Stability of arc lower crust: Insights from the Talkeetna arc section, south central Alaska, and the seismic structure of modern arcs: Journal of Geophysical Research B: Solid Earth, v. 111, p. , doi: 10.1029/2006JB004327.

Behn, M.D., Hirth, G., and Kelemen, P.B., 2007, Trench-parallel anisotropy produced by foundering of arc lower crust: Science (New York, N.Y.), v. 317, p. 108, doi: 10.1126/science.1141269.

Bender, J.F., Hodges, F.N., and Bence, A.E., 1978, Petrogenesis of basalts from the project FAMOUS area: experimental study from 0 to 15 kbars: Earth and Planetary Science Letters, v. 41, p. 277-302, doi: 10.1016/0012-821X(78)90184-X.

Bohrson, W.A., and Spera, F.J., 2001, Energy-Constrained Open-System Magmatic Processes II: Application of Energy-Constrained Assimilation–Fractional Crystallization (EC-AFC) Model to Magmatic Systems: Journal of Petrology, v. 42, p. 1019-1042.

Cleveland, W.S., 1993, Visualizing data: Summit, NJ, Hobart Press, p. 360.

Conrad, W.K., and Kay, R.W., 1984, Ultramafic and mafic inclusions from Adak Island; crystallization history, and implications for the nature of primary magmas and crustal evolution in the Aleutian Arc: Journal of Petrology, v. 25, p. 88-125, doi: 10.1093/petrology/25.1.88.

Davidson, J., Handley, H., Macpherson, C., Turner, S., and Dosseto, A., 2007, Amphibole "sponge" in arc crust? Geology, v. 35, p. 787-790, doi: 10.1130/G23637A.1.

DeBari, S.M., Coleman, R.G., 1989, Examination of the deep levels of an island arc: evidence from the Tonsina ultramafic-mafic assemblage, Tonsina, Alaska
: Journal of Geophysical Research, v. 94, p. 4373-4391.

Debari, S., Mahlburg Kay, S., and Kay, R.W., 1987, Ultramafic xenoliths from Adagdak volcano, Adak, Aleutian Islands, Alaska; deformed igneous cumulates from the Moho of an island arc: Journal of Geology, v. 95, p. 329-341, doi: 10.1086/629133.

DeMets, C., Gordon, R.G., Argus, D.F., and Stein, S., 1994, Effect of recent revisions to the geomagnetic reversal time scale on estimates of current plate motions: Geophysical Research Letters, v. 21, p. 2191-2194, doi: 10.1029/94GL02118.

Depaolo, D.J., 1981, Trace element and isotopic effects of combined wallrock assimilation and fractional crystallization: Earth and Planetary Science Letters, v. 53, p. 189-202, doi: 10.1016/0012-821X(81)90153-9.

Efron, B., and Tibshirani, R., 1993, An introduction to the bootstrap: New York, New York : Chapman & Hall, .

Fliedner, M.M., and Klemperer, S.L., 2000, Crustal structure transition from oceanic arc to continental arc, eastern Aleutian Islands and Alaska Peninsula: Earth and Planetary Science Letters, v. 179, p. 567-579, doi: 10.1016/S0012-821X(00)00142-4.

Fowler, C.M.R., 1990, The solid earth : an introduction to global geophysics: Cambridge England, Cambridge University Press, .

Fujii, T., and Scarfe, C., 1985, Composition of liquids coexisting with spinel lherzolite at 10 kbar and the genesis of MORBs: Contributions to Mineralogy and Petrology, v. 90, p. 18-28, doi: 10.1007/BF00373037.

Ghiorso, M.S., Hirschmann, M.M., Reiners, P.W., and Kress, V.C., 2002, The pMELTS: A revision of MELTS for improved calculation of phase relations and major element partitioning related to partial melting of the mantle to 3 GPa: Geochemistry, Geophysics, Geosystems, v. 3, p. 1-35, doi: 10.1029/2001GC000217.

Gill, J.B., 1981, Orogenic andesites and plate tectonics: Berlin ; New York, Berlin ; New York : Springer-Verlag, .

Glazner, A.F., 1994, Foundering of mafic plutons and density stratification of continental crust: Geology, v. 22, p. 435-438, doi: LOTTSO>2.3.CO;2.

Greene, A.R., DeBari, S.M., Kelemen, P.B., Blusztajn, J., and Clift, P.D., 2006, A Detailed Geochemical Study of Island Arc Crust: the Talkeetna Arc Section, South–Central Alaska: Journal of Petrology, v. 47, p. 1051-1094, doi: 10.1093/petrology/egl002.

Griffin, W.L., and O'Reilly, S.Y., 1987, Is the continental Moho the crust- mantle boundary? Geology, v. 15, p. 241-244, doi: ITCMTC>2.0.CO;2.

Hacker, B., Mehl, L., Kelemen, P., Rioux, M., Behn, M.D., and Luffi, P., 2008, Reconstruction of the Talkeetna intraoceanic arc of Alaska through thermobarometry: Journal of Geophysical Research-Solid Earth; J.Geophys.Res.-Solid Earth, v. 113, , doi: 10.1029/2007JB005208.

Hacker, B.R., and Abers, G.A., 2004, Subduction Factory 3: An Excel worksheet and macro for calculating the densities, seismic wave speeds, and H2O contents of minerals and rocks at pressure and temperature: Geochemistry, Geophysics, Geosystems, v. 5, p. n/a, doi: 10.1029/2003GC000614.

Hildreth, W., and Moorbath, S., 1988, Crustal contributions to arc magmatism in the Andes of Central Chile: Contributions to Mineralogy and Petrology, v. 98, p. 455-489, doi: 10.1007/BF00372365.

Holbrook, W.S., Lizarralde, W.S., McGeary, W.S., Bangs, W.S., and Diebold, W.S., 1999, Structure and composition of the Aleutian island arc and implications for continental crustal growth: Geology, v. 27, p. 31-34, doi: SACOTA>2.3.CO;2.

Hora, J.M., Singer, B.S., Wörner, G., Beard, B.L., Jicha, B.R., and Johnson, C.M., 2009, Shallow and deep crustal control on differentiation of calc-alkaline and tholeiitic magma: Earth and Planetary Science Letters, v. 285, p. 75-86, doi: 10.1016/j.epsl.2009.05.042.

Jagoutz, O., and Schmidt, M.W., 2013, The composition of the foundered complement to the continental crust and a re-evaluation of fluxes in arcs: Earth and Planetary Science Letters, v. 371-372, p. 177-190, doi: 10.1016/j.epsl.2013.03.051.

Jagoutz, O., 2014, Arc crustal differentiation mechanisms: Earth & Planetary Science Letters, v. 396, p. 267-278, doi: 10.1016/j.epsl.2014.03.060.

Jagoutz, O., and Behn, M.D., 2013, Foundering of lower island-arc crust as an explanation for the origin of the continental Moho: Nature, v. 504, p. 131-135, doi: 10.1038/nature12758.

Janoušek, V., 2016, Geochemical Modelling of Igneous Processes – Principles And Recipes in R Language : Bringing the Power of R to a Geochemical Community: Berlin, Heidelberg : Springer Berlin Heidelberg : Imprint: Springer, .

Jicha, B.R., Scholl, D.W., Singer, B.S., Yogodzinski, G.M., and Kay, S.M., 2006, Revised age of Aleutian Island Arc formation implies high rate of magma production: Geology, v. 34, p. 661-665, doi: 10.1130/022433.1.

Jull, M., and Kelemen, P.B., 2001, On the conditions for lower crustal convective instability: Journal of Geophysical Research: Solid Earth, v. 106, p. 6423-6446, doi: 10.1029/2000JB900357.

Jun-Ichi Kimura, 2017, Modeling chemical geodynamics of subduction zones using the Arc Basalt Simulator version 5: Geosphere, v. 13, p. 992-1026.

Kay, R.W., 1978, Aleutian magnesian andesites: Melts from subducted Pacific ocean crust: Journal of Volcanology and Geothermal Research, v. 4, p. 117-132, doi: 10.1016/0377-0273(78)90032-X.

Kay, S.M., and Kay, R.W., 1985, Role of crystal cumulates and the oceanic crust in the formation of the lower crust of the Aleutian arc: Geology, v. 13, p. 461-464, doi: ROCCAT>2.0.CO;2.

Kay, S.M., Kay, R.W., and Citron, G.P., 1982, Tectonic controls on tholeiitic and calc-alkaline magmatism in the Aleutian arc
: Journal of Geophysical Research, v. 87, p. 4051-4072, doi: 10.1029/JB087iB05p04051.

Kelemen, P. B., G. M. Yogodzinski, D. W. Scholl, 2003, Along strike variation in the Aleutian Island Arc: Genesis of high Mg# andesite and implications for continental crust
, in Inside the Subduction Factory: The American Geophysical Union, p. 223.

Kelemen, P.B., Hanghoj, K., Greene, AR., 2004, One view of the geochemistry of subduction-related magmatic arcs with an emphasis on primitive andesite and lower crust
, in Holland, H.D., Turekian, K.K., ed., Treatise on Geochemistry: Amsterdam, Elsevier Pergamon, p. 593-647.

Kelemen, P.B., and Behn, M.D., 2016, Formation of lower continental crust by relamination of buoyant arc lavas and plutons: Nature Geoscience, v. 9, , doi: 10.1038/ngeo2662.

Kodaira, S., Sato, T., Takahashi, N., Ito, A., Tamura, Y., Tatsumi, Y., and Kaneda, Y., 2007, Seismological evidence for variable growth of crust along the Izu intraoceanic arc: Journal of Geophysical Research B: Solid Earth, v. 112, p. , doi: 10.1029/2006JB004593.

Lizarralde, D., Holbrook, W., Mcgeary, S., Bangs, N., and Diebold, J., 2002, Crustal construction of a volcanic arc, wide-angle seismic results from the western Alaska Peninsula: Journal of Geophysical Research-Solid Earth, v. 107, , doi: 10.1029/2001JB000230.

Mangan, M., Miller, T., Waythomas, C., Trusdell, F., Calvert, A., and Layer, P., 2009, Diverse lavas from closely spaced volcanoes drawing from a common parent: Emmons Lake Volcanic Center, Eastern Aleutian Arc: Earth & Planetary Science Letters, v. 287, p. 363-373, doi: 10.1016/j.epsl.2009.08.018.

Medard, E., Schmidt, M.W., Schiano, P., and Ottolini, L., 2006, Melting of Amphibole-bearing Wehrlites: an Experimental Study on the Origin of Ultra-calcic Nepheline-normative Melts: Journal of Petrology, v. 47, p. 481-504, doi: 10.1093/petrology/egi083.

Meissner, R., 1986, The continental crust : a geophysical approach: Orlando, Fla., Academic Press, .

Nye, C.J., Reid, M.R., 1986, Geochemistry of primary and least fractionated lavas from Okmok volcano, Central Aleutians: implications for arc magmagenesis
: Journal of Geophysical Research, v. 91, p. 10,287.

Pearce, J.A., and Parkinson, I.J., 1993, Trace element models for mantle melting: Application to volcanic arc petrogenesis: Geological Society Special Publication, v. 76, p. 373-403, doi: 10.1144/GSL.SP.1993.076.01.19.

Plank, T., Kelley, K.A., Zimmer, M.M., Hauri, E.H., and Wallace, P.J., 2013, Why do mafic arc magmas contain ∼4 wt% water on average? Earth and Planetary Science Letters, v. 364, p. 168-179, doi: 10.1016/j.epsl.2012.11.044.

Rapp, R., and Watson, E., 1995, Dehydration melting of metabasalt at 8-32 kbar; implications for continental growth and crust-mantle recycling: Journal of Petrology; J.Petrol., v. 36, p. 891-931, doi: 10.1093/petrology/36.4.891.

Rudnick, R.L., 1995, Making continental crust: Nature, v. 378, p. 571-579.

Rudnick, R.L., and Fountain, D.M., 1995, Nature and composition of the continental crust: A lower crustal perspective: Reviews of Geophysics, v. 33, p. 267-309.

Ryan, W.B.F., Carbotte, S.M., Coplan, J.O., O' Hara, S., Melkonian, A., Arko, R., Weissel, R.A., Ferrini, V., Goodwillie, A., Nitsche, F., Bonczkowski, J., and Zemsky, R., 2009, Global Multi‐Resolution Topography synthesis: Geochemistry, Geophysics, Geosystems, v. 10, p. n/a, doi: 10.1029/2008GC002332.

Shillington, D.J., Van Avendonk, Harm J A, Behn, M.D., Kelemen, P.B., and Jagoutz, O., 2013, Constraints on the composition of the Aleutian arc lower crust from VP/VS: Geophysical Research Letters, v. 40, p. 2579-2584, doi: 10.1002/grl.50375.

Shillington, D.J., Van Avendonk, Harm J A, Holbrook, W.S., Kelemen, P.B., and Hornbach, M.J., 2004, Composition and structure of the central Aleutian island arc from arc‐parallel wide‐angle seismic data: Geochemistry, Geophysics, Geosystems, v. 5, p. n/a, doi: 10.1029/2004GC000715.

Singer, B.S., Jicha, B.R., Leeman, W.P., Rogers, N.W., Thirlwall, M.F., Ryan, J., and Nicolaysen, K.E., 2007, Along-strike trace element and isotopic variation in Aleutian Island arc basalt: Subduction melts sediments and dehydrates serpentine: Journal of Geophysical Research B: Solid Earth, v. 112, p. , doi: 10.1029/2006JB004897.

Spera, F. J., Bohrson, W. A., 2001, Energy-Constrained Open-System Magmatic Processes I: General Model and Energy-Constrained Assimilation and Fractional Crystallization (EC-AFC) Formulation: Journal of Petrology, v. 42, p. 999-1019.

Syracuse, E.M., and Abers, G.A., 2006, Global compilation of variations in slab depth beneath arc volcanoes and implications: Geochemistry, Geophysics, Geosystems, v. 7, p. n/a, doi: 10.1029/2005GC001045.

Stanley, C., 2017, Lithogeochemical classification of igneous rocks using Streckeisen ternary diagrams: Geochemistry: Exploration, Environment, Analysis, v. 17, p. 63-91.

Tatsumi, Y., Shukuno, H., Tani, K., Takahashi, N., Kodaira, S., and Kogiso, T., 2008, Structure and growth of the Izu-Bonin-Mariana arc crust: 2. Role of crust-mantle transformation and the transparent Moho in arc crust evolution: Journal of Geophysical Research: Solid Earth, v. 113, p. , doi: 10.1029/2007JB005121.

Tatsumi, Y., 1982, Origin of high-magnesian andesites in the Setouchi volcanic belt, southwest Japan, II. Melting phase relations at high pressures: Earth and Planetary Science Letters, v. 60, p. 305-317, doi: 10.1016/0012-821X(82)90009-7.

Taylor, S.R., and White, A.J.R., 1965, Geochemistry of Andesites and the Growth of Continents: Nature, v. 208, p. 271, doi: 10.1038/208271a0.

Van Avendonk, Harm J A, Shillington, D.J., Holbrook, W.S., and Hornbach, M.J., 2004, Inferring crustal structure in the Aleutian island arc from a sparse wide‐angle seismic data set: Geochemistry, Geophysics, Geosystems, v. 5, p. n/a, doi: 10.1029/2003GC000664.

Walker, J., Carr, M., Patino, L., Johnson, C., Feigenson, M., and Ward, R., 1995, Abrupt change in magma generation processes across the Central American arc in southeastern Guatemala: flux-dominated melting near the base of the wedge to decompression melting near the top of the wedge: Contributions to Mineralogy and Petrology, v. 120, p. 378-390, doi: 10.1007/BF00306515.

Wright, T.L., and Doherty, P.C., 1970, A linear programming and least squares computer method for solving petrologic mixing problems: Bulletin of the Geological Society of America, v. 81, p. 1995-2008, doi: ALPALS]2.0.CO;2.

Yang, X., Fischer, K., and Abers, G., 1995, Seismic anisotropy beneath the Shumagin Islands segment of the Aleutian-Alaska subduction zone: Journal of Geophysical Research-Solid Earth, v. 100, p. 18165-18177, doi: 10.1029/95JB01425.

Zimmer, M.M., Plank, T., Hauri, E.H., Yogodzinski, G.M., Stelling, P., Larsen, J., Singer, B., Jicha, B., Mandeville, C., and Nye, C.J., 2010, The Role of Water in Generating the Calc-alkaline Trend: New Volatile Data for Aleutian Magmas and a New Tholeiitic Index: Journal of Petrology, v. 51, p. 2411-2444, doi: 10.1093/petrology/egq062.

APPENDIX - FIGURES AND CAPTIONS

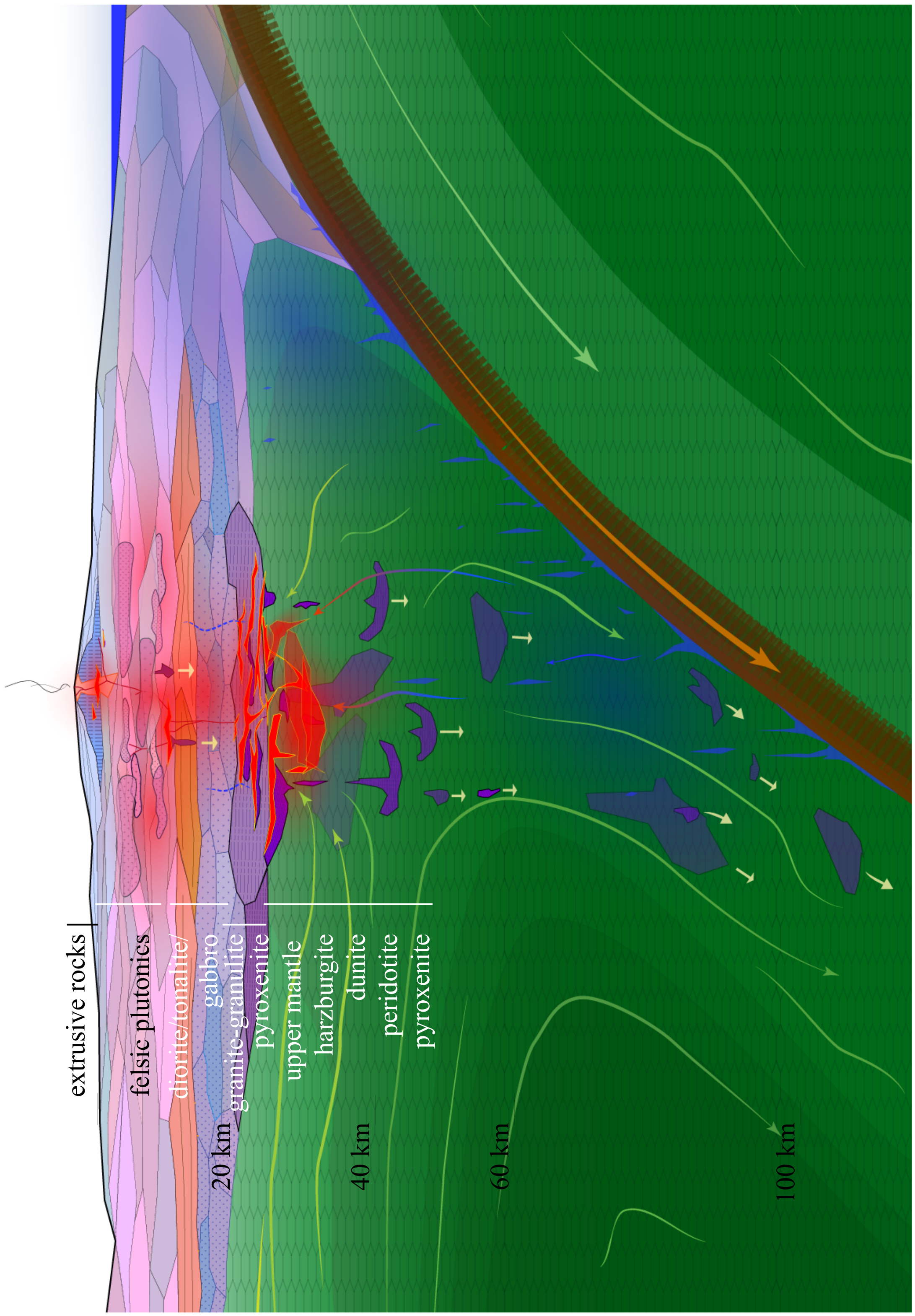

extrusive rocks
felsic plutonics
diorite/tonalite/
gabbro
granite-granulite
pyroxenite
upper mantle
harzburgite
dunite
peridotite
pyroxenite
20 km
40 km
60 km
100 km

Figure 2.1

Figure 2.1: Fractionation and delamination in arc crust genesis.
Schematic diagram encapsulates the main magmatic process occurring beneath magmatic arcs. A typical oceanic magmatic arc undergoing flux- and decompression-melt generation, fractionation at the Moho, delamination of cumulate masses at the Moho, fractionation and melting within the crust with foundering of mafic cumulate and restite masses toward the Moho. Fractionation and density settling processes within the crust produce its stratifications (labeled at left) while fractionation of primary magma and delamination of cumulates from the Moho drive the overall crust compositions. Crustal hot zones are idealized as red glows around melt sills. Matured crustal hot zones induce thermal breakdown of amphibole-rich cumulate releasing the stored water into the crust (thin blue broken lines). Also depicted are local mantle flows induced by sinking ultramafic cumulate masses, resulting in enhanced decompression melting beneath the Moho. The depiction approximates the amount of ultramafic mass foundered into the mantle as estimated in the Discussion section.

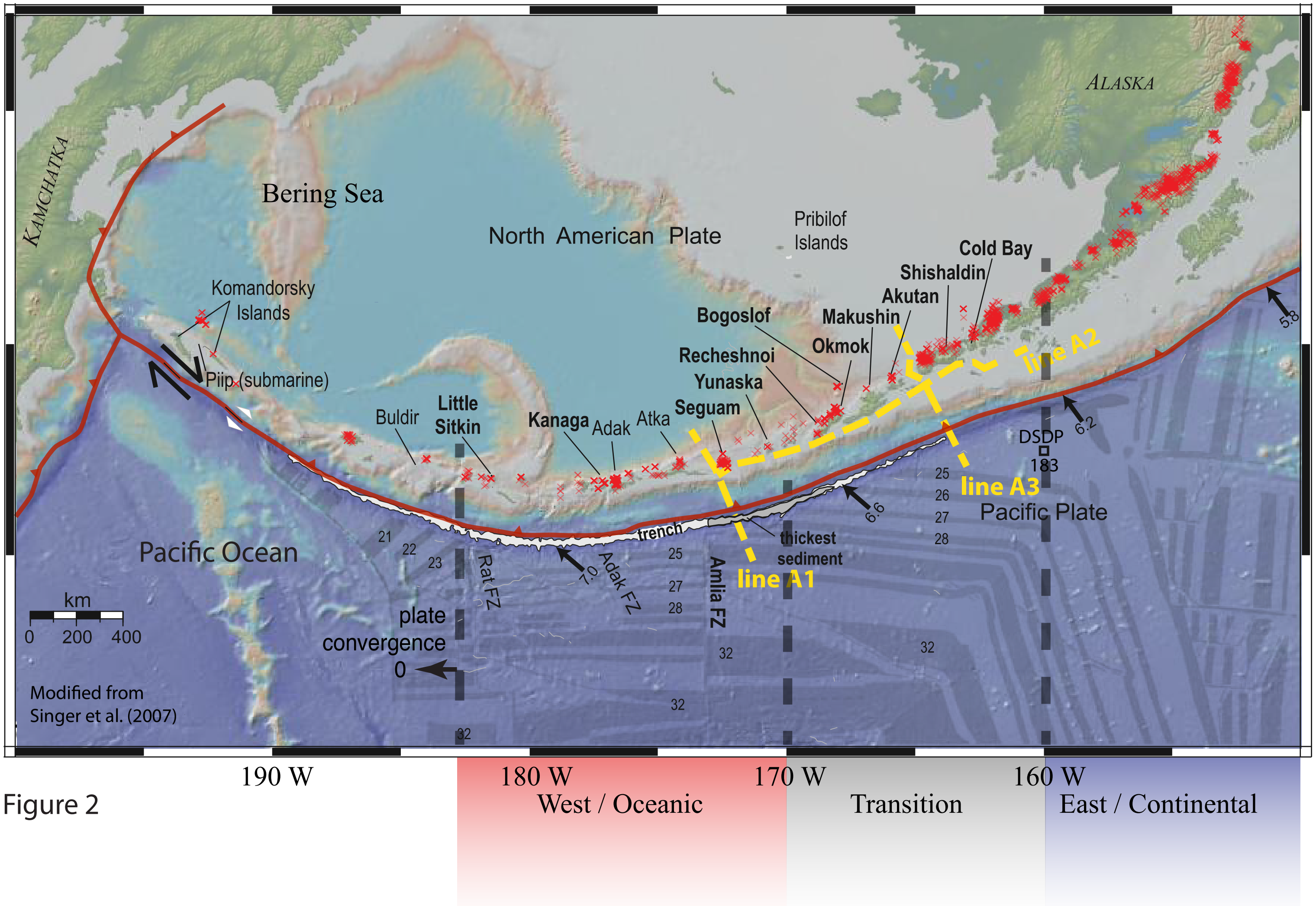

KAMCHATKA
Bering Sea
North American Plate
Pribilof Islands
ALASKA
Komandorsky Islands
Piip (submarine)
Buldir
Little Sitkin
Kanaga
Adak
Atka
Seguam
Yunaska
Recheshnoi
Bogoslof
Okmok
Makushin
Akutan
Shishaldin
Cold Bay
line A1
line A2
line A3
DSDP 183
Pacific Plate
Pacific Ocean
trench
thickest sediment
Rat FZ
Adak FZ
Amlia FZ
plate convergence
km
0 200 400
Modified from Singer et al. (2007)
60 N
55 N
50 N
45 N
190 W
180 W
170 W
160 W
West / Oceanic
Transition
East / Continental

Figure 2

Figure 2.2: The Alaska-Aleutian convergent margin.
The Alaska-Aleutian subduction zone with volcanic sample locations plotted as 'x's. The approximate boundary between oceanic (Aleutian) and continental (Alaska Peninsula) portions of the arc system is near 165ºE. Approximately ±5º on either side of 165°E is designated as the "Transition" segment, labeled at bottom. "East/Continental" and "West/Oceanic" segment used in this study are designated as shown. Major volcano /island names are labeled on the map. "line A1", "line A2", and "line A3" are tracks from the Alaska Seismic Experiment (ASE) of 1994. The map is modified from Singer et al. (2007), it includes relative plate velocity from DeMets et al. (1994) and marine magnetic anomalies from Atwater (1989). The colored base map was generated with GeoMapApp (www.geomapapp.com, Ryan, et al., 2009).

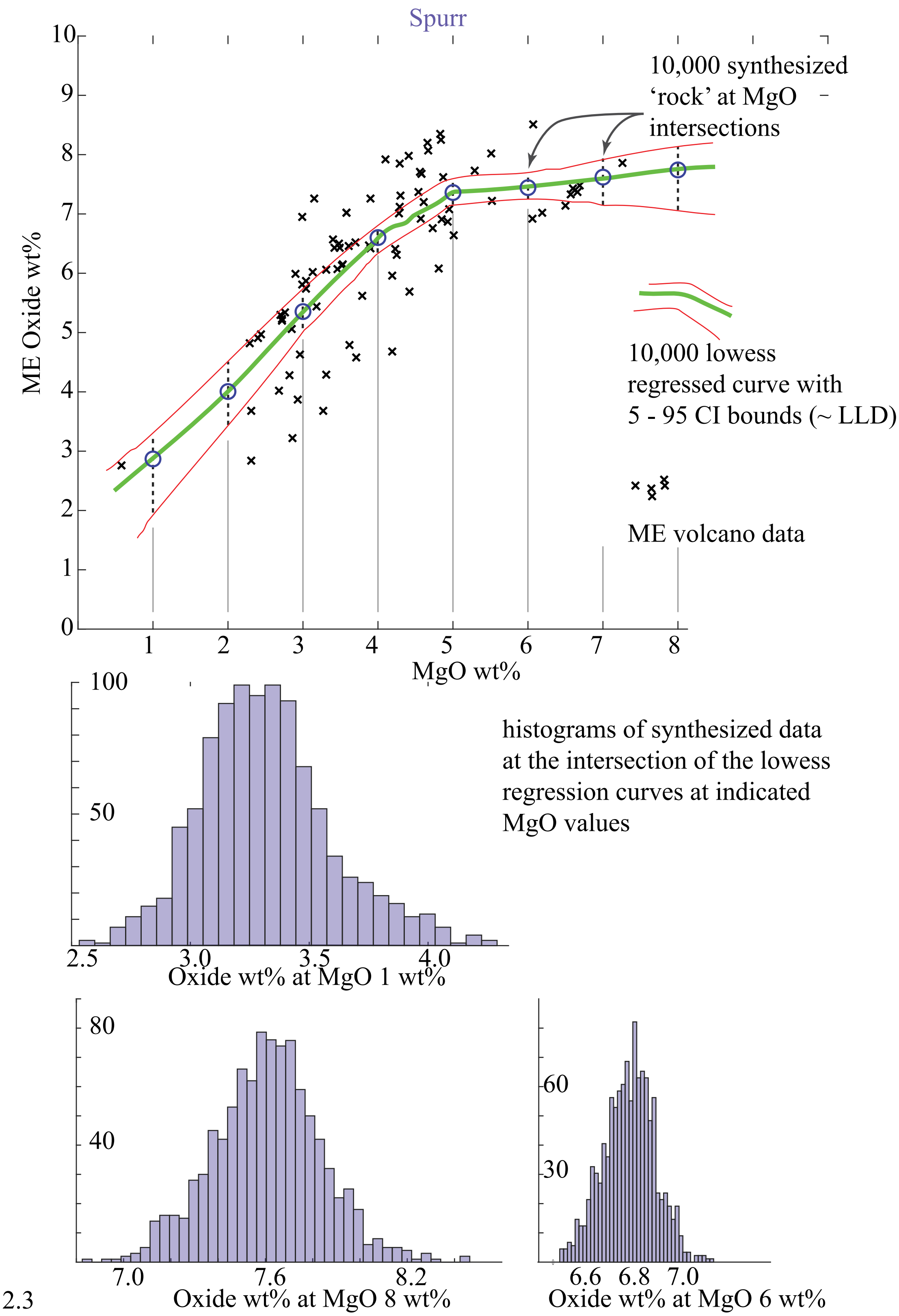
Spurr
10,000 synthesized
'rock' at MgO
intersections
10,000 lowess
regressed curve with
5 - 95 CI bounds (~ LLD)
ME volcano data
ME Oxide wt%
MgO wt%
histograms of synthesized data
at the intersection of the lowess
regression curves at indicated
MgO values
Oxide wt% at MgO 1 wt%
Oxide wt% at MgO 8 wt%
Oxide wt% at MgO 6 wt%

Figure 2.3

Figure 2.3: Synthesizing oxides.
The figure shows a schematic explanation of creating the 10,000 oxides for each of the 8 MgO wt% steps for one oxide of one volcano (Spurr). Harker diagram with lowess regression curves constructed from existing downloaded volcano sample data here plotted as black ‘x’s. Shown is the median curve (green), with the 5- and 95-% confidence curves bounding the 10,000 bootstrapped curves (not shown). These curves are proposed to approximate the liquid line-of-descent for the indicated oxides and are used to create the oxide values at the MgO wt% 8, 7,...,1 resulting in 7 steps of 10,000 values each that are used in the step-wise least square parent-daughter fractionation scheme. The right panel shows typical sample histograms of the distribution of the population of the synthesized data.

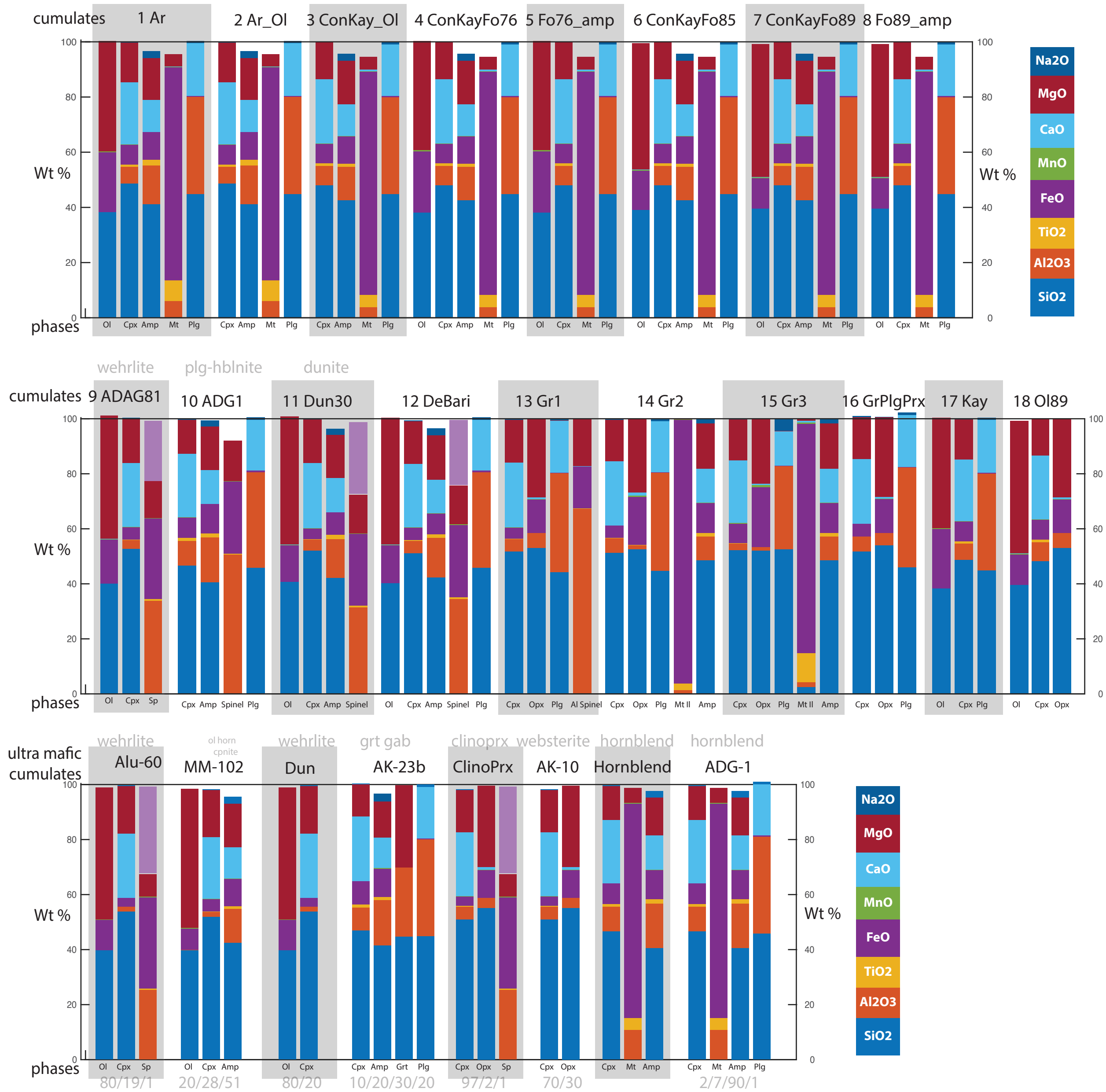

Figure 2.4

Figure 2.4: Major element compositions of cumulate assemblages used in this study. Cumulates used in the least square method are shown with the proportion of major oxides represented by color bars. Each column depicts the compositions of the phase identified at the base of the column. Color legend indicating oxides is shown at right. The phases that compose a particular cumulate rock are distinguished by the presence/absence of a gray box, labels at the top identify the cumulate name (see Method section for references). Top two rows are cumulate phases used for mafic steps (1 to 7), lowest row shows cumulate phases used for ultramafic steps (0).

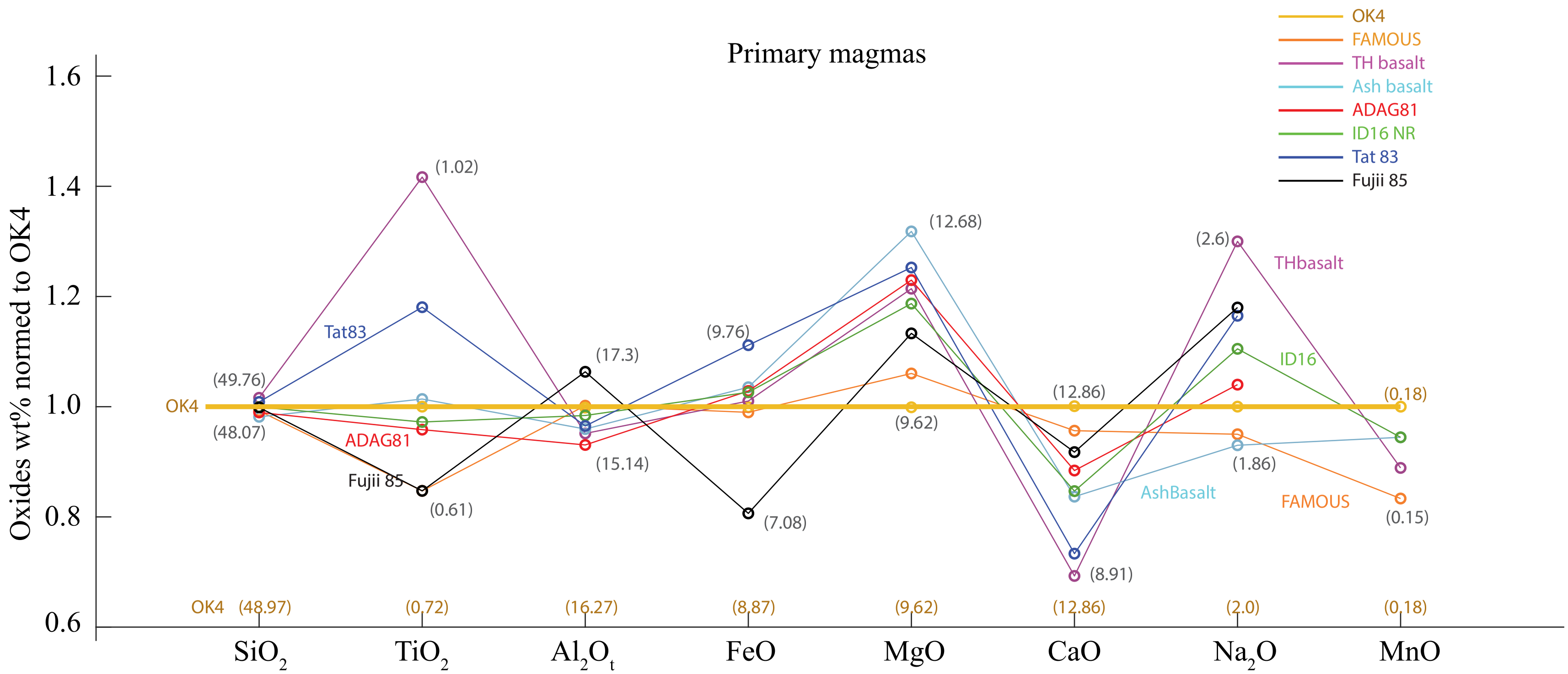

Figure 2.5

Figure 2.5: Primary magmas compositions.
Primary magmas major elements Primary magmas employed as unfractionated mantle-derived parental magma for least-square modeling step 0. Major element compositions of the eight candidate parental magmas are normalized to values of OK4. Colored lines link oxides of the eight candidate primary magmas. Numbers in parentheses next to colored circles identify oxides in wt %.

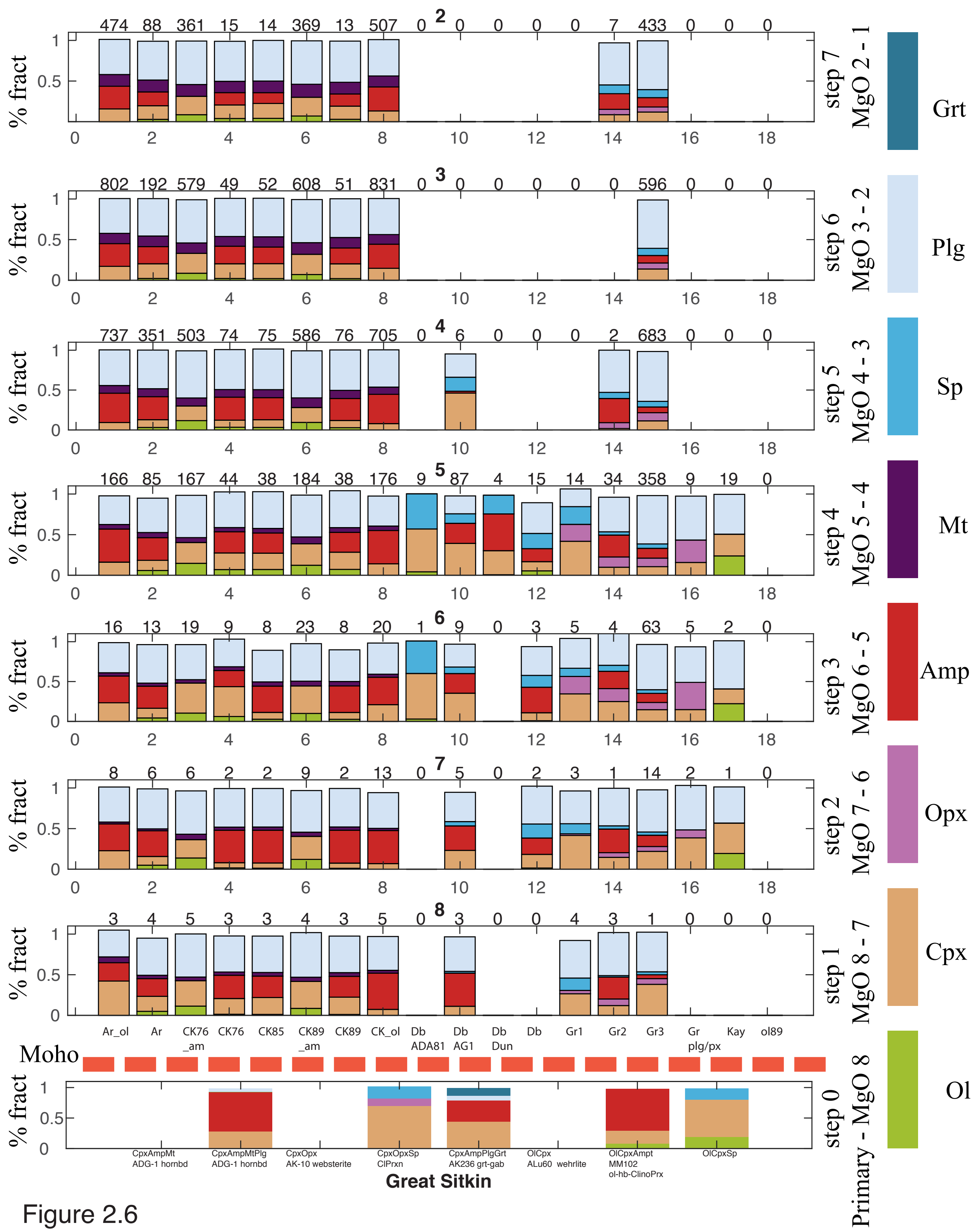

Figure 2.6

Figure 2.6: Least square solutions of cumulate proportions, step 0, and steps 1 to 7.
Phase proportions from the least square solutions (after filtering) for a volcano, 7 + 1 fractionation steps, and 18 + 8 cumulate mineral assemblages, the " +1" and "+8" refer to the fractionation of the primary magma (step 0). This is the typical scheme for displaying the least squares solution per volcano. One (Great Sitkin) is shown here. The other 27 volcanoes are found in the appendix. The name of the volcano is displayed at the bottom. Each long-horizontal box contains solutions for 1 steps (with step number at right), with 18 mineral assemblages within each step (identification of assemblage at the bottom of the second-from-bottom long box, see text for details of each assemblage). The bottom long box contains solutions of the primary-magma-to-MgO-8wt% (step 0) with its 8 cumulate mineral assemblages (see text for details of each assemblage). The "Moho" line separates the primary magma fractionation from those of the lavas'. The solution of mineral proportions for one step with one mineral assemblage is one stacked bar with the minerals coded by color (color keys shown at extreme right margins). Each stacked bar's colored division represents medians of phase proportion of the cumulate solutions. The number of solutions obtained per 1,000 trials (as described in the text) is indicated by the numeral on top of each stacked bar. The number of solution/1000 trials also serves as a weight (as a proportion of the total number of solution for that step) used when extracting quantities from these solutions: cumulate assemblage at a particular step having a greater number of solutions is weighted more for the overall calculation.

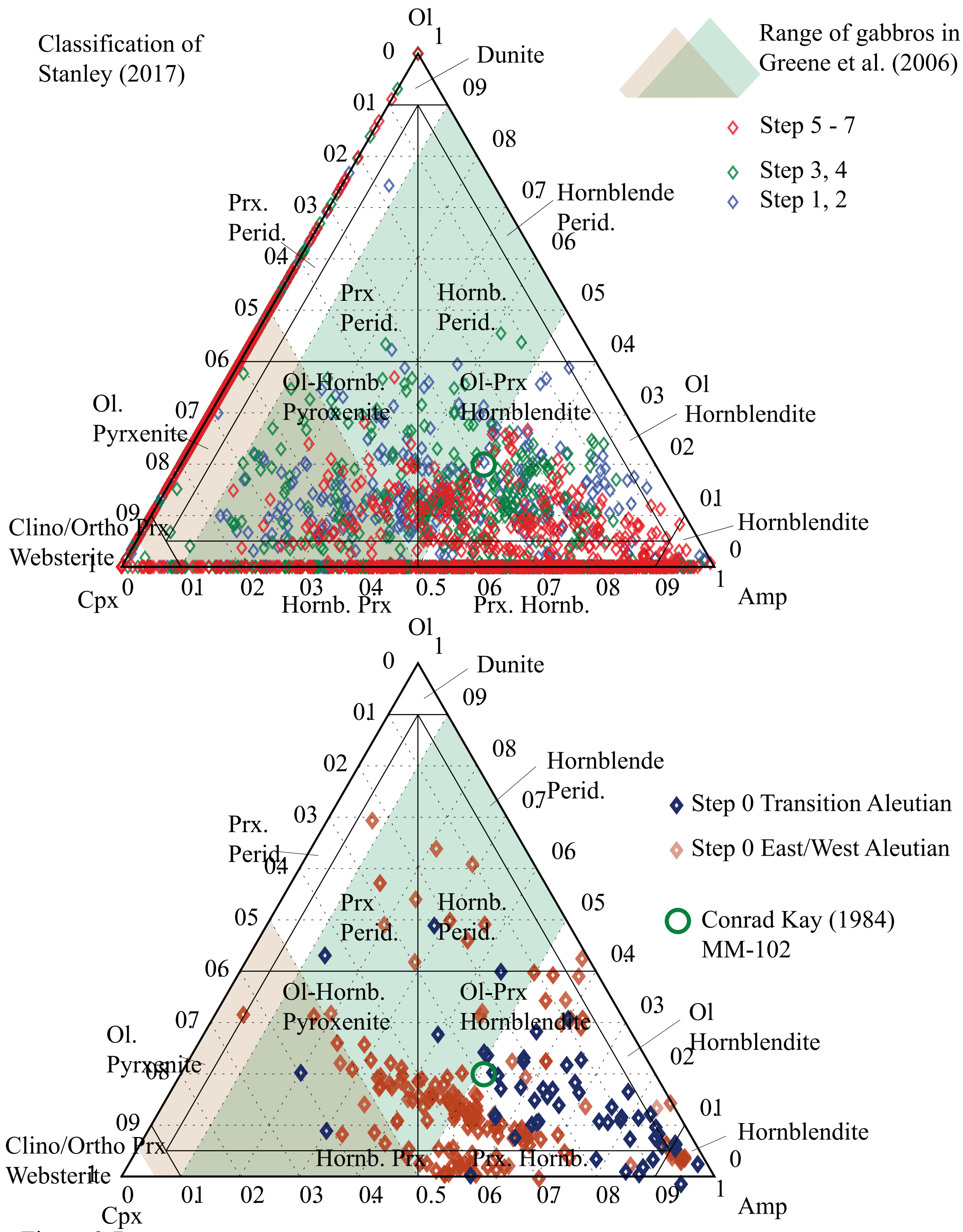
Classification of
Stanley (2017)
Range of gabbros in
Greene et al. (2006)
Step 5 - 7
Step 3, 4
Step 1, 2
Ol
Dunite
Hornblende
Perid.
Prx.
Perid.
Prx
Perid.
Hornb.
Perid.
Ol-Hornb.
Pyroxenite
Ol-Prx
Hornblendite
Ol.
Pyrxenite
Ol
Hornblendite
Hornblendite
Clino/Ortho Prx
Websterite
Cpx
Amp
Hornb. Prx
Prx. Hornb.
Step 0 Transition Aleutian
Step 0 East/West Aleutian
Conrad Kay (1984)
MM-102

Figure 2.7

Figure 2.7: Ternary diagrams 1.
Fractionated cumulates on clinopyroxene-olivine-amphibole ternary diagrams. Steps 1 to 7 and step 0 cumulates plotted on the left and right diagram, respectively. Most cumulates from all steps occupied the olivine pyroxenite or olivine hornblendite fields. Fields showing ranges of gabbros and norites of Greene et al. (2006) are superimposed on the diagrams. The synthesized cumulates are richer in amphibole than the Greene et al.'s Talkeetna gabbro composition.

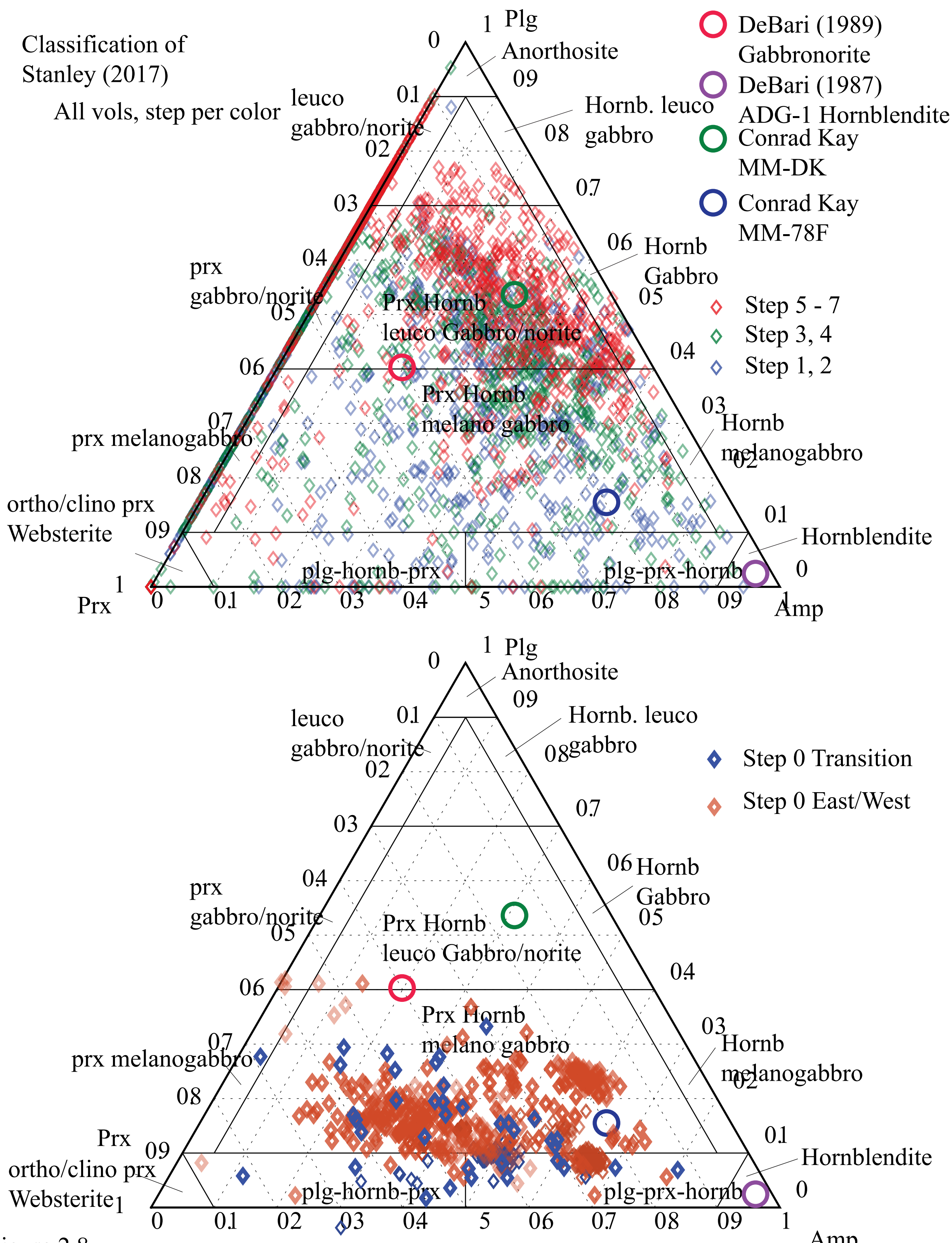
Classification of
Stanley (2017)
All vols, step per color
Plg
Anorthosite
leuco
gabbro/norite
Hornb. leuco
gabbro
prx
gabbro/norite
Hornb
Gabbro
Prx Hornb
leuco Gabbro/norite
Prx Hornb
melano gabbro
prx melanogabbro
Hornb
melanogabbro
ortho/clino prx
Websterite
Hornblendite
plg-hornb-prx
plg-prx-hornb
Prx
Amp
DeBari (1989)
Gabbronorite
DeBari (1987)
ADG-1 Hornblendite
Conrad Kay
MM-DK
Conrad Kay
MM-78F
Step 5 - 7
Step 3, 4
Step 1, 2
Step 0 Transition
Step 0 East/West

Figure 2.8

Figure 2.8: Ternary diagrams 2.
Fractionated cumulates on pyroxene-plagioclase-amphibole ternary diagrams. Steps 1 to 7 and step 0 cumulates plotted on the left and right diagram, respectively. Step 0 gabbros tend to be poorer in plagioclase than the intracrustal gabbros.

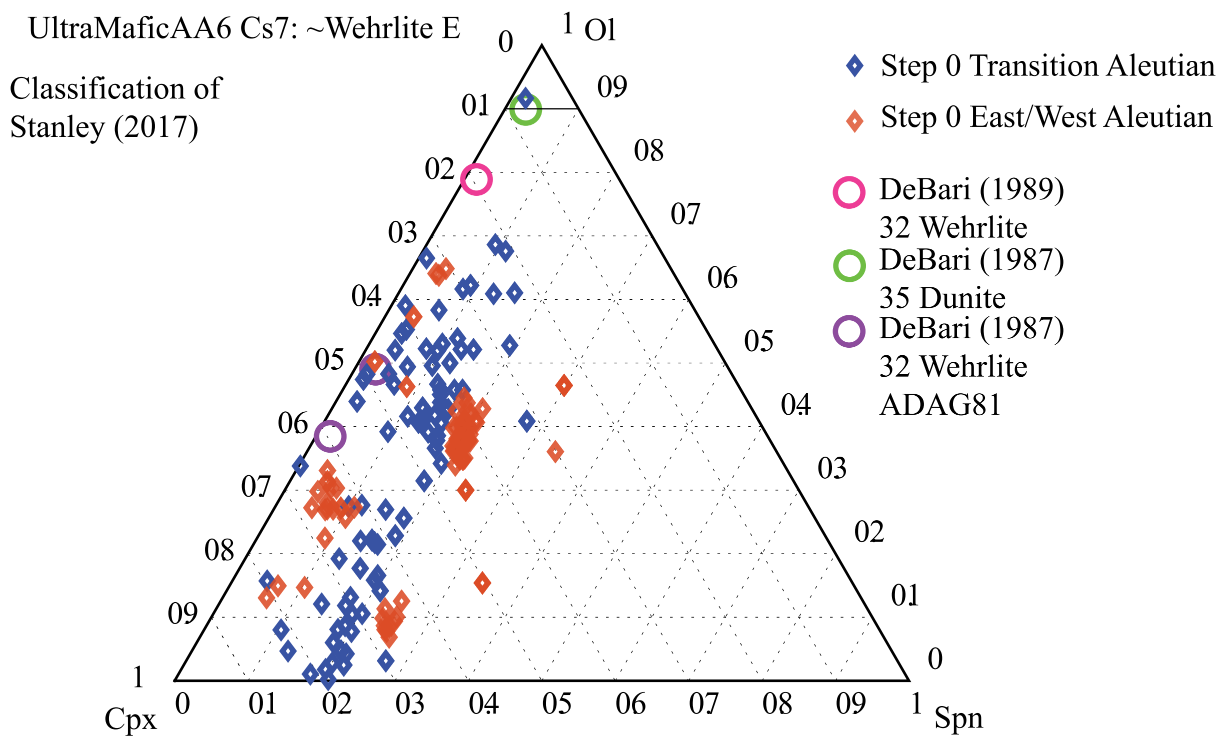

Figure 2.9: Ternary diagram 3.
Spinel-bearing wehrlites of the step 0 cumulates.

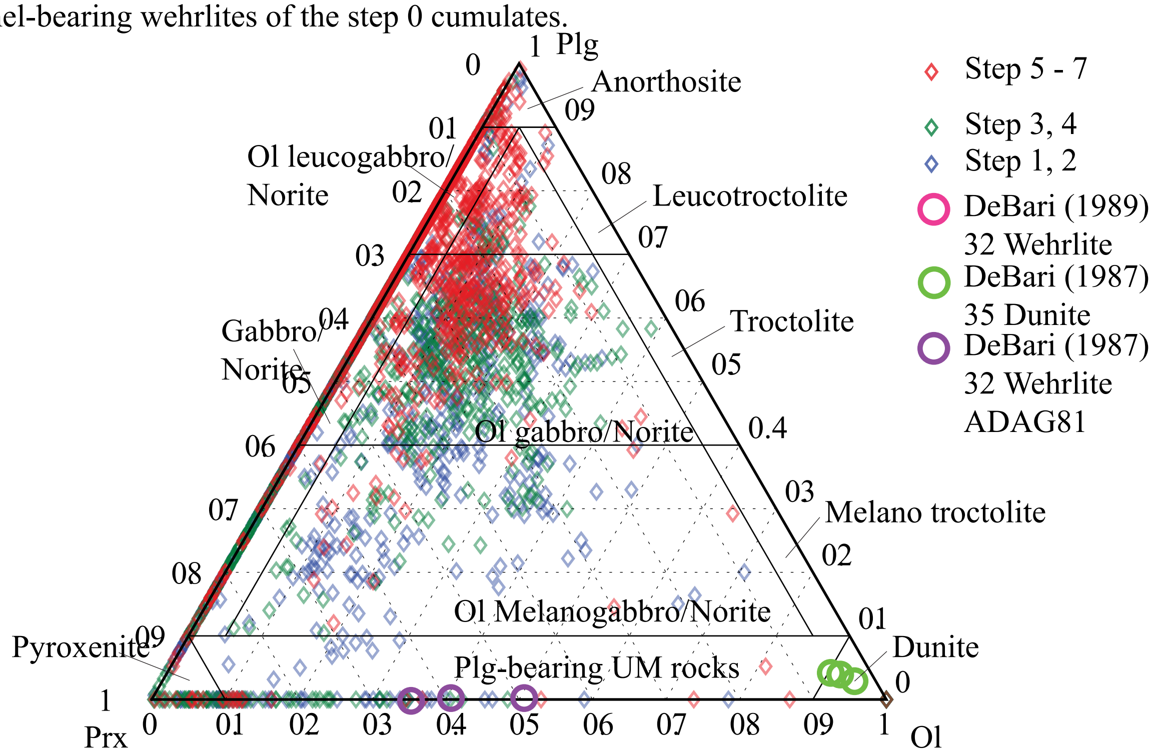

Figure 2.10: Ternary diagram 4.
Intracrustal gabbros, norites, and olivine-bearing gabbro/norites.

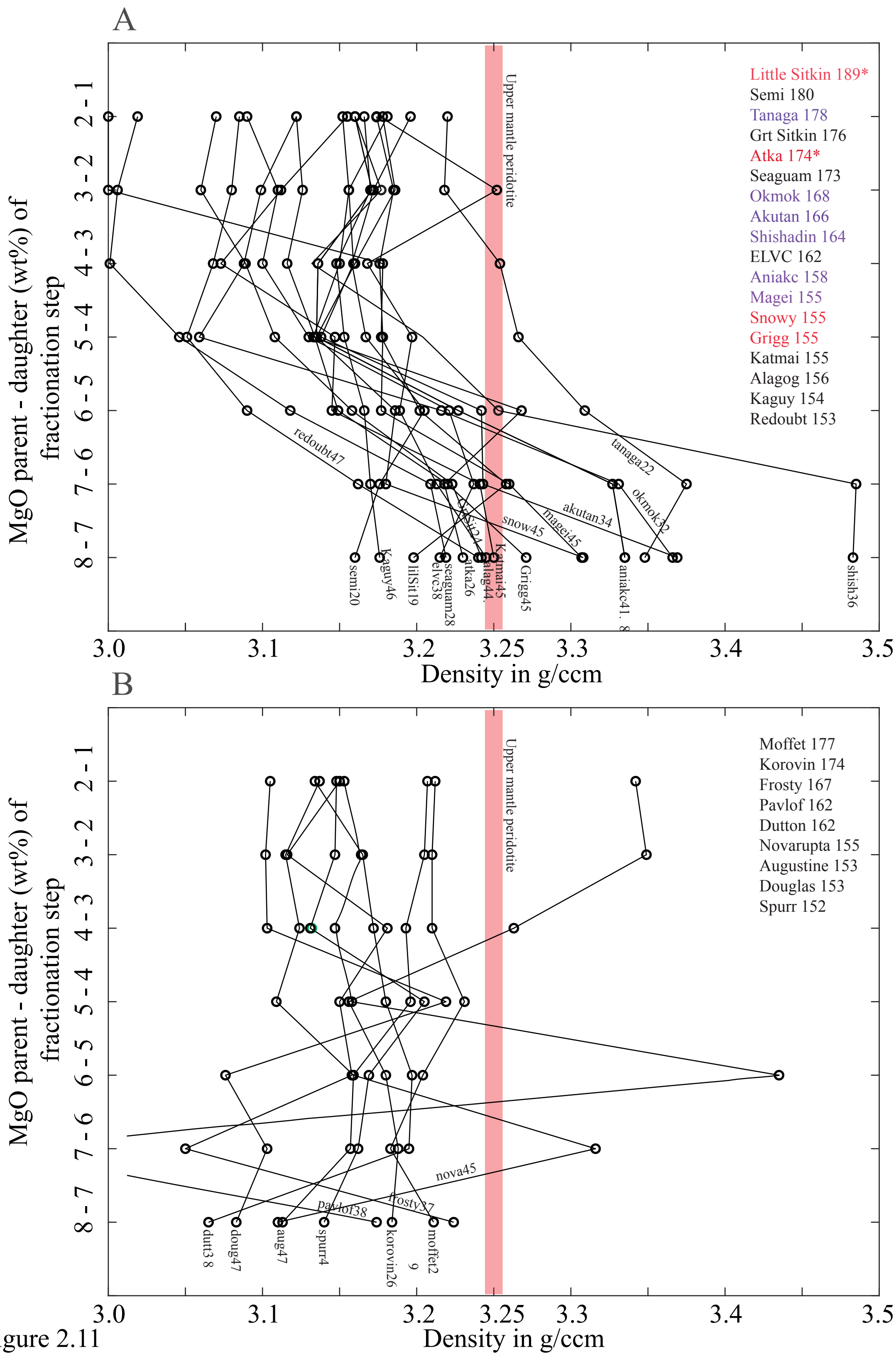

A
B
Upper mantle peridotite
Little Sitkin 189*
Semi 180
Tanaga 178
Grt Sitkin 176
Atka 174*
Seaguam 173
Okmok 168
Akutan 166
Shishadin 164
ELVC 162
Aniakc 158
Magei 155
Snowy 155
Grigg 155
Katmai 155
Alagog 156
Kaguy 154
Redoubt 153
Moffet 177
Korovin 174
Frosty 167
Pavlof 162
Dutton 162
Novarupta 155
Augustine 153
Douglas 153
Spurr 152
MgO parent - daughter (wt%) of fractionation step
Density in g/ccm

Figure 2.11

Figure 2.11:
Cumulate densities calculated using the algorithm from Hacker and Abers (2004). Each volcano is divided into the 7 fractionation steps (y-axis, wt % of parent and daughter MgO). (A) shows 18 volcanoes with “crustal column” (a MgO wt% proxy) stratified in density: open circles denote median of least square solutions of cumulate density at each fractionation step (y-axis), lines link the median solutions of individual volcanoes. The density of the upper mantle (~3.25 gm/ccm) is shown as a thick vertical line. The density of cumulates is seen to increase with increasing MgO wt% in a parent-daughter pair. List of volcanoes with “lower crust” cumulates density greater than the upper mantle are highlighted in red fonts. Volcanoes are listed in W - E longitude order (numbers after the names). Nine volcanoes whose cumulate density profiles show no increase with “depth” (MgO wt %) are excluded from (A) and plotted in (B).

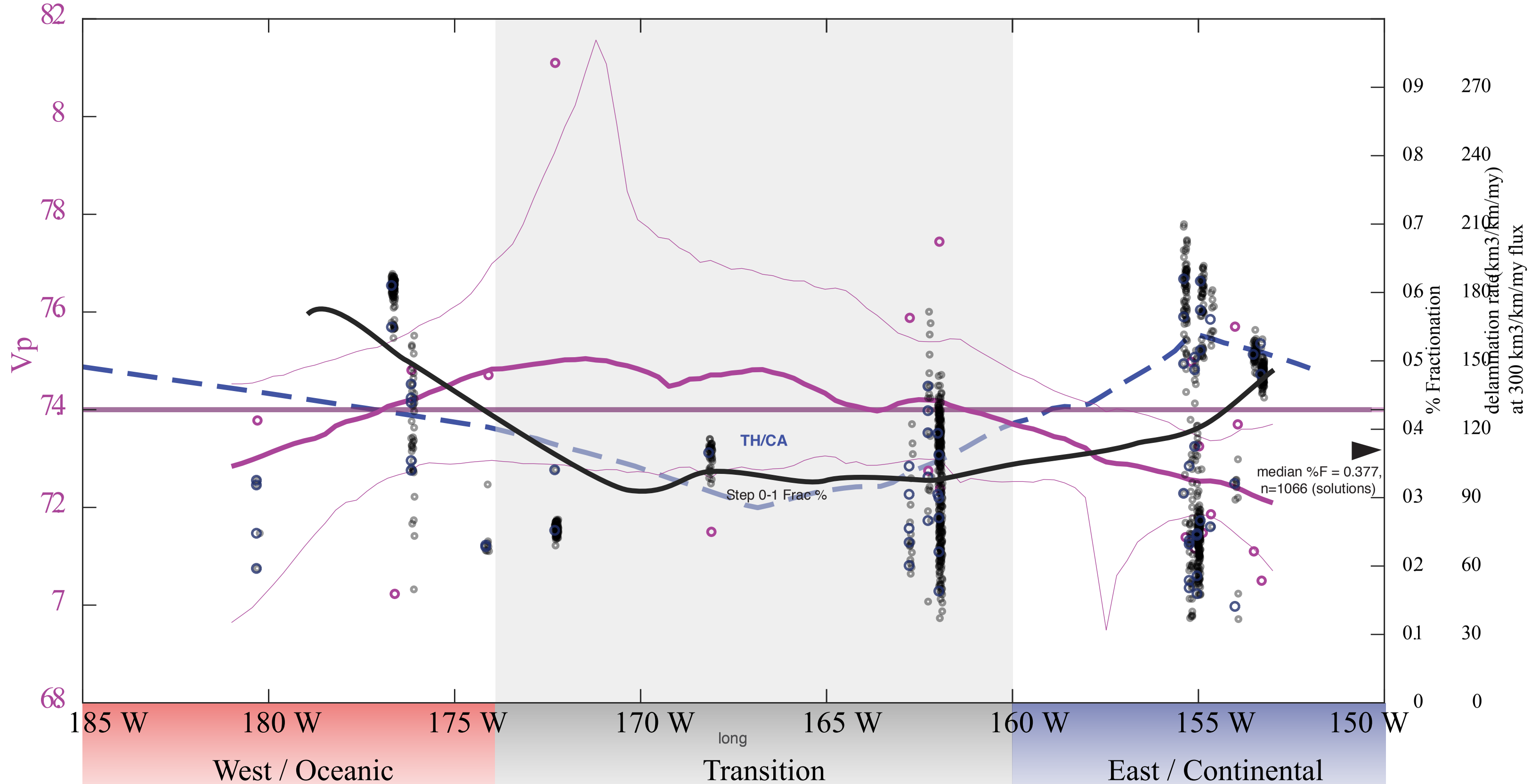
Vp
82
8
78
76
74
72
7
68
185 W
180 W
175 W
170 W
165 W
160 W
155 W
150 W
long
West / Oceanic
Transition
East / Continental
TH/CA
Step 0-1 Frac %
median %F = 0.377,
n=1066 (solutions)
% Fractionation
09
08
0.7
0.6
0.5
0.4
03
02
0.1
0
delamination rate(km3/km/my)
at 300 km3/km/my flux
270
240
210
180
150
120
90
60
30
0

Figure 2.12

Figure 2.12: Primary magma fractionation % and cumulate Vp.
The black curve is the lowess regressed primary magma fractionation % as calculated from least square modeling of the 8 primary magmas differentiating to 8 wt. % MgO synthesized lavas from the arc volcanoes and ultramafic cumulates listed in the Methods section. Black dots are individual solutions of % fractionation of each cumulate. Purple curve is the lowess regressed curve for calculated Vp step 0 fractionated cumulates' following Hacker and Abers (2004). The curve is derived from calculated median cumulates of each volcano (purple dots). A horizontal line at Vp = 7.4 km/s divides cumulates with 1 GPa P-wave velocity; cumulates with higher Vp than 7.4 km/s are related to lithologies considered unstable compared to the mantle (Behn and Kelemen, 2006). The dashed line divides tholeiitic and calc-alkaline suites as defined in Lieu and Stern (2018), where the shaded region from 160° W to 175° W (transition segment) tends to host tholeiitic volcanoes, calc-alkaline volcanoes are more common to the east and west (western Aleutian and eastern Alaskan segments). High Vp region coincides with the transitional tholeiitic, high melt fraction segment of the arc.

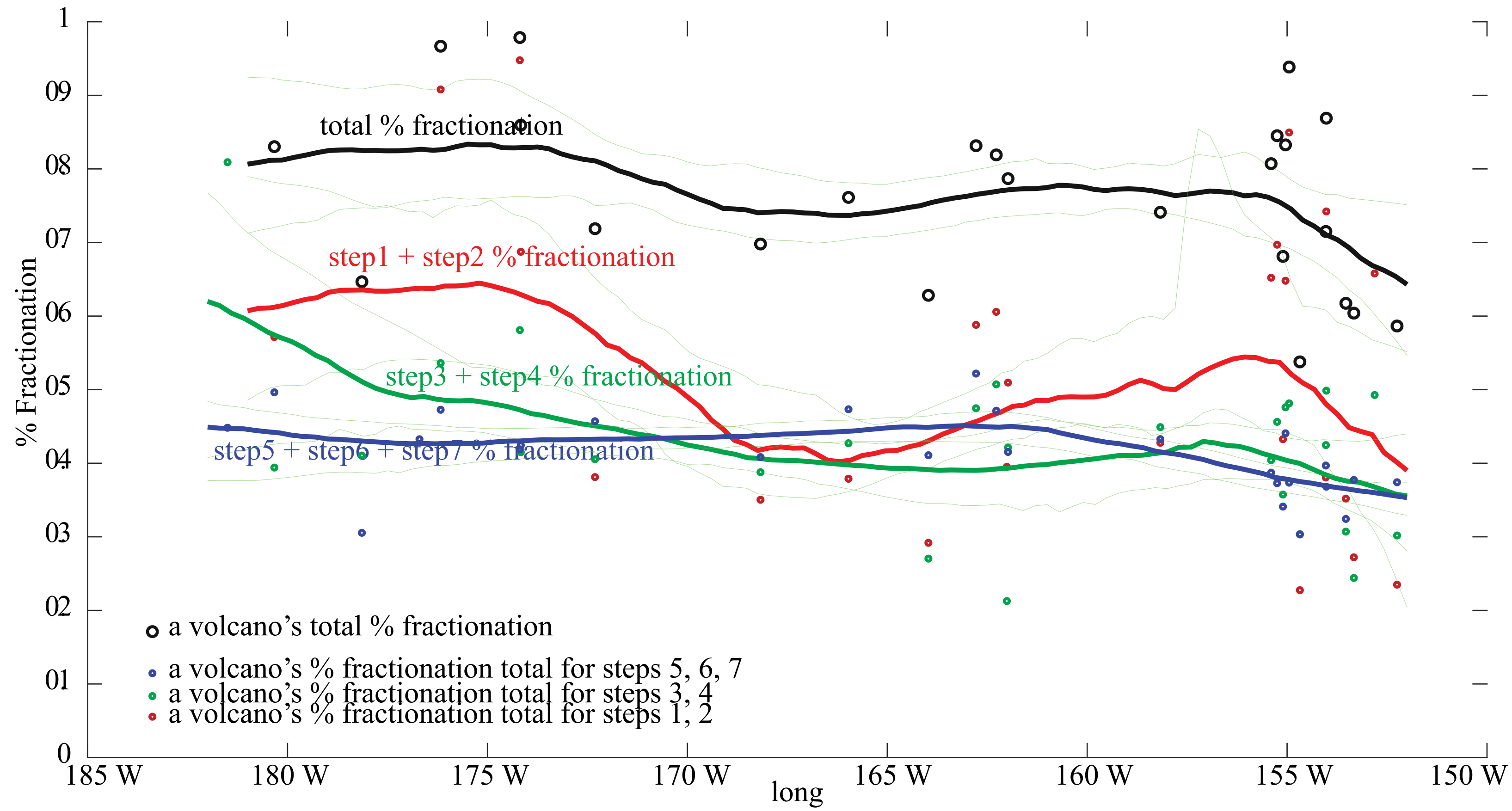

Figure 2.13

Figure 13: Fractionation for Alaskan-Aleutian arc volcanoes.
Shown are % fractionation per volcano (colored dots, color per grouped step) for the least-square solutions of steps 1 to 7 grouped in 3 combined steps, and the summed total fractionation plotted against the along-arc location of the volcanoes. The combined steps are color coded, as shown in the legend. Bootstrapped lowess regression curves are derived for the volcanoes for each step; curves are color-matched for each step. 5 and 95% confidence curves bound the median (50%) most likely curve. Top curve and points (blue) are the fractionation summed the steps.

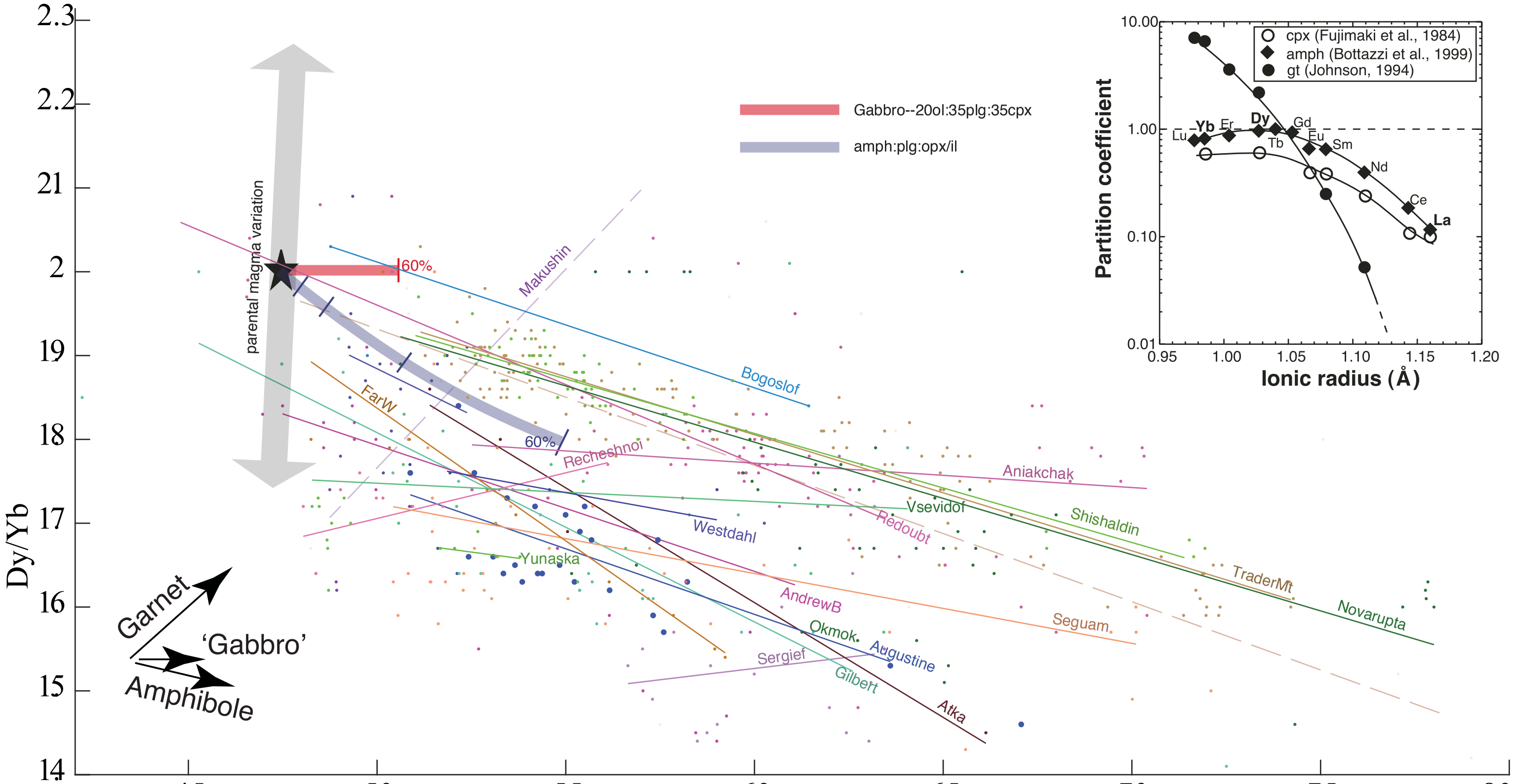

Figure 2.14

Figure 2.14: Dy/Yb systematics on amphibole fractionation.

Linear regressed lines (colored matched with samples dots) of Dy/Yb vs. SiO2 for samples from the labeled volcano adapted from Davidson et al. (2007). Fractionation vectors from Rapp and Watson (1995) of gabbroic and amphibole assemblages are shown with % fractionation ticks. Star and thick gray vector with arrows denote probable parental magma composition and its variational range, respectively. Gabbro and hornblende gabbronorite fractionation vectors are shown with ticks at every 10% F. For MREE/HREE in magma fractionation, amphibole and garnet show opposite slope due to the reversed partitioning variations of Dy/Yb between the two minerals in MREE and HREE (Inset, copied from Davidson et al. (2007)). 20 of the 28 Alaska-Aleutian volcanoes show an amphibole-controlled trend. Garnet and gabbroic assemblages do not seem to have a significant role in the cumulate composition. Gabbro (20ol:35plg:35cpx) fractionation depletes SiO2 such that, at 60% fractionation, it is not able to drive the liquid's silica beyond basaltic (brown vector).

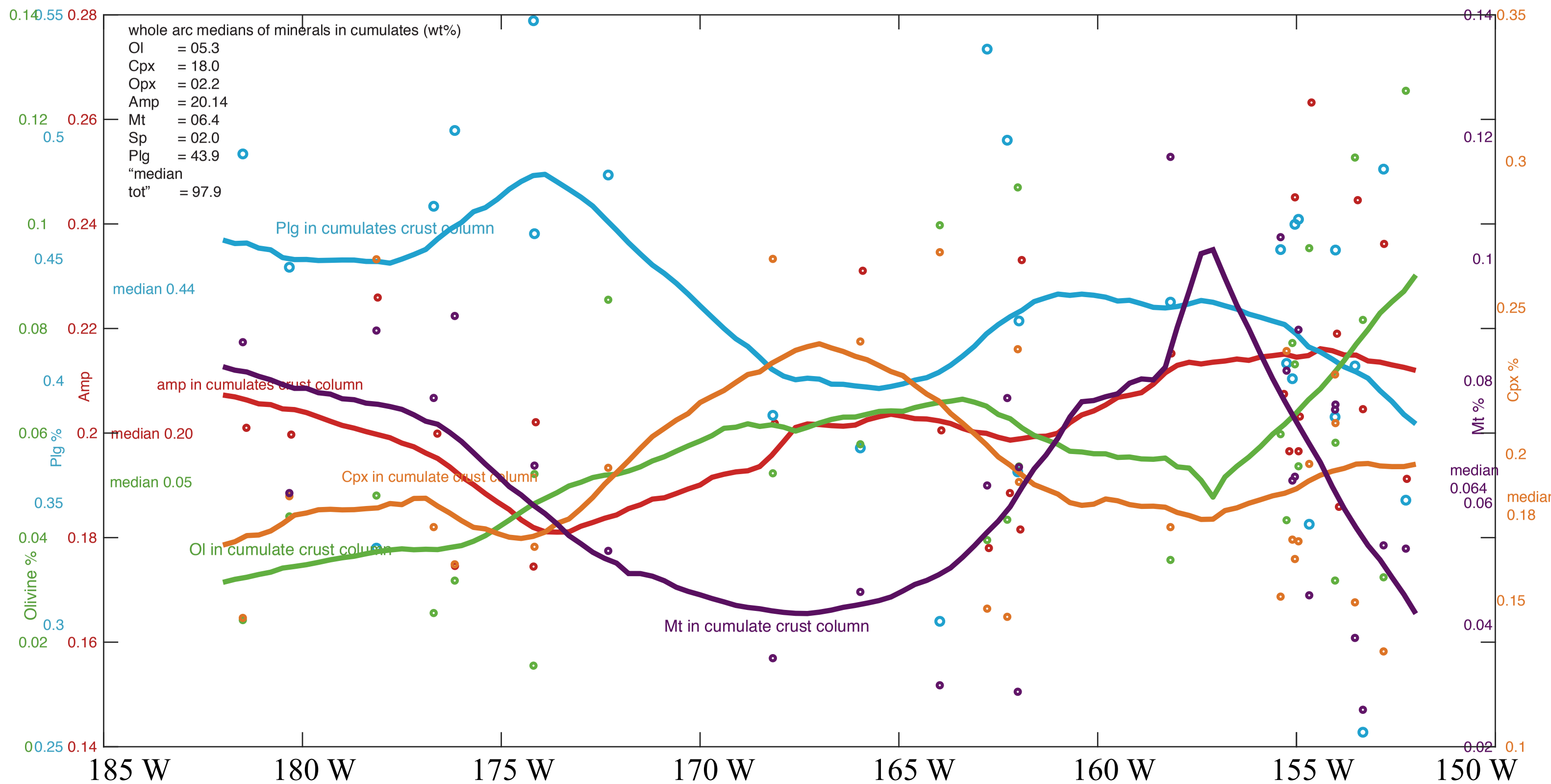

Figure 2.15

Figure 2.15: Fractionated phases along the Alaska-Aleutian arc.

Along-arc crustal composition in % of minerals fractionated. Derived minerals from the total crust column are coded in colored dots (per volcano) with their respective lowess regression curve (all along-arc volcanoes). Colored dots correspond to a volcano's total mineral % estimated from cumulate modeled in the least square procedure. Estimates are calculated per discussion in the text. Shown are Ol (olivine), Cpx (clinopyroxene), Amp (amphibole), Mt (magnetite), and Plg (plagioclase) with the whole-arc median of each mineral shown at upper left. The phase % variations are modest along the arc for amp, plg, and cpx. Mt and Ol vary by close to 250% and 300% respectively.

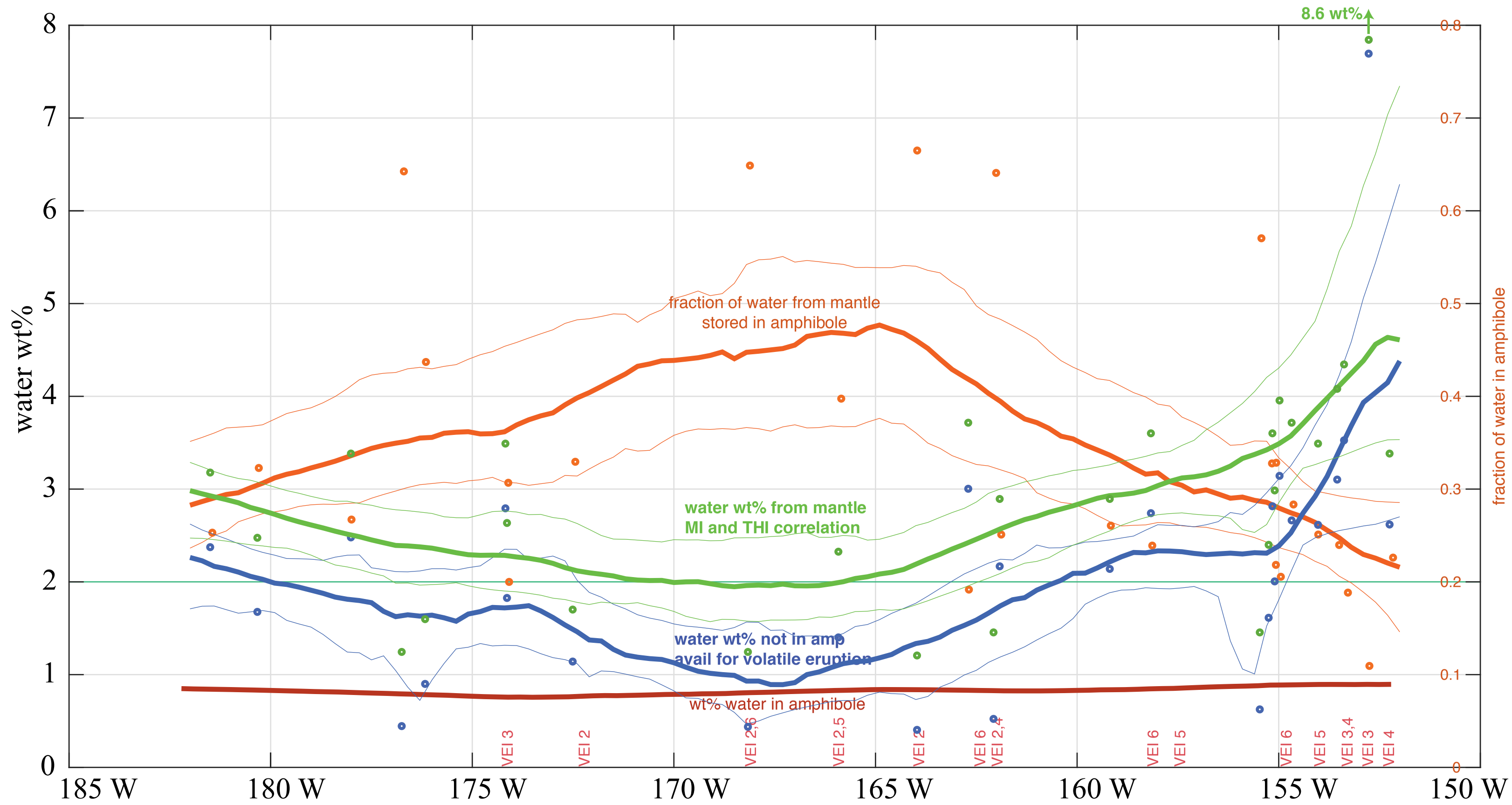

Figure 2.16

Figure 2.16: Water and amphibole in cumulates of the Alaska-Aleutian arc.
Curves representing mantle water wt.% (green, derived from Zimmer et al., 2010), fraction of mantle water stored structurally in amphibole (brown), and remaining water migrating upward, perhaps erupting (blue). Curves are lowess regressions of the three values from each arc volcano(corresponding colored dots), see text for the derivation of those values.

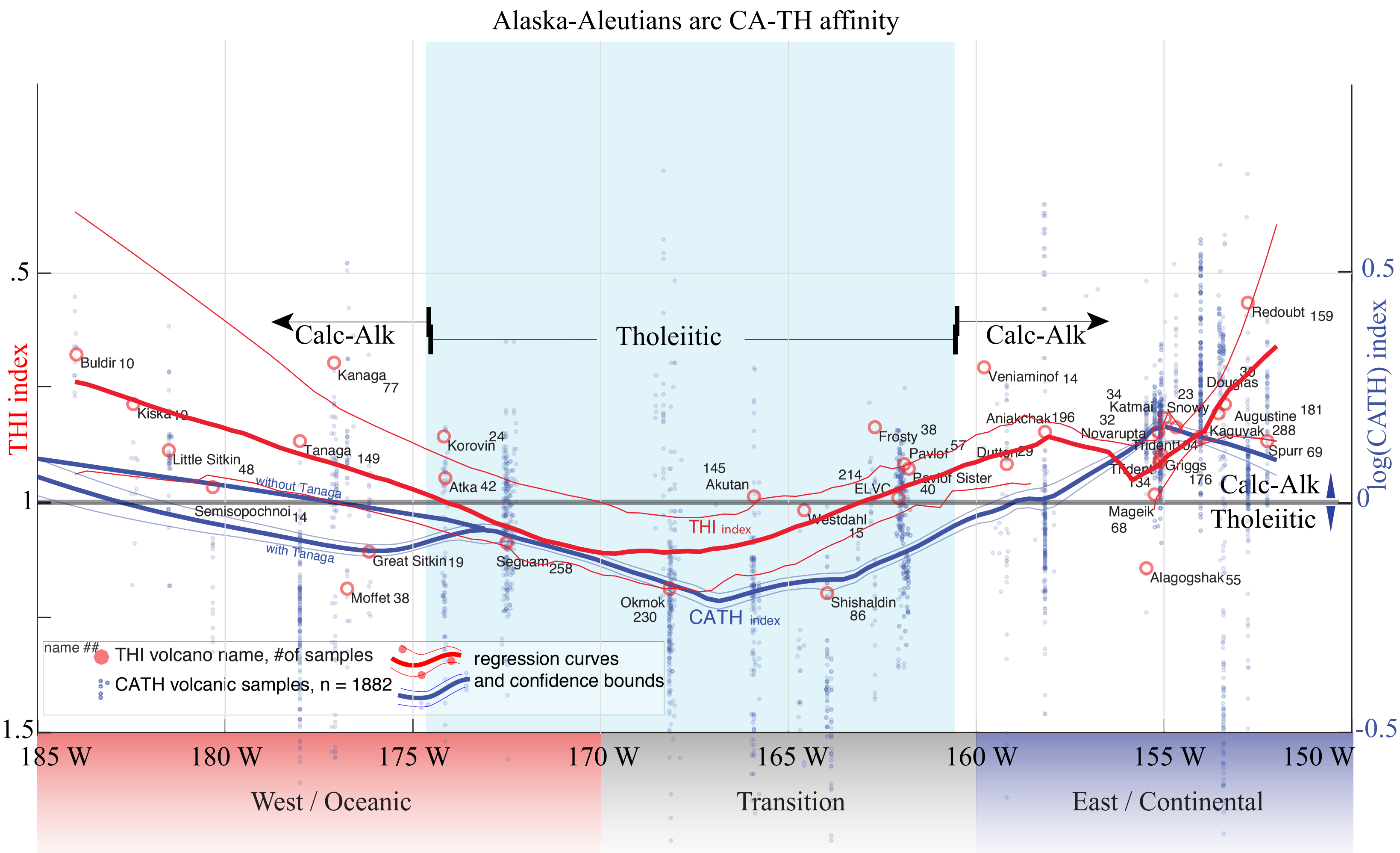

Alaska-Aleutians arc CA-TH affinity
THI index
log(CATH) index
.5
1
1.5
0.5
0
-0.5
Calc-Alk
Tholeiitic
Calc-Alk
Calc-Alk
Tholeiitic
Buldir 10
Kiska 10
Little Sitkin 48
Semisopochnoi 14
Tanaga 149
Kanaga 77
without Tanaga
with Tanaga
Great Sitkin 19
Moffet 38
Korovin 24
Atka 42
Seguam 258
Okmok 230
145 Akutan
THI index
CATH index
Westdahl 15
Shishaldin 86
214 ELVC
Frosty 38
Pavlof 57
Pavlof Sister 40
Dutton 29
Veniaminof 14
Aniakchak 196
Mageik 68
Alagogshak 55
Redoubt 159
Augustine 181
Kaguyak 288
Spurr 69
name ## THI volcano name, #of samples
CATH volcanic samples, n = 1882
regression curves and confidence bounds
185 W
180 W
175 W
170 W
165 W
160 W
155 W
150 W
West / Oceanic
Transition
East / Continental

Figure 2.17

Figure 2.17: Calc-alkaline and tholeiitic lavas.
Variations in affinities of Alaska-Aleutian arc lavas, from calc-alkaline to tholeiitic, as characterized by the CATH and THI indices of Hora et al. (2009) and Zimmer et al. (2010), respectively. Weighted lowess regression of THI (per volcano, red dots, weighted by the number of samples per volcano) and CATH (rock sample, blue points) are shown. The horizontal line at THI = 1 (left ordinate) and CATH = 0 (right ordinate) separates the tholeiitic/calc-alkaline affinity of the volcanoes and samples. Note the discrepancy between the two curves, especially at Tanaga, Akutan, and Aniakchak where the indices give opposite indications. This is caused by the complexity of including silica in the CATH index (see discussion in Zimmer et al., 2010). I take THI to be the more robust index and use it to define the tholeiitic region of the arc (THI < 1, shaded blue) that coincides with the region of thinner crust.

$$\text{CATH index} = (\text{wt\%}SiO_2 - 42.8) / (6.4 \times FeO^*/MgO), \quad (4)$$

$$\text{THI} = FeO_{4.0}/FeO_{8.0} \quad (5)$$

(subscripts on FeO indicate MgO wt %)

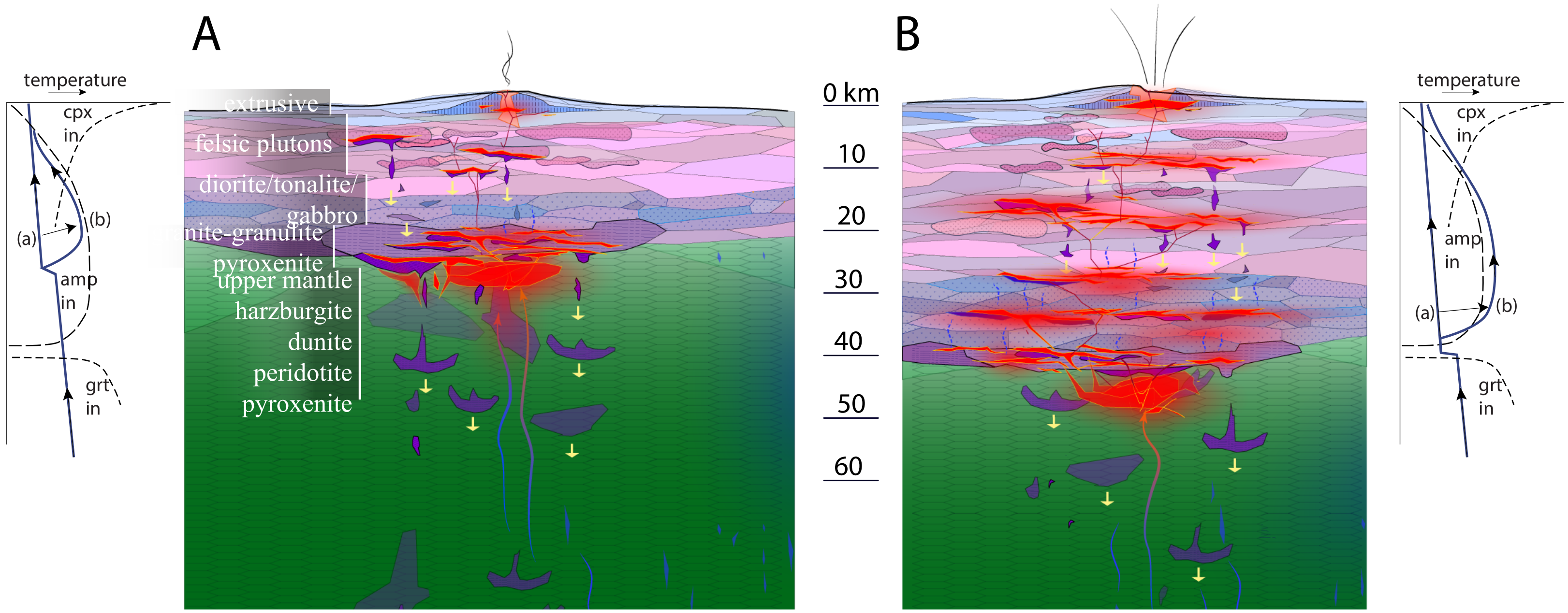
A
B
temperature
cpx
in
amp
in
grt
in
(a)
(b)
extrusive
felsic plutons
diorite/tonalite/
gabbro
nite-granulite
pyroxenite
upper mantle
harzburgite
dunite
peridotite
pyroxenite
0 km
10
20
30
40
50
60
temperature
cpx
in
amp
in
grt
in
(a)
(b)

Figure 2.18

Figure 2.18: Schematic drawing summarizing the main results of this study. Two sections of arc crust with different thicknesses are shown, along with intra-crustal and crust/mantle processes. Idealized lithologies of the section are colored differently. Flux melting is depicted as blue-to-red arrows rising from the mantle to melt lens at Moho. Melts and melt lens are red, with the fractionated products in pink for felsic plutons and dark purple for mafic cumulates. Yellow arrows indicate mafic cumulates foundering through the crust. These masses descend, stall and amass over the Moho, with the densest ones falling through into the mantle. Ultramafic cumulates and restites sink into the mantle after fractionated from the mantle-derived melt. Red glows represent thermal energy imparted to the crust at sills where magma injection alter the local geotherm, promoting the thermal maturity of the lithology and the breakdown of amphibole and releasing the structural water stored there (blue streaks emanating from sills). This process is more efficient for the thicker crust (right) where it is hotter at the base of the crust where there is volumetrically more amphibole. The hydration promotes the calc-alkalic magma trend that is more prevalent in the thick-crust Alaska-Aleutian continental arc segment versus the thinner crust tholeiitic transition segment. Far right and left show schematic phase diagrams for garnet, amphibole, cpx with geotherms (blue curves with arrows) of a pre-thermal matured (a) with stable amphibole, and a post-thermal matured (b) with amphibole breakdown. Table 1 Numeric summary of data displayed in Figure 17. See text for the derivation of amphibole phase from a volcano's crustal column. H2Omantle is water content from mantle melt based on correlation with THI, the tholeiitic index from Zimmer et al. (2010).

CONCLUSIONS

I have applied statistical techniques to the analysis of geochemical processes of trace element partitioning and major element fractionation and modeled useful results that can be compared to geophysical results. Trace element partitioning (Chapter 1) was used in combination with empirical correlation to obtain crustal thickness estimates of three arcs that rival those derived from active seismic methods. The discrepancy in the case with the Alaska-Aleutian arc may in face give insight to the dynamic processes of the crust itself. Specifically active seismic techniques may measure a spatially averaged of the mixture of delaminated ultra-mafic cumulate rocks that have detached from the lower crust with the lithologies of the upper mantle. If this is the case, arc with active delamination will render the Moho hard-to-distinguish by seismic technique. In the trace element depth proxy adapted here from the empirical correlations, the Moho depth is determined by the pressure at which Sr, Yb, Y, and La begin their partitioning into mineral. This is insensitive to delamination and in fact marks where the depth where this process take place. This may be a more relevant way of defining the Moho.

For the least-squares modeling of major element, I have applied the same statistical techniques (LOWESS regression and bootstrapping) to estimated liquid-line-of-descent from a volcanic suite of lava. Monte Carlo simulation in combination with bootstrapping of the lava samples provided a mean to synthesize any number of co-related lava suite from first melts to highly evolved felsic lavas. I used least-square modeling to relate pairs of lava to derive their cumulate composition, assuming that they obeyed mass-conserved, least square approximated evolution. Analysis of these cumulates derived from synthetic co-related lavas gave first-order insights into a totally "exposed" crustal column beneath a volcano. I perform this modeling for the volcanoes of the Alaska-Aleutian arc and extract physical characteristics from these cumulates such that I could estimate compositions and density through the crust along the entire arc. The resulting depiction is of a mid and lower crust that accommodated lavas that fractionate amphibole-rich cumulates that are dense enough to sink toward the lowermost crust and accumulate there, thus making the lowermost crust a reservoir for water. This water may be release when repeated injection of mantle-derived magma perturbs the local geotherm to pass the liquidus. This may explains the episodic cycling of tholeiitic and calc-alkaline lavas that erupts from the same volcanic complex of this arc.

In repositories around the world sits geochemical data collected and categorized over the past data. These data are the remnants after they have generated manuscripts and published papers. However their uses have not been exhausted. They await techniques that are well suited to extract even more inferences and structures from them. They are especially well-suited for meta-analysis where their combined number can illuminate areas of inquiry that are

BIOGRAPHICAL SKETCH

Warren Lieu' s interests have kept him in pursuit of the arts and the sciences. Having a childhood interest in astronomy he entered university and completed his Bachelor of Science degree in physics. Also having an aptitude in drawing and spatial design he decided on a post-college career in architecture. He subsequently worked in several design firms before he entered and completed with honor a master's program in architecture. A series of design jobs followed where he worked as a team member in designing award-winning buildings. However, the sciences beckoned and he returned to university to pursue a master's degree in geology. Ultimately, he continued on this path and dedicated his time, resources and energy to pursue a Doctor of Philosophy degree from The University of Texas at Dallas, the result of which is this Dissertation.

CURRICULUM VITAE

Warren K. Lieu

lieu.warren@gmail.com

Education:

Ph.D. (pending), Geosciences, University of Texas at Dallas, 2019

Concentration: Geochemistry; Dissertation: Statistical treatment and modeling of geochemical data from volcanic arcs Dissertation Advisor: Robert J. Stern, Ph.D.

M.S., Geosciences, University of Texas at Dallas, 2013

M.S., Architecture, University of Texas at Arlington, 1998

B.S., Physics, University of Texas at Austin, 1988

Employment:

Teaching Assistant 2013 - 2018

University of Texas at Dallas

Course: Petrology laboratory, Paleobiology laboratory, Field Geology, Signal Processing.

Substitute Lecturer 2015, 2016

University of Texas at Dallas

Course: Petrology, Exoplanets

Architectural Designer 1998 - 2010

Companies: 5G Studio, Beck Group, Domiteaux+Howard

Tasks: Concept design, project documentation, trades coordination, and construction administration for a variety of building types: hotels, schools, restaurants, churches, and residences.

Teaching Assistant 1997 - 1998
University of Texas at Arlington
Course: Computer Aid Design

Skills:

Matlab scripting for scientific calculations
CAD software
Graphics software
Concept sketching

Publications:

Warren Lieu and Robert Stern (in press); "The robustness of Sr/Y and La/Yb as proxies for crust thickness in modern arcs."
Robert Stern, Warren Lieu, Asya Mantey, Andrew Ward, Todd Fechter, Eric Farrar, Sean McComber, Jeffrey Windler; "A new animation of subduction zone processes developed for the undergraduate and community college audience." Geosphere ; 13 (3): 628–643.

Research Experiences:

Geology and petrology in the southern Mariana margin: science team member, RV Thomas Thompson, cruise TN273, December 2011 to February 2012.
University of California at Santa Cruz subduction geochemistry workshop, Summer 2012, 2013.

Patent:

Lieu, Warren. "Pet habitat." Patent D523,182S. 13 June 2006.

Presentation:

Lieu, Warren (2012) "Contouring bivariate diagram of large dataset", AGU short course.

Awards and Honors:

College of Natural Science Outstanding Teaching Assistant, 2016.

Architectural Design Competition Awards:

3rd place 1996, honorable mention 1997.